

**NASA
Technical
Memorandum**

NASA TM-82541



**THE MARSHALL SPACE FLIGHT CENTER KC-135
ZERO GRAVITY TEST PROGRAM FOR FY 1982**

Edited by R. E. Shurney
Systems Analysis and Integration Laboratory

May 1983

(NASA-TM-82541) THE MARSHALL SPACE FLIGHT
CENTER KC-135 ZERO GRAVITY TEST PROGRAM FOR
FY 1982 (NASA) 90 p HC A05/MF A01 CSCL 22A

N83-33914

Unclas
G3/12 36064



National Aeronautics and
Space Administration

George C. Marshall Space Flight Center

TECHNICAL REPORT STANDARD TITLE PAGE

1. REPORT NO. NASA TM-82541		2. GOVERNMENT ACCESSION NO.		3. RECIPIENT'S CATALOG NO.	
4. TITLE AND SUBTITLE The Marshall Space Flight Center KC-135 Zero Gravity Test Program for FY 1982				5. REPORT DATE May 1983	
				6. PERFORMING ORGANIZATION CODE	
7. AUTHOR(S) Edited by R. E. Shurney				8. PERFORMING ORGANIZATION REPORT #	
9. PERFORMING ORGANIZATION NAME AND ADDRESS George C. Marshall Space Flight Center Marshall Space Flight Center, AL 35812				10. WORK UNIT NO.	
				11. CONTRACT OR GRANT NO.	
12. SPONSORING AGENCY NAME AND ADDRESS National Aeronautics and Space Administration Washington, D.C. 20546				13. TYPE OF REPORT & PERIOD COVERED Technical Memorandum	
				14. SPONSORING AGENCY CODE	
15. SUPPLEMENTARY NOTES Prepared by Systems Analysis and Integration Laboratory, Science and Engineering					
16. ABSTRACT <p>During FY82, researchers and experimenters from Marshall Space Flight Center (MSFC) conducted 11 separate investigations during 26.3 hr of testing aboard the KC-135 zero-gravity aircraft, based at Ellington Air Force Base, Texas. Although this represented fewer hours than initially projected, all experiment and test objectives were met or exceeded. This Technical Memorandum compiles all results achieved by MSFC users during FY82, a year considered to be highly productive.</p> <p>We thank the aircraft operations people at Johnson Space Center for their enthusiastic support this year and in years past.</p>					
17. KEY WORDS Model Immiscible/critical wetting low gravity test Ice crystal growth SLI crew verification of restraints for BRS Bubble and drop motion in rotating liquid field			18. DISTRIBUTION STATEMENT Unclassified -- Unlimited		
19. SECURITY CLASSIF. (of this report) Unclassified		20. SECURITY CLASSIF. (of this page) Unclassified		21. NO. OF PAGES 88	
				22. PRICE NTIS	

TABLE OF CONTENTS

	Page
I. Model Immiscible/Critical Wetting KC-135 Low Gravity Flights (D. Frazier)	2
II. Acoustic and Electrostatic Material Science Containerless Processing Modules KC-135 Reduced Gravity Test (D. D. Elleman, A. Croonquist, W. K. Rhim, E. Trinh and T. G. Wang)	6
III. Growth of Ice Crystals From Salt Solution in Low Gravity (V. Keller, R. Owen and O. Vaughan, Jr.)	16
IV. Spacelab 1 Crew Restraints KC-135 Reduced Gravity Test (Ulf Merbold)	21
V. Reduced Gravity Positioning Device for the Upgrading of Glass Microballoons (S. A. Dunn)	23
VI. Bubble and Drop Motion in Rotating Liquid Fields (N. Shanker, P. Kondos, R. S. Subramian and R. Cole)	25
VII. Thermal Wave Experiment Comparisons of Measurements and Model Predictions (D. Bowdle, B. J. Anderson, and V. Keller) ...	30
VIII. Science Report on the Directional Solidification of Hypereutectic Cast Iron During KC-135 Low-G Maneuvers (P. A. Curreri, D. M. Stefanescu, and J. C. Hendrix)	37
IX. Influence of Low Convective Velocities on Crystal Growth (John Hallett, Gary Keyser, Rick Purcell, Nam Cho, Anna Lord, Clive Saunders, and V. Keller)	54
X. Optical Observations of Unidirectional Solidification in Microgravity (M. H. Johnston, R. B. Owen and R. E. Shurney)...	64

PRECEDING PAGE BLANK NOT FILMED

TECHNICAL MEMORANDUM

THE MARSHALL SPACE FLIGHT CENTER KC-135 ZERO GRAVITY TEST PROGRAM FOR FY1982

INTRODUCTION

Since 1959, aircraft flying parabolic trajectories have been used by the National Aeronautics and Space Administration (NASA) and the Department of Defense (DOD) to create cyclic periods of weightlessness within the aircraft cabins. While several aircraft have been and still are being used in this capacity, the specially modified KC-135, based at Ellington AFB, Texas, is the largest and most widely used. This aircraft, which offers 20 to 30 sec of weightlessness per maneuver, features a working volume measuring 60-ft long, 10-ft wide, and 7-ft high. Universal user services include a tiedown grid pattern, special photo-flood lighting, and a variety of ac and dc power supplies.

Initially, aircraft-based weightless simulations were employed primarily to test human reaction to zero gravity and to help in the development of crew aids. As we gained extensive experience with actual manned space flight, the aircraft has been increasingly used as a test bed for proposed scientific flight experiments and spacecraft systems. Engineers and scientists observe first-hand the strengths and weaknesses of their designs.

Compiled in this report are papers which collectively document the FY1982 Marshall Space Flight Center (MSFC) KC-135 program. The papers were prepared by the individuals who proposed the investigations, provided the hardware, or conducted test operations aboard the aircraft. The overall program was coordinated and facilitated by Man/Systems Integration Branch, EL15.

The editor expresses his sincere thanks to each participant and author whose work is presented herein.

I. MODEL IMMISCIBLE/CRITICAL WETTING KC-135 LOW GRAVITY FLIGHTS

By D. Frazier

Succinonitrile- H_2O solution phase densities may be equalized at room temperature using the appropriate amount of D_2O substituted for H_2O during solution make-up. Unfortunately, density stabilization can only be accomplished at one temperature; therefore, while density-driven separation may be minimized during a solidification process, it cannot be completely eliminated on Earth.

Quenching studies were conducted with 40 mole % (75.1 V %) succinonitrile H_2O/D_2O mixtures in pyrex tubes (preferentially wet by H_2O) and in plastic tubes (preferentially wet by succinonitrile). The density was adjusted to be neutral near the $18.5^\circ C$ monotectic temperature. The tubes were heated above the consolute point to homogenize the mixture, and then quenched by immersing them in liquid nitrogen.

Cross sectional slices, particularly in the pyrex tube case, reveal that massive separation did occur. In both cases, the H_2O -rich phase formed a symmetric H_2O -rich core throughout the length of the tube (though to a lesser extent in the plastic tube cases). Karl Fisher analyses revealed that the succinonitrile-rich annulus surrounding the H_2O -rich core in the pyrex tube case, contained 8 wt. % H_2O , which corresponds to the monotectic composition. Testing in plastic tubes showed a similar trend, although a somewhat more uniform dispersion of water occurred throughout the succinonitrile matrix (Table I-1.) The annulus H_2O compositions are, on average, higher than the 8 wt. % H_2O number determined in the pyrex tube case. Since 8 wt. % H_2O is exactly the monotectic composition, the SN- H_2O separations in the plastic tube cases do not appear as complete. Potard's work suggests that if the majority phase (succinonitrile-rich) is wetting, then the minority phase (H_2O -rich) will have no container sites on which nucleation and growth can be enhanced. Particle growth is retarded and thermal migration velocities reduced. There would be more H_2O , therefore, in the succinonitrile-rich phase, as Table I-1 indicates, than in the corresponding phase in pyrex. In the pyrex tube, however, we should expect to see a water-rich layer adjacent to the container wall. The analysis did not detect such a layer, but there is reason to assume that a water-rich film was lost while photographing the slices and preparing them for analysis.

An objective of one of the KC-135 experiments flown in June 1982 was to track the motions of the water-rich phase near the advancing interface during directional solidification in a quartz cell. Two samples, A (10 m% succinonitrile) and B (46 m% succinonitrile), were filmed in shadowgraph. Ground-based film showed upward migration of the rejected low density water-rich phase while solidifying a homogeneous sample from the bottom of the cell. The primary difference between cells A and B was that the higher viscosity matrix in cell B significantly damped convective fluid flow and slowed droplet migration. Sample A, in flight, showed normal density-induced phase separation during 2 g pull-out while solidifying the sample. As the plane entered the microgravity zone, however, water-rich phase droplet motion suddenly slowed, but continued along its previous path toward the hotter end of the cell (opposite direction of heat flow). As the solidification front (or, at least, the opaque zone) approached the slowly moving water-rich phase, the latter suddenly stopped

and reversed direction. The droplets were then totally engulfed by the advancing opaque zone. The temperature gradient, measured during ground-based studies, was approximately 8°C/cm. Possibly, all liquid phase material responded to newly formed voids (by moving to fill them) resulting from the density increase corresponding to the liquid to solid phase transition of succinonitrile. Nevertheless, there was no indication of lateral motion toward the cell wall. The most probable occurrence of wetting activity, according to our proposed mechanisms, would have been in sample B, the succinonitrile-rich solution. The H₂O-rich solution A wet the quartz cell wall; hence, no driving force for H₂O-rich particles, rejected at the solid-liquid interface, to move toward the wall were assumed. In the succinonitrile-rich case, however, H₂O-rich droplets, as they are rejected from the solid-liquid interface or as they form just above the monotectic temperature, may have such a velocity component. Thus far, however, filming of solidifying B solution has not yet synchronized passage of the interface through the optical path with microgravity portions of the flight parabolas. The B solution will again be observed on an upcoming flight. The current data is still being studied and ground-based/microgravity film strips for split screen viewing have been prepared.

Differences in thermal conductivity between pyrex and plastic tubes in the aforementioned laboratory experiments obscure results. Measurements show that heat transfer through the plastic tubes lags significantly behind that of pyrex. It is feasible to reverse the wetting characteristics of pyrex by coating and baking the pyrex surface with dimethyl polysiloxane (silicon oil-50 cps). This allows direct comparisons between solutions of identical minority phase volume fraction and contained in identical heat transfer media. Observation of cloud points upon cooling such solutions from above T_c (58°C) to 42°C (neutral density temperature for normal H₂O/D₂O isotopic composition) reveal interesting results. In succinonitrile-rich solutions contained in treated tubes (SN-rich phase wetting), cloud times are significantly shorter than those of the same solution in untreated tubes (H₂O-rich phase wetting). Conversely, cloud times of H₂O-rich solutions contained in untreated tubes are shorter than cloud times of the same solution contained in treated tubes. This result disagrees with the aforementioned mechanism (re: Potard, Perepezco). Further ground-based experiments, including a re-solidification of SN-H₂O systems and subsequent Karl Fisher analyses should add clarity to the sequence. Complete analysis must include photographs of solidifying B solution in a microgravity environment.

A short experiment to observe contact angle variations with temperature also flew on the June KC-135 flight. The main difficulty in measuring contact angles in a 1-g field is that the two liquid phases generally have a significant density difference. As temperature approaches the critical temperature, T_c, the interfacial tension between the two phases becomes very small, and the large density difference causes the phase boundary to become very flat. The contact angle appears to be 90°, when according to theory, it is approaching 0°. The extremely small radius of curvature of the interface near the surface makes it extremely difficult to obtain good contact angle measurements (Fig. I-1). The purpose of the short KC-135 experiments was to circumvent the situation caused by the density difference and allow interfacial tension to dominate the interface shape. Rapid adjustment of the interface from 1-g to 0-g allows photography of the interface at microgravity conditions. Succinonitrile/ethanol solution (55 wt. % ethanol) was sealed in a 1 mm path length cuvette. The critical temperature of this system is about 32°C, hence, temperature variation near T_c is

simple. The density difference between L_1 and L_2 is large enough so that the 1-g - 0-g transition should be dramatic.

The experiment demonstrated the desired phenomena. The apparently flat interface curved dramatically as the flight entered the microgravity zone. Liquid crystal strips attached to the cuvette gave an indication of the temperature of fluid inside the cell (the strips were calibrated in the laboratory). The cell was photographed in flight. Actual measurements of contact angle were not feasible from these photographs, but the experiment served as a precursor to a more detailed experiment in which a cuvette containing the desired solution was flown on Dr. R. Owen's optics palette during the September flight.

Because of the existing cell compartment design, a 1 cm path length cell replaced the 1 mm cell of the hand-held demonstration. Photography was in shadow-graph. Contrary to demonstrated feasibility, the record of activity inside the cell showed violent fluid flow during the microgravity part of the flight parabola. The high degree of activity removes any possibility of making contact angle measurements from this set of data. There were two distinct differences between the earlier demonstration and the latter. First, the cell volume in the latter cell was 10 fold larger than the former. Second, the hand-held experiment was more "free floating" than the latter which was anchored to the aircraft and possibly experiencing intermittent forces. A newly purchased cell having a 2 mm path length and compatible with the optical palette, will replace the 1 cm path length cell during the next flight. In the event the problem remains, a free floating device to house the cell is in preparation for a later flight.

TABLE 1. SUCCINONITRILE MATRIX

<u>Initial Composition</u>	<u>Tube Material</u>	<u>Annulus</u>
40 m% succ.	polystyrene	7.3 wt. % H ₂ O
40 m% succ.	polystyrene	16.4 wt. % H ₂ O
40 m% succ.	polypropylene	8.9 wt. % H ₂ O
40 m% succ.	polypropylene	11.8 wt. % H ₂ O

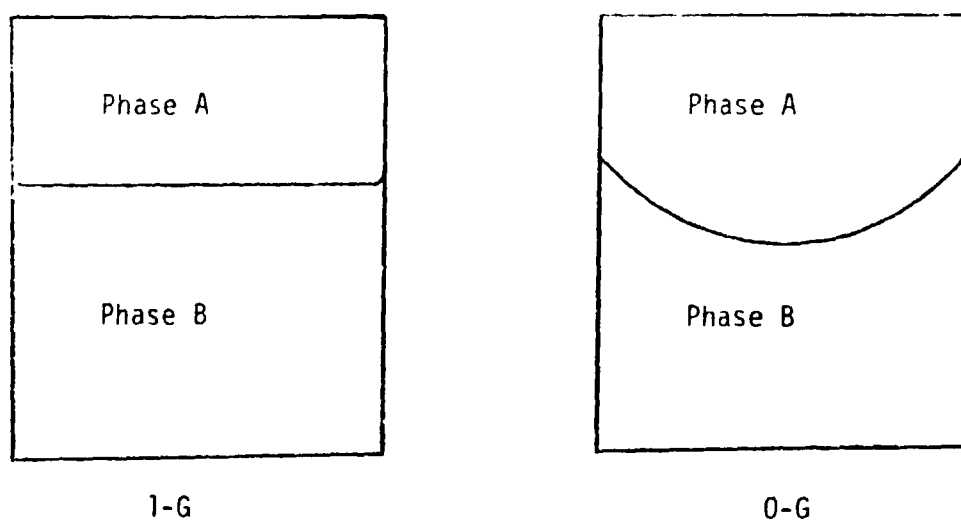


Figure I-1. Expected behavior of two-fluid/solid interface near the critical-wetting point in normal gravity and in low-gravity. As the interfacial tension between the two fluids becomes small, the contact angle approaches zero. In the 1-g case, hydrostatic pressure flattens the interface making small contact angles difficult to measure. In 0-g, this pressure is removed and the interface shape is determined solely by interfacial effects. Now small contact angles can be easily measured.

II. ACOUSTIC AND ELECTROSTATIC MATERIAL SCIENCE CONTAINERLESS PROCESSING MODULES KC-135 REDUCED GRAVITY TEST

By D. D. Elleman, A. Croonquist, W. K. Rhim,
E. Trinh and T. G. Wang

During FY82, the Jet Propulsion Laboratory conducted a series of reduced gravity tests on the JSC KC-135 aircraft. The primary emphasis of these tests was the development and verification of both acoustic and electrostatic material science containerless processing modules.

The acoustic module has undergone a series of low gravity tests over the past five years. The electrostatic positioning module low-gravity tests were initiated in the last half of FY82. Two major modifications to the acoustic module were tested in FY82: complementary phase modulation and the elongated acoustic chamber.

Complementary Phase Modulation

The standard technique to position and rotate objects in three-axis acoustic levitation chambers has been to have two of the dimensions equal in order to take advantage of interference effects. To levitate liquids in this type of chamber for nonrotation conditions the equal-frequency signals must be modified from simple sinusoidal waves. Complementary modulation of the signals is one of the techniques which has been used successfully to position liquid and solid samples during times when rotation is not desired in a chamber with a square cross-section. Complementary phase modulation is a more versatile system which can be used both for rotation and nonrotation situations.

Acoustic waves of the same frequency interfere with each other and distort the symmetry of the acoustic centering forces in the plane of the two speakers. If the relative phase between the signals at the center of the chamber is 0 deg, a rigid object can be stably positioned in the center even though the restoring force is unbalanced - the force is maximum along the diagonal between the two speakers and minimum along the second diagonal in the plane of the two drivers. As the phase separation increases so does the acoustic torque which is proportional to the sine of the phase difference. When the relative phase is ± 90 deg, the condition for maximum torque, the centering force becomes symmetric. With simple sinusoidal signals, simultaneous levitation and rotation is practical for liquid samples only very near ± 90 deg while positioning, without applying either a torque or distorting force to the drop, is not possible.

The signals which have been used in rectangular chambers with two equal dimensions were sinusoids of the same frequency with a relative phase difference of ± 90 deg when rotation was desired and complementary modulation when torque on the sample was not wanted. During complementary modulation, the signals are turned alternately on and off at the frequency f_m so that only one of the two axes is being driven at any given time. Thus, interference occurs only during and shortly after the transitions are made. The modulation frequency was chosen to be much lower than the frequency of the chamber's resonance to insure that transitions occurred during only a small fraction of the time and to be higher than any of the lower modes of natural oscillation for the expected drop to prevent the sample's stimulation and deformation. Experiments in the laboratory, the KC-135, and the SPAR have been

performed using these techniques. A problem with using simple sine-wave signals in a chamber with equal dimensions has been that it has not been practical to vary the acoustic torque between its extreme values. To decrease the torque from its maximum value at a phase difference of 90 deg, two choices were available: to change the relative phase or to decrease the amplitude of the acoustic pressure. When the relative phase was not ± 90 deg, the acoustic potential well was not circularly symmetric at the chamber's center which caused an unwanted distortion to deformable objects in this field. Although the torque decreased when the acoustic pressure was reduced, the centering force also diminished.

A scheme, which provides the entire range of torque from zero to the maximum possible value without changing the strength or the symmetry of the acoustic centering force, was found in which each signal was phase-modulated in a complementary switching pattern. For lack of a more clear name, this idea has been called complementary phase modulation (or just phase modulation).

In the nonrotation mode, the signal generator for the complementary phase modulation switches the phase of each of the acoustic waves two times every $t_m = (f_m)^{-1}$ sec. There are three phase combinations which have been implemented.

1) 0 deg mode - Constant relative phase. The two signals remain in phase while the absolute phase of each channel changes by $+90$ deg and -90 deg every t_m sec.

This mode is used to study the effects of the phase modulation upon the average acoustic power. It is not a useful operational mode as all deformable levitated objects are quickly flattened.

2) ± 90 deg mode - Alternating torques. The relative phase switches from $+90$ deg to -90 deg to $+90$ deg, etc. This is accomplished by changing the phase of both channels by 90 deg but in opposite directions. Averaged over time [i.e., times $\gg (f_m)^{-1}$], there is no net torque and the centering force remains circularly symmetric.

However, on a shorter time frame, the object will feel two equal torques opposite in direction every t_m . This mode can be used for positioning without rotation. Because the centering force is always circularly symmetric, the chances of distorting liquid samples are minimized.

3) 0 deg, 180 deg mode - Alternating assymetric field. The relative phase between the two channels alternates between 0 deg and 180 deg. Like the ± 90 deg mode each signal is shifted ± 90 deg, only the initial relative phase is different. This mode can be used for acoustic positioning and because the imbalance in the acoustic forces oscillates at the frequency f_m , this frequency can be adjusted so that surface oscillations are stimulated on a liquid sample.

The first three sets of curves in Figure I-1 illustrate the signals sent to the acoustic drivers for these non-rotation modes. When one looks at the output of a microphone in a chamber into which these signals are being injected, the discontinuities cause a decrease in the amplitude which then returns to the original level. To minimize the disruptive effect that this switching produces, the frequency of the modulation used for both complementary and phase modulation schemes is $1/30$ of the resonance frequency of the chamber. (In the figure it is only $1/7$).

When clockwise rotation of a sample is desired, the proportion of time in which the signal generator produces the clockwise torque is increased at the expense of the counter clockwise torque: the duty cycle of the ± 90 deg mode is changed from 50 percent, which give the nonrotation mode presented above, to any other value. Zero percent and 99 percent correspond to the maximum torques in opposite directions. The centering force does not change for these three conditions. The bottom curves illustrate the signals used to obtain 50 percent of the maximum torque: for 25 percent of the time, the object is under the effect of a torque opposite to the desired direction and in the proper direction for the remainder of the time. The result is an average torque which is 50 percent of the maximum torque in that direction which is obtain when the duty cycle is set for 1/99. To achieve a torque of the same magnitude in the other direction, a duty cycle of 75/25 is used.

Experimental study of the phase modulation design has been conducted in the laboratory and on KC-135 flights over the past year. In the lab, a styrofoam ball has been levitated while the various nonrotation and rotation modes were tested. The sample behaved as expected for all four modes.

The three-axis acoustic positioning modules are not able to levitate solid high density material or liquid samples in a 1-g environment due to their limited levitation force. It is particularly important to verify the ability for the complementary phase modulation (CPM) system to handle liquid samples since this type of sample simulates molten samples that will eventually be used in material science experiments. Therefore, an extensive test program in the reduced gravity KC-135 aircraft was conducted with the three-axis CPM system using both solid high density samples and liquid samples.

The results of these tests confirm that the CPM technique does not distort the drop in either the ± 90 deg mode (alternating torque) or the 0, 180 mode (alternating asymmetric field). In addition, it has been demonstrated that in the ± 90 deg mode the sample can be rotated with an adjustable torque while independently controlling the acoustic positioning force. The ability to position with a large force and at the same time rotate with a small torque is important when solid body rotation of liquid samples is required.

To date, the CPM system has qualitatively been verified. In FY83 quantitative torque measurements will be obtained.

Elongated Triaxial Acoustic Chamber

The three-axis acoustic positioning chambers that have been tested and flown on KC-135 and SPAR rocket tests in the past are rectangular with all three axes nearly the same dimension. Such chambers, when used in a high temperature furnace for material science experiments, have several disadvantages; (1) the acoustic power has to be piped into the chamber by acoustic wave guides since the acoustic transducers cannot operate in a high temperature environment, and (2) sample cooling in a contactless manner cannot be accomplished rapidly since the entire chamber and furnace must be brought down in temperature so as to cool the sample.

For these reasons an elongated three-axis acoustic chamber, approximately 3 by 3 by 20 in, has been constructed and tested in the 1-g environment of the laboratory and in the reduced gravity environment provided by the KC-135 aircraft. The elongated chamber has all of the advantages and capabilities of the three-axis rectangular chamber; i.e., it can position, rotate, and oscillate the sample. In addition, the elongated chamber can be constructed with the acoustic transducers at

one end of the chamber rather than on three orthogonal faces as shown in Fig II-2. With this arrangement of the acoustic transducers, one end of the chamber, the one without transducers, can be placed in the furnace while the other end of the chamber with the transducers remains cool. Furthermore, the chamber can be acoustically driven in a higher harmonic mode in the long dimension so that there are multiple nodal points along the length of the chamber. Thus, samples can be positioned at any of these nodal points. This allows one to position a sample in the heated end of the chamber then transport the sample to the cool end of the chamber for rapid cooling.

A ground-based experiment with low density samples demonstrated the ability of this chamber to position samples at various nodal points while the chamber was driven in 2nd, 3rd, 4th and 5th harmonic mode in the long dimension. Also, the chamber was operated with one end at 1000°C and the other end at room temperature.

True transportation of the sample without the aid of gravity could only be tested in a reduced gravity environment. A series of tests was conducted with both low-density and intermediate-density samples in the KC-135 aircraft. The chamber was operated in the (1,0,0) lateral mode and in the 2nd, 3rd, 4th and 5th longitudinal harmonic mode. Transportation was accomplished shifting the sample to various longitudinal nodal points by switching to the appropriate harmonic modes. Transportation and positioning of low-density samples was successfully demonstrated in the 10^{-2} g environment provided by the KC-135 aircraft; however, some difficulty was encountered when higher density samples were used. Large oscillation in the acoustic potential well developed due to gravity jitter of 10^{-2} g due to aircraft motion and by the translation velocity of the sample as it is moved from one nodal point to another nodal point.

Plans are now underway to incorporate a position feedback control system in order to reduce the sample oscillation. Low-gravity tests of the improved system are planned for FY83.

Electrostatic Positioning Module

Efforts at JPL have centered on the development of two types of electrostatic levitators for the low gravity environment: the ring levitator and the tetrahedral levitator. A schematic diagram of the ring levitator is shown in Figure II-3. The ring levitator derives its name from two annular electrodes which are used to create a radially symmetric field which places a charged object in a potential energy well with respect to its movement in a lateral plane, thus passively centering the object. Active control is restricted to the vertical (as shown in Fig. II-3) dimension with the ring levitator. The tetrahedral levitator, in contrast, makes use of full, 3-dimensional active feedback control, using two solid-state cameras to sense the 3-dimensional position of the object being levitated, and using 4 electrodes in a tetrahedral arrangement to control that object's position.

Despite the above differences, a single block diagram of the control electronics for the two levitators may be produced. As shown in Figure II-4, the primary components of the control system are (1) CCD camera(s) for sensing object position, (2) interface logic to convert the video raster signal from the camera(s) to one binary integer representing object position for each dimension of interest, (3) a micro-computer digitally implementing the control algorithm, (4) four digital to analog converters which generate control voltages for (5) four programmable 0-20

kilovolt voltage sources, and (6) a levitation chamber containing four electrodes. The object itself completes the closed loop system. Two additional components, a cathode-ray-tube monitor and a keyboard interfaced to the control computer, display the status of the system and allow an operator to alter control parameters.

The CCD cameras employ a self-scan photodiode array to generate a 50-row by 50-column binary threshold light/dark image representing the field-of-view. Diffuse back-lighting is used to make the levitated object appear as a dark group of pixels on a light background. The camera interface logic computes the centroid of the image from the camera's raster signal, essentially by summing the row and column coordinates of each dark pixel, and dividing the sums by the total number of darkened points in the frame. The resulting x-y measurements are fed to the control computer at the frame rate of the cameras, 120 times a second. Whereas a single camera and interface unit are all that is required for the one-dimensional control employed with the ring levitator, the tetrahedral levitator makes use of two cameras oriented at 90 deg to one another to supply x-y-z coordinate measurements to the computer. Although it may be noted that the measurements obtained in this manner with standard optics will not be in exact agreement with an ideal cubical grid due to perspective distortion, they are quite adequate for the control purposes of this application.

The levitation apparatus, as implemented, may be properly described as a discrete-time, sampled-data, digital control system. In this case, the position of the levitated object is sampled at discrete intervals of 1/120th of a sec and this measurement used to digitally compute 8 bit unsigned output values for controlling electrode voltages, and in turn object position. The basic method of determining the outputs is the popular proportional-integral-derivative or PID servo algorithm for implementing a second order linear feedback system, wherein an error signal equal to the difference between the measured variable and its desired value determine the output.

Laboratory test of the electrostatic systems and the position feedback control subsystem were conducted with low density samples in a 1-g environment. In addition, reduced gravity tests were simulated with high density samples, both solid and liquid, in a neutral buoyancy tank. The success of these laboratory experiments led to the first reduced gravity test of the electrostatic module on July 20, 1972.

The module was tested in the strap down mode. No free float tests with the module were conducted. It was felt that with the feedback system, the electrostatic module could overcome the larger g jitter, ± 0.1 g that occurs in the strap down mode.

The specific objectives of the tests were as follows:

- 1) Test of launching system
- 2) Test of tetrahedral levitator
- 3) Test of ring levitator
- 4) Overall performance of electronic equipments within the KC-135 environment
- 5) Levitation of high density balls
- 6) Collect information required to design the future liquid levitation experiments.

The results of the experiment were successful and all test objectives were met. A detailed investigation of the test data is in progress. The data are recorded on video tape. This tape includes not only the visual recording of the behavior of the levitated object, but also records outputs from the feedback system in graphical and numerical form. From preliminary analysis, it has been determined that:

- 1) The launching system was functioning perfectly.
- 2) The tetrahedral levitator not only levitated light glass shells but also those plastic balls of density ~ 1 .
- 3) The ring levitator could levitate light balls.
- 4) All electronic equipment functioned properly most of the time. Temporary malfunctioning of one of the high voltage units is under investigation.

From the results gained in the first low-gravity test, several minor modifications to the feedback control system were made. A second series of reduced gravity experiments using the electrostatic module was carried out in September 1982. The primary emphasis of these tests was the demonstration and control of high density material $>3\text{gm/cc}$ and liquid samples. The results of these tests show that the electrostatic module can position and control the higher density samples to within 2 mm of the set point while the system is subjected to $\pm 5 \times 10^{-2} \text{ g}$ loads produced by aircraft motion and vibration. Several liquid samples were also successfully positioned in the chamber after in-flight modifications were made to the liquid delivery subsystem.

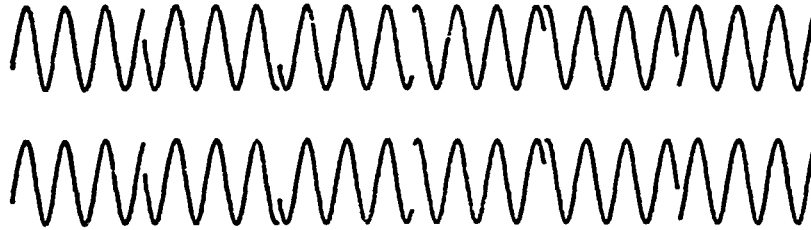
Additional tests of the system with liquid samples will be conducted in FY83 so as to determine internal perturbation within liquid samples while they are positioned by the electrostatic system. Also, detailed data will be gathered on the actual g-perturbation the sample receives and relate this g-jitter to the aircraft motion. Proper adjustment of the feedback control parameters can reduce acceleration forces on the sample to less than the aircraft jitter.

ACKNOWLEDGMENT

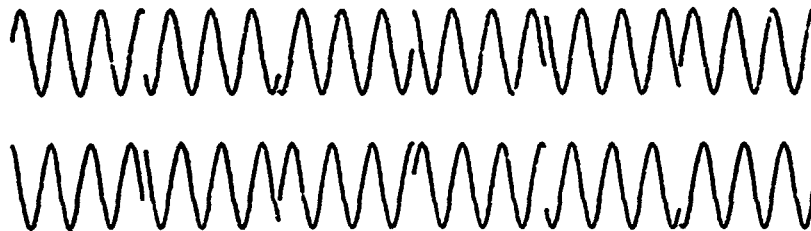
The authors would like to thank the KC-135 flight crew at JSC for their efforts and assistance in conducting the reduced gravity experiments. In addition, a special note of appreciation is in order for Robert Shurney of MSFC, without whose help many of these experiments could not have been conducted.

Non-Rotation Configurations:

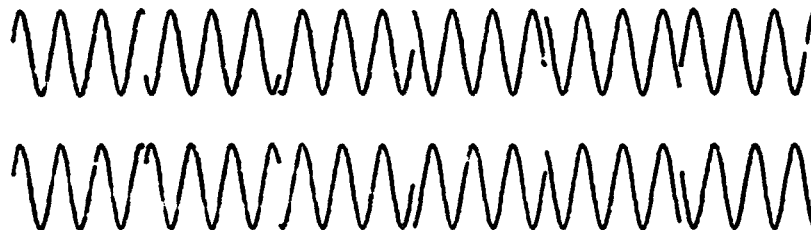
0° mode - 50/50 duty cycle



$\pm 90^\circ$ mode - 50/50 duty cycle



$0^\circ, 180^\circ$ mode - 50/50 duty cycle



Rotation Configuration:

$\pm 90^\circ$ mode - 25/75 duty cycle

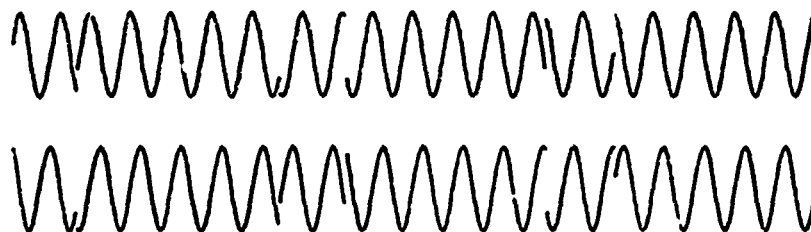


Figure II-1. Complementary phase modulation examples of waveforms.

ORIGINAL PAGE IS
OF POOR QUALITY

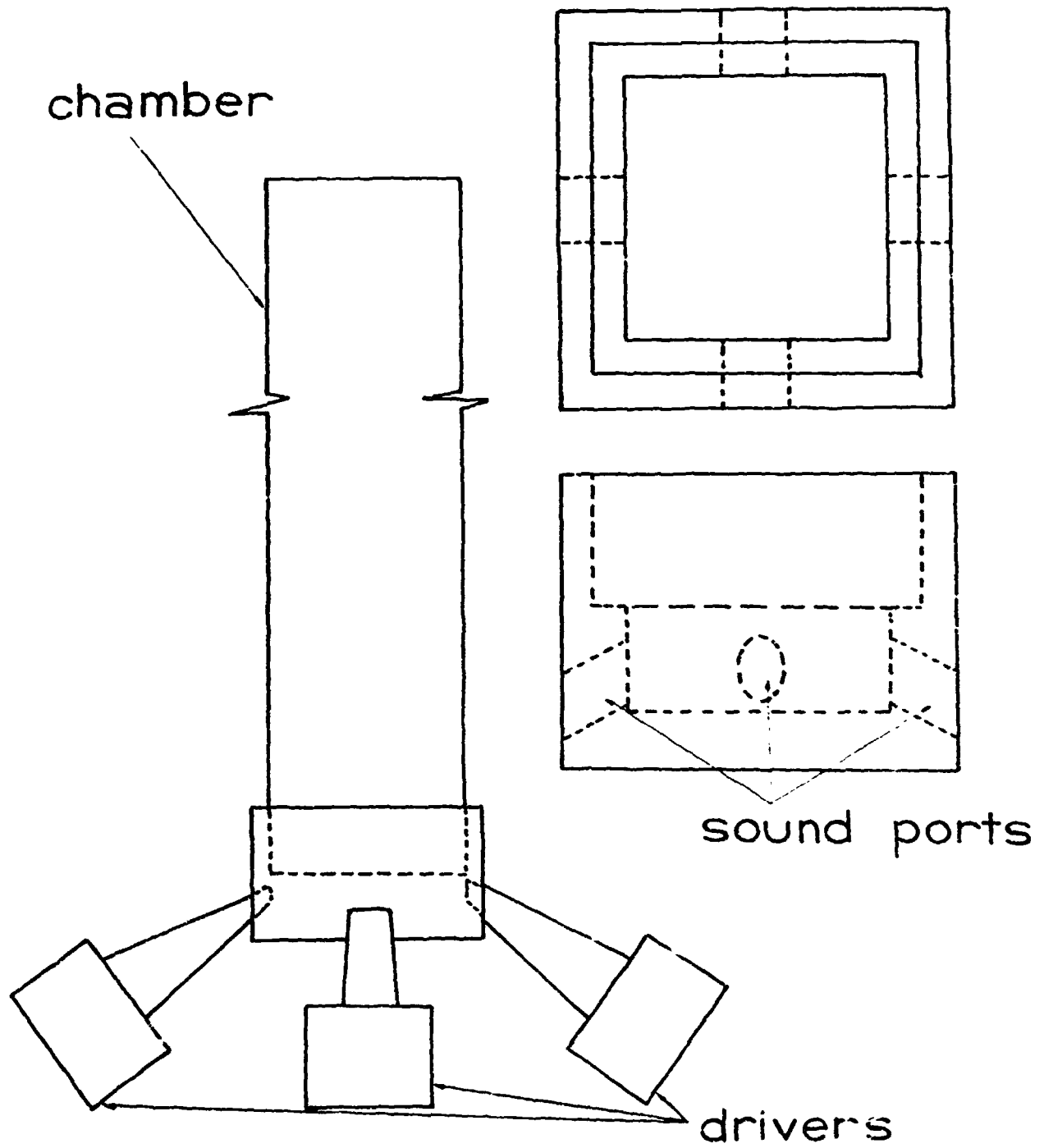


Figure II-2. Rectangular elongated vibration chamber.

ORIGINAL PAGE 19
OF POOR QUALITY

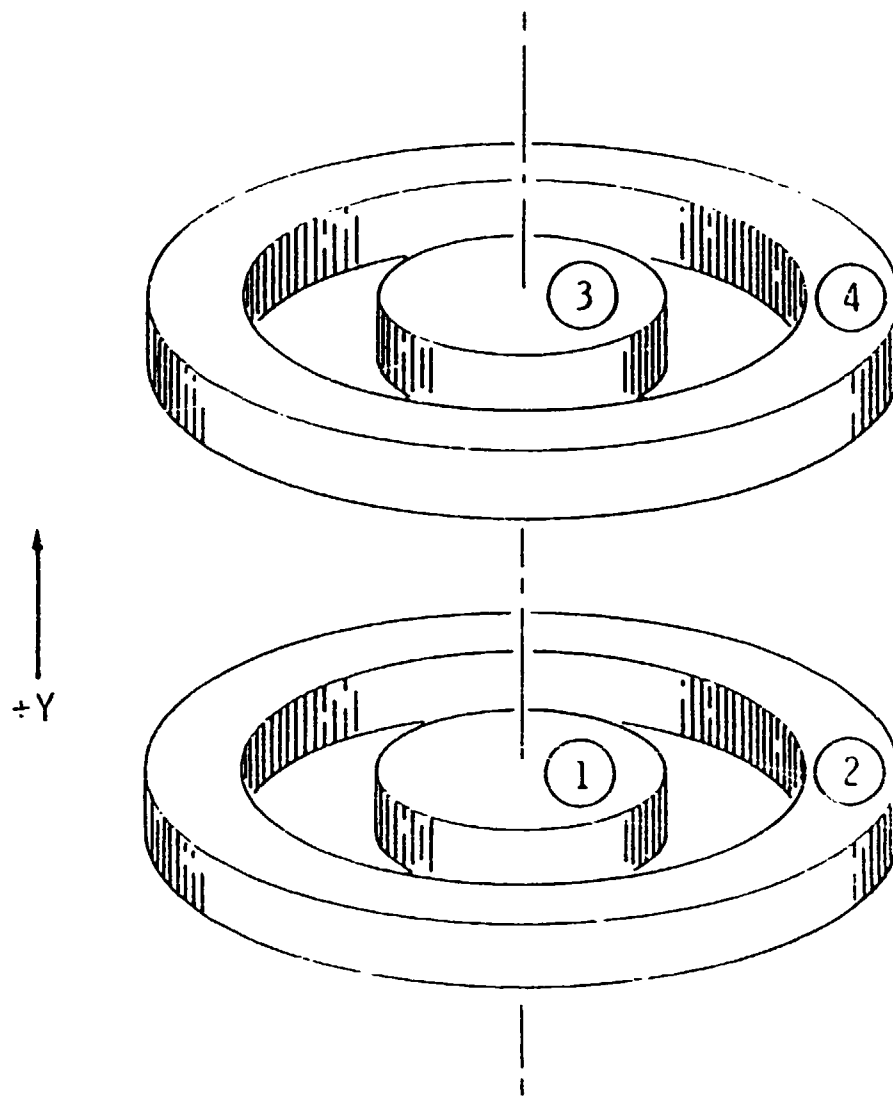


Figure II-3. Ring levitator schematic diagram.

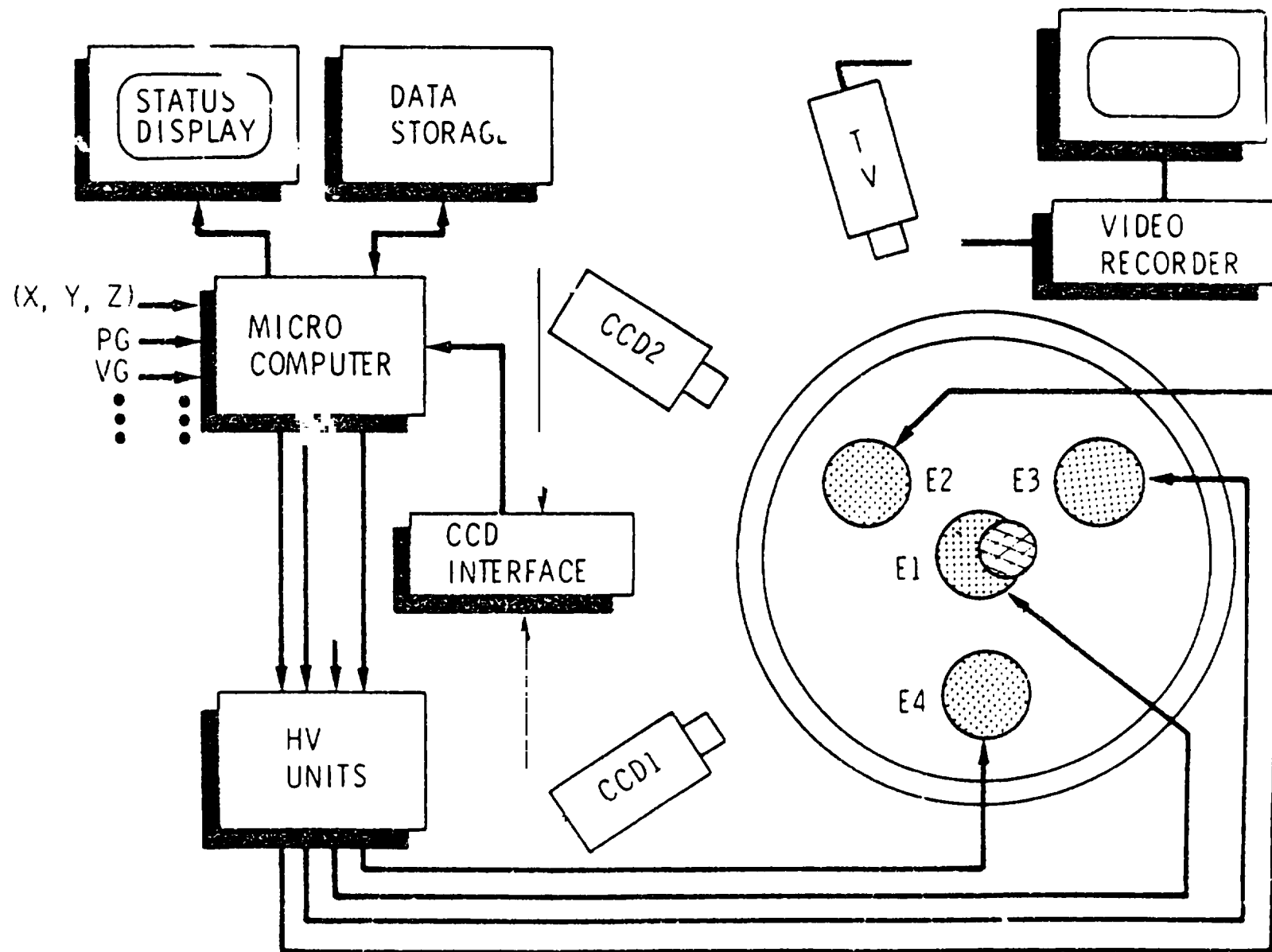


Figure II-4. Control system primary components.

III. GROWTH OF ICE CRYSTALS FROM SALT SOLUTION IN LOW GRAVITY

By V. Keller, R. Owen and O. Vaughan, Jr.

Introduction

As an ice crystal grows in a supercooled salt solution, water molecules from the solution are preferentially incorporated into the crystalline lattice leaving a higher concentration of salt at the crystal-solution interface. The density differences due to the concentration gradient near the crystal surface may be substantial; i.e., it is estimated that they may be as much as 100 times greater in 1.0 percent NaCl solution than the temperature induced density gradients in pure water. Working in an earth-based laboratory, Vlahakis and Barduhn (1974)¹ observed that in 0.5 to 1.0 percent NaCl solutions ice crystals grew as much as 2.5 times as fast as in pure water at the same supercooling instead of the 0.8 to 0.9 times predicted. Present models simply predict a regular decrease in growth rate with increasing solute concentration. They also found that the effect was enhanced at low forced flow rates and high subcoolings and tended to disappear at low subcoolings and high forced flow rates. They suggested that natural convection induced by concentration gradients may be the reason the ice crystal linear growth rate versus solute concentration is anomalous in that the growth rate increases to a maximum value and then decreases as the solute concentration is increased.

If this explanation were correct, then the linear crystal growth rate should change markedly as a crystal alternately grows in low gravity and high gravity. Furthermore, under low gravity conditions, the linear ice crystal growth rate in distilled water should be comparable or even greater than the growth rate in 0.5 percent NaCl at the same supercooling.

Experiments

Ice crystals are nucleated and grown in both supercooled distilled water and supercooled salt solutions (0.5 to 10.0 percent NaCl) in the alternately low gravity-high gravity environment available on NASA KC-135 aircraft parabolic flights. For each experiment run, an optical glass cell filled with 15 ml of water or salt solution is placed into the cylindrical water-ethylene glycol filled cavity of the temperature-controlled growth chamber. The cell contains a thermistor for temperature measurement and a capillary nucleation tube approximately 2.5 mm OD. The temperature inside the optical cell, as well as the temperature of the growth chamber, is monitored and recorded during flight using two digital meters and a three-channel strip chart recorder. Accelerometer data is recorded on the third channel of the recorder. Although the cell is pre-cooled to 0°C in an ice water bath before being placed into the growth chamber, the time necessary to insure that the temperature of the liquid in the cell is uniform and has come to within at least 0.1°C of the growth chamber temperature is still on the order of 45 min. This limits the number of experimental runs on each flight to two or at most three.

When temperature equilibrium is achieved, a nucleation probe, pre-cooled to dry ice temperature, is inserted into the capillary nucleation tube. Ice crystals then grow

1. Vlahakis, J. G., and A. J. Barduhn: AICHE Journal, Vol. 20, No. 3, pp. 581-591, 1974.

from the end of the capillary tube into the bulk of the supercooled liquid and are photographed. Using this technique, ice crystals are nucleated from a point; i.e., the end of the capillary tube, at any time desired in the flight parabola. Condensation on the windows of the growth chamber is prevented by heating the outer optical glass windows of both the illumination and camera ports.

Laboratory runs were made with a range of NaCl concentrations and supercoolings to determine the optimum conditions to give crystal growth rates ($\sim 10^{-2}$ cm s $^{-1}$) compatible with the time available in a low gravity parabola (~ 25 secs).

Shadowgraph, Moire, and Mach-Zehnder optical systems have all been used on the low gravity flights. The crystal growth was recorded photographically.

Results

Both the Moire and Mach-Zehnder systems recorded greatly reduced convection around the growing crystals in the low gravity (10^{-2} to 10^{-3} g) portion of the parabolas. Figures III-1, III-2, and III-3 are Mach-Zehnder interferograms taken respectively in the high-gravity, low-gravity (i.e., after 20 sec of low gravity), and high-gravity portion of a parabola sequence. Waves in the fringe patterns indicate index of refraction gradients which are associated with density gradients and indirectly with convection. Convection is downward in these experiments due to rejection of salt, which is heavier than water, at the crystal interface (primary effect) and heating of the liquid surrounding the growing crystals due to latent heat release, which for water at these temperatures increased its density (secondary effect). A comparison between Figures III-1 and III-2 shows that convection was significantly reduced in low gravity. It should be noted that even after convection ceases a considerable time is required in low gravity to smooth out density gradients by molecular diffusion.

These experiments have demonstrated that the linear ice crystal growth rate in dilute salt solution is not strongly a function of natural convection. The growth rate is not dramatically different between low gravity and high gravity. Furthermore, for the same supercooling, the growth rate was substantially greater in 0.5 percent NaCl solution than in distilled water even when growth took place in low gravity; i.e., anomalous growth occurs even in low gravity.

We conclude that the anomalously rapid growth is due to crystal growth kinetics. Possibilities to explain this anomaly include but are not limited to such mechanisms as: (1) the effect of preferential ion incorporation into the ice lattice on the nucleation rates of different crystalline faces (freezing potential measurement demonstrates that Cl $^{-}$ ions are preferentially incorporated into the ice lattice leaving excess Na $^{+}$ ions in solution); (2) the effect of small amounts of solute on the ice crystal thermal conductivity (increased conductivity implies more rapid heat removal and faster growth); and (3) the effect of solution temperature rather than just undercooling temperature on the crystal thickness (slightly colder temperatures may result in substantially thinner crystals for the same undercooling of different solution concentrations). An attempt is being made to develop an alternate explanation for this anomaly.

Acknowledgments

ORIGINAL PAGE IS
OF POOR QUALITY

The dedicated efforts of Robert Shurney, MSFC, Robert Williams, JSC, Lawrence Magers, JSC, and pilots and crew of the KC-135 aircraft contributed immensely to this investigation.



Figure III-1. Mach-Zehnder interferogram of ice crystals growing from 6.0% NaCl solution in high gravity ($\sim 2g$) preceding the low gravity portion of a flight parabola.

ORIGINAL PHOTOGRAPH
OF POOR QUALITY



Figure III-2. Mach-Zehnder interferogram of ice crystals growing from 6.0% NaCl solution in low gravity (i.e., after 20 sec of low gravity).

ORIGINAL PHOTOGRAPH
OF POOR QUALITY



Figure III-3. Mach-Zehnder interferogram of ice crystals growing from 6.0% NaCl solution in high gravity ($\sim 2g$) following the low gravity portion of the flight parabola.

IV. SPACELAB 1 CREW RESTRAINTS KC-135 REDUCE GRAVITY TEST

By Ulf Merbold

Spacelab 1 Crew Restraints

Spacelab 1 Life Science experiments call for a support crewman to impart translational and rotational oscillations, a second crewman (or subject) restrained to a chair-like Body Restraint System (BRDS). The ability of the originally baselined suction cup foot restraints to secure a crewman had for some time been questioned by investigators; these doubts increased when early Shuttle crews repeated poor flight results with suction cups.

The test reported in the following memorandum led to a recommendation that Skylab-like grid panels and triangle shoes be flown on Spacelab 1.

Three different foot restraint systems; e.g.,

- Triangular Grid and Special Shoes
- Improved Suction Cup Shoes
- Foot Straps

were verified on two KC-135 flights which took place on August 24 and August 25, 1982. The participants were Bob Shurney, Bob Parker, Wubbo Ockels, Ulf Merbold, and Tom Grubbs (ISC Suction Cup Shoe Engineer). My assessment of the different systems is as follows:

1. High Load Activities

For high load activities, like oscillating a test subject (1ES201, 1ES28), the improved suction cup shoes are inadequate because they will break loose frequently and without any preceding warning.

The best restraint system is clearly the triangular grid in combination with special shoes.

The foot straps can be used; however, they do not assure smooth operations since the operator is not securely attached to the SL floor.

2. Low Load Operations

The problems we encountered with the high load operations raise the question whether suction cup shoes are reliable enough to be used during low load operations such as operating the DDU.

I have come to the conclusion that they will probably be sufficient for a lot of activities; however, additional work needs to be done to improve my confidence in the shoes. So far, I do not consider them a proven system.

Obviously, foot straps as well as the triangular grid can be used to restrain a crewman while he is executing low load operations. They are more reliable, but not quite as flexible as suction cup shoes.

NOTE: As a result of the tests reported above, an ECR was submitted calling for additional grid as shown on the attached figure. As shown, grid is to be attached to the center isle floor, off of the body restraint system and to each of the four portable foot restraints (one side only).

V. REDUCED GRAVITY POSITIONING DEVICE FOR THE UPGRADING OF GLASS MICROBALLOONS

By S. A. Dunn

Bjorksten Research Laboratories, Inc., is engaged in the development of a reduced-gravity materials-processing system originally intended for the purpose of upgrading glass microballoons (GMB's). This work is being performed under NASA Contract NAS8-33513. The objective of the current phase of the project is the development of a reduced gravity materials positioning device of general applicability.

Adjustments in position are made with directional pulses of air from opposed pairs of transducers situated along three orthogonal axes. The transducers generate the directional air pulses from sound energy upon command from a microcomputer. Each transducer, termed a sonic pump, involves an audio speaker whose output is funnelled through a collimated hole structure (CHS). During each sound pulse, flow into the CHS is omnidirectional, while the flow from it is unidirectional and aligned with the CHS axis. The end result is an axial net outward flow of air a short distance above the CHS.

The computer receives positional data through a split screen video camera which, with the aid of mirrors, tracks an object in two orthogonal planes. Deviation of the object from preset coordinates provokes output pulses from appropriate speakers until original position is restored.

A reduced gravity environment such as that of the KC-135 flight regime is essential to test the position keeping capabilities of the computer controlled sonic pump system. While in Earth's gravity stable levitation of a 1 mm GMB is readily accomplished, the stability of the levitation is controlled by other agencies as well as by the triaxial sonic pump system. Lateral stability, for example, can be attained through the Bernoulli forces associated with the main upward flow alone. The reduced gravity of the KC-135 flight would eliminate this steady flow from one of the sonic pumps and with it accompanying Bernoulli forces and thereby place the burden of lateral and other elements of stability solely upon the computerized positioning device.

The positioning system was designed to work against acceleration of a milligravity or less, in consequence of a response time, camera to computer to transducer of the order of 100 milliseconds. In the first test series aboard the KC-135, however, the equipment was bolted to the deck where it picked up aircraft vibrations. These oscillations involved accelerations of the order of hundreds of milligravity, and in conjunction with amplitudes of the order of millimeters, they exceeded the position keeping capability of the device.

Accordingly, modifications were made for free floating test equipment in a second flight and thus avoiding the unwanted airframe vibrations. A retractable positioning probe was provided which permitted the operator to load and position the GMB during level flight. It then held the GMB during multigravity and released it upon command in the reduced gravity portion of the flight regime.

The probe functioned well in tests on the ground. On in-flight video tape, however, it appeared that retraction of the probe created eddy currents which gave rise to unacceptable forces on the GMB. There was also evidence of comparable accelerations from other forces, presumably electrostatic. These accelerations appeared to be

of the order of a large fraction of gravity and well beyond the system's response capability.

The use of quadrant photo detectors for tracking information of levitated objects is currently being investigated. Response times of 200 microseconds appear possible, an improvement of over two orders of magnitude relative to the present system. Employment of this system will enable levitation and positional maintenance of objects in rapidly changing gravitational environments, such as experienced in the KC-135 flight regime.

Funding to implement these improvements has been proposed along with further KC-135 testing.

VI. BUBBLE AND DROP MOTION IN ROTATING LIQUID FIELDS

By N. Shanker, P. Kondos, R. S. Subramanian and R. Coie

Abstract

Experiments concerned with the trajectory of small bubbles or drops in rotating liquid fields, were carried out in the near-free-fall environment provided by the NASA KC-135 flight program. Bubble trajectories were observed in a rotating, liquid-filled glass sphere; in an unconstrained liquid drop centered within a rotating, liquid-filled glass sphere; and in an acoustically rotated, levitated liquid drop. Drop trajectories were observed in a rotating glass sphere filled with a liquid which was immiscible with and less dense than the drop.

Introduction

Containerless space processing may well involve the interaction of liquids in the form of drops. For example it may be desirable to form an alloy in space by merger of two or more drops. Encapsulation of a volatile liquid by a second less volatile and immiscible liquid might be a means for avoiding volatilization. Rotation, oscillation, etc., of such systems would enhance mixing where desirable and/or provide means for drop management.

The presence of bubbles in drops is often to be expected. They may result from air originally entrapped in raw materials or they may be formed by chemical reaction as in the manufacture of glass. Bubbles might also result from a reduction in system pressure. In some instances bubbles are desirable. Examples include the development of foamed metals and the formation of hollow shells for use as targets in the laser fusion program. In the making of glass, bubbles are almost always undesirable and their complete removal is critical to the production of optical quality components. In orbit, the near-free-fall conditions which make containerless processing feasible, diminish substantially the buoyant forces which would normally act to eliminate many of the bubbles. Also diminished is buoyant convection which would influence the motion of drops and bubbles and would also aid in the mixing process.

Subramanian and Cole [VI-1, VI-2] have proposed alternate means such as thermocapillarity, rotation, oscillation, expansion/contraction, etc., for the elimination and/or management of bubbles in an orbital environment. Papers describing the ground-based studies supporting these experiments have recently appeared in the literature [VI-3, VI-7]. The latter two papers [VI-6, VI-7] deal with bubble and drop motion in rotating liquid fields and provide the background and motivation for the preliminary flight experiments reported here. These flight experiments represent a second phase in ongoing investigations and have been initiated to further aid in the design and interpretation of our Shuttle experiments.

Test Apparatus and Procedure

Rotating, liquid-filled glass sphere. For these preliminary experiments a very simple hand-held device has been developed for observing bubble and drop trajectories in a rotating field. The device consists of an 8 x 10 cm "Plexiglas" base on which is mounted a 1.5 V AAA alkaline battery, a small dc motor, a switch, and a potentiometer for varying the speed of the motor. Cemented to the motor shaft is a 2 cm diameter hollow glass sphere filled with the appropriate liquid.

For the first experiments, the hollow glass sphere was filled with a Dow-Corning DC-200 silicone oil having a nominal viscosity of 12.5 Pa·s (12,500 times as viscous as water). The small air space left in the hollow sphere formed a bubble which upon rotation of the sphere had a diameter on the order of 6 mm. The procedure was simply to turn the switch on when near-free-fall conditions prevailed and to observe the trajectory of the bubble in the rotating, silicone oil-filled glass sphere. Real time motion pictures were taken of the rotating system by NASA photographers. Between parabolas the potentiometer setting was changed to allow the effect of different rotation rates to be observed.

The second set of experiments were somewhat more involved in that the glass sphere was filled with water and silicone oil. As the two liquids are immiscible, with silicone oil being slightly less dense ($\sim 920 \text{ kg.m}^{-3}$), a layered structure forms under normal gravity conditions with the silicone oil on top. As before, a bubble results from the small air space left in the sphere. The procedure was the same as for the first experiments; the sphere was caused to rotate when near-free-fall conditions prevailed and the trajectories of the silicone oil drop and air bubble were observed. In this second set of experiments, the water was the continuous phase. Again, the sphere rotation rate was varied from parabola to parabola.

A third set of experiments utilized a semi-transparent plastic sphere which was filled with silicone oil and a slight amount of water. The latter formed a more dense drop which was colored purple for increased visibility. The behavior of the drop during rotation of the sphere was observed in the aircraft both during free-fall conditions and in level flight.

JPL, 3-axis acoustic levitator. A 3-axis acoustic positioning module, described elsewhere in this combined report, was kindly made available to us by the Jet Propulsion Laboratory to conduct preliminary experiments on the migration of small bubbles in rotating liquid drops. The system has the capability of injecting liquid drops into a chamber, positioning them with a 3-axis acoustic field, and acoustically inducing rotation.

The experimental procedure was (upon attaining near-free-fall conditions) to introduce a water drop of 1- to 2-cm diameter into the chamber by means of two diametrically opposite stings. Simultaneously, a few (one to five) small bubbles were introduced into the drop by prior entrapment in the liquid line leading to one of the stings. The stings were retracted and the drop captured in the acoustic well created by the three orthogonal acoustic drivers and reflectors. After a waiting period of several seconds (for disturbances to decay), drop rotation was induced. The run was usually terminated by the drop escaping from the acoustic well and splashing against the wall as free-fall conditions were lost. Two orthogonal views of the drop and the resulting bubble motion were recorded on motion picture film throughout the duration of the experiment.

Results and Discussion

1. Rotating, liquid-filled glass sphere. Prior ground-based experiments [6] have established that in a 1-g environment, rotation will cause a bubble to migrate inwards toward the axis of rotation under the influence of inertial, pressure, viscous, and gravitational forces. Theory [VI-8] predicts the asymptotic scaled radial position of the bubble to be proportional to the dimensionless group $ag/\nu\Omega$. Here, "a" is the bubble radius, "g" the gravitational acceleration, " ν " the kinematic viscosity, and Ω

the rate of rotation. Hence it was anticipated that under free-fall conditions, the asymptotic radial position would be the axis of rotation. It was further anticipated that for spin-up times much less than the bubble migration time, the bubble trajectory would always lie in a plane normal to the rotation axis, independent of its initial position.

As far as could be determined both from visual observations of the bubble motion during the experiments, and from the film record, the final position of the bubble was along the axis of rotation. Although the bubble appeared to be spherical during the migration path to the rotation axis, once it reached that axis it would elongate to some equilibrium shape which for a given fluid was dependent upon the rotation rate of the sphere. The greater the sphere rotation rate, the greater the bubble elongation. Rosenthal [VI-9] and Princen [VI-10] among others have developed equations for the equilibrium shape of bubbles under just such conditions. Deliberate reorientation of the rotation axis relative to the aircraft during the free-fall period produced no discernable movement of the bubble from its position on the rotation axis. In a 1-g environment the bubble would move upwards along the axis due to buoyancy.

It was also desired to vary the initial position of the bubble (to some position at the sphere wall other than in the equatorial plane of the sphere), by changing the angle of inclination of the sphere axis relative to the gravity vector just before entering the free-fall environment. However due to the handheld nature of the experiment, the difficulty in maintaining a stable position during the entry into free fall, and the camera being held by a NASA photographer undergoing similar difficulties, no definitive statement can be made about the nature of the migration path except that it was towards the rotation axis.

Observed migration times were somewhat shorter than had been anticipated. From [6], a simplified analysis yields the following expression for the time of migration (the time required for the bubble to be within 1 radius of the sphere axis) in the absence of gravity.

$$t_m = \frac{3\nu}{a^2\omega} \ln \frac{R}{a} \quad (\text{VI-1})$$

where ν is the kinematic viscosity, a the bubble radius, R the sphere radius, and ω the sphere rotation rate. For the conditions of these experiments (assuming $\omega = 20\pi \text{ rad}\cdot\text{s}^{-1}$), equation (VI-1) predicts a migration time of 4 sec. Typical observed migration times were on the order of 2 to 3 sec.

The second set of experiments more closely simulated our proposed shuttle experiments [VI-1, VI-2] in that the bubble migrates within a rotating unconstrained liquid drop. It differs from the shuttle experiments in that the drop is contained in a more dense medium (water) rather than a less dense medium (gas). Prior to the start of the experiment the less dense silicone oil ($\mu = 1 \text{ Pa}\cdot\text{s}$, $\rho = 920 \text{ kg}\cdot\text{m}^{-3}$) and the air bubble were at the top of the water-filled sphere. Upon rotation of the sphere, the silicone oil detached from the sphere wall and formed a spherical drop which proceeded to migrate toward the axis of rotation. The bubble was retained within the silicone oil drop, at the silicone oil-water interface. While the drop migrated toward the axis of rotation, neither the drop nor the bubble appeared to rotate. When the drop reached the rotation axis of the sphere, it began to rotate and the bubble detached from

the interface and began to migrate within the rotating drop toward the rotation axis. In a time interval of only a few seconds, the bubble appeared to be centered within the silicone oil drop, which was itself centered within the water-filled sphere.

The third set of experiments were designed to obtain information on the behavior of a liquid drop in an immiscible, less dense liquid medium. The drop was colored water and the less dense medium was silicone oil ($\mu = 1 \text{ Pa}\cdot\text{s}$). Previous ground-based investigations [VI-7] had revealed the rather surprising result that under certain conditions, the more dense phase (drop) may migrate inwards toward the rotation axis. With the aircraft in normal flight, the sphere was caused to rotate and the behavior of the colored drop observed. There was no doubt that the drop initially migrated inwards towards the rotation axis, stayed there momentarily and then behaved as expected; migrating outwards to the sphere wall. The behavior of the drop under free-fall conditions was not quite as clear. The experiment was repeated many times by many persons. It was the consensus of opinion that the drop did not leave the wall. Thus, it appears that the inward migration of the more dense drop is due in part at least to the existence of a gravitational field. In confirmation of this, the experiment was conducted a number of times during the 2-g pullout of the aircraft. The drop was found to migrate closer to the rotation axis than in 1-g, and to stay at this location longer before migrating back to the wall.

2. JPL, 3-axis acoustic levitator. The experiments with the JPL 3-axis acoustic positioning module were all preliminary in nature. Bubbles usually appeared within the levitated drop as a result of entrainment, but the number and size were random. Further, JPL scientists were in the process of determining optimum procedures for best producing controlled rotation. However several drops containing only a few small bubbles were levitated and rotated. Those runs should provide useful preliminary information when analyzed.

Conclusions

Preliminary experiments concerned with the behavior of small bubbles or drops in rotating liquid fields under free-fall conditions have yielded qualitative information on trajectories and migration times. Of most interest are the observations that the bubble migration time appears to be shorter than had been anticipated from ground based studies, and that the unusual behavior of more dense liquid drops reported in [VI-7] is apparently a gravity induced phenomenon.

Acknowledgement

This work was supported by the Materials Processing in Space Program Office of the National Aeronautics and Space Administration through a contract (NAS8-32944) from the Marshall Space Flight Center to Clarkson College of Technology. We are grateful to Dr. Taylor Wang for making the JPL 3-axis acoustic positioning module available for our experiments and to Dr. D. Elleman and Mr. A. Croonquist for their kind cooperation. We are also grateful to the Dow-Corning Corporation for providing us with free samples of the DC-200 series silicone oils used in the sphere rotation experiments.

References

- VI- 1. P. Annamalai, N. Shankar, R. Cole, and R. S. Subramanian: Bubble Migration Inside a Liquid Drop in a Space Laboratory. *Appl. Sci. Res.*, Vol. 38, pp. 179-186, 1982.
- VI- 2. R. S. Subramanian and R. Cole: Experiment Requirement and Implementation Plan (ERIP) for "Physical Phenomena in Containerless Glass Processing." Experiment MPS 77F010, NASA Marshall Space Flight Center, Document 77FR010, August 1979.
- VI- 3. N. Shankar, R. Cole, and R. S. Subramanian: Thermocapillary Migration of a Fluid Droplet Inside a Drop in a Space Laboratory. *Int. J. Multiphase Flow*, Vol. 7, pp. 581-594, 1981.
- VI- 4. K. Jayaraj, R. Cole, and R. S. Subramanian: Combined Thermocapillary and Buoyant Flow in a Drop in a Space Laboratory. *J. Colloid Interface Sci.*, Vol. 85, pp. 66-77, 1982.
- VI- 5. R. B. Jucha, D. Powers, T. McNeil, R. S. Subramanian, and R. Cole: Bubble Rise in Glassmelts. *J. Am. Cer. Soc.*, Vol. 45, pp. 289-292, 1982.
- VI- 6. P. Annamalai, R. S. Subramanian, and R. Cole: Bubble Migration in a Rotating, Liquid-Filled Sphere. *Phys. Fluids*, Vol. 25, pp. 1121-1126, 1982.
- VI- 7. P. Annamalai and R. Cole: Drop Motion in a Rotating Immiscible Liquid Body. XXIV COSPAR Conference, Ottawa, Canada, May 1982.
- VI- 8. P. Annamalai, R. S. Subramanian, and R. Cole: Bubble Motion in a Rotating Liquid Body, in *Materials Processing in the Reduced Gravity Environment of Space*. Ed. by Guy E. Rindone, Proc. Materials Res. Soc. Meeting, Boston, November 1981, Elsevier, New York, 1982.
- VI- 9. D. K. Rosenthal: The Shape and Stability of a Bubble at the Axis of a Rotating Liquid. *J. Fluid Mech.*, Vol. 12, pp. 358-366, 1962.
- VI-10. H. M. Princen, I.Y.Z. Zia, and S. G. Mason: Measurement of Interfacial Tension from the Shape of a Rotating Drop. *J. Colloid Interface Sci.*, Vol. 23, pp. 99-107, 1967.

VII. THERMAL WAVE EXPERIMENT COMPARISONS OF MEASUREMENTS AND MODEL PREDICTIONS

By D. Bowdle, B. J. Anderson, and V. Keller

Introduction

This study is designed to evaluate a low-gravity cloud chamber, coupled with a cloud microphysics model, as a tool for verifying the fundamental theory of droplet growth and evaporation. For this study, a controlled thermal wave is generated in a cloud of water droplets in low gravity. The droplets grow and evaporate in response to the thermal forcing. Photographic records of the cloud development and dissipation are compared to predictions from a detailed numerical model of the cloud microphysical processes. Model parameters are adjusted to reduce the mismatch between measurements and model predictions. Results to date show qualitative agreement between experiment and theory.

Research Method

Updated or otherwise pertinent details of the equipment design and other aspects of the thermal wave experiment are given below. Additional information about supporting equipment, chamber design, and results of a proof-of-concept thermal wave experiment may be found in Anderson, et al. (1982).

Instrumentation

The primary element of the thermal wave equipment is the experiment chamber, a 5.1 cm diameter cavity in the side of a large solid aluminum cylinder. Spatial and temporal uniformity of the chamber wall temperature is maintained by the high thermal conductivity and the large thermal inertia of the chamber block. The chamber air is initially held at water saturation at the temperature of the wall by a water-soaked lining of charcoal-impregnated filter paper. The thermal wave is generated by a 3 cm x 3 cm thermoelectric module (TEM), which is mounted on the side of the cylindrical cavity near the center of the chamber. The rear surface of the TEM is in good thermal contact with the chamber body. The front surface of the TEM can be operated with a wick (a 3 cm x 3 cm piece of moistened lens paper), in the wet mode; or without a wick, in the dry mode.

The experimental droplet cloud is illuminated by an off-axis beam and photographed at 30 deg forward scattering angle by a motor-driven 35 mm Nikon camera, at 1/3 magnification, with a framing rate of approximately 1/sec. The chamber wall temperature is measured by an embedded thermistor. The TEM temperature is measured by a fine thermocouple on a corner of the TEM surface. Chamber air pressure and local acceleration are also measured. Analog signals from the sensors and timing pulses from the cameras are recorded on two multichannel strip chart recorders.

Experimental Procedure

Several minutes before entering a low-gravity parabola, the test chamber is flushed and filled with aerosol-laden air, and then sealed. The time delay assures

temperature and water vapor equilibration and also stilling of residual air motions. After low gravity conditions (usually ± 0.02 G) are attained, the camera is turned on and for about 25-30 sec the TEM is externally driven through several sinusoidal cooling/heating cycles centered on the dew point temperature of the sample air. As the thermal wave propagates outward from the TEM surface, water droplets nucleated from the test aerosols alternately grow and evaporate. Photographic records of the droplet cloud clearly show cloud density and cloud/clear-air interfaces (Anderson, et al., 1982).

Several experimental parameters can be independently varied from one run to the next: namely, the period, amplitude, and phase of the thermal wave (usually about 10 sec, 10°C peak-to-peak, and initial cooling); the nature of the test aerosol particles (usually $0.234\text{ }\mu\text{m}$ diameter polystyrene latex spheres, or equivalent, with a laboratory-determined critical supersaturation of about 1%); and the freshness of the sample air in the chamber (usually refilled before each run). Somewhat less control is available for other parameters, namely the TEM surface condition (which can be changed between dry-mode and wet-mode from one day's flight series to the next), the chamber block temperature (which decreases by about 1°C/hr due to aircraft cabin cooling during a two-hour flight), and the chamber pressure (which is initially fixed by cabin pressure during pressure equalization of the chamber just before a run). Pressure variations during a run, which arise from air temperature changes driven by the TEM and from imperfections in the chamber seals, are accounted for by the model treatment (see following section).

Data Analysis

Measurements of TEM and chamber body temperatures and air pressure from suitable runs are used as boundary value inputs to a detailed numerical model of the thermal wave experiment. This model, which is part of NASA's Atmospheric Cloud Physics Laboratory Numerical Simulator, treats the growth and evaporation of solution droplets, the diffusion of heat and water vapor, and bulk air motions induced by temperature or gas concentration gradients, in a one-dimensional grid. Forcing options include externally driven pressure changes and/or wall effects. Model outputs of droplet size and cloud position at selected times are compared with micro-densitometric measurements of cloud density and position from the corresponding photographic negatives.

Adjustable model parameters are varied to reduce mismatches between model predictions and experimental measurements. Adjustable parameters include the number concentration and critical supersaturation of the test nuclei, the thermal and mass accommodation coefficients for condensation/evaporation, and the water vapor boundary condition at the TEM surface.

Low-Gravity Flight Series

The thermal wave experiment has been flown on four series of low-gravity flights on the NASA KC-135 aircraft. The initial flight series (September 1980) yielded a successful proof-of-concept experiment. The second and third flight series (April and May 1981), which used an upgraded aerosol supply system, yielded several cloud formation events which were suitable for detailed analysis. The fourth flight series (July 1982) used a wet-mode TEM surface, where all previous flights had used dry-mode conditions. Dramatic differences in the experimental cloud development were observed between the wet-mode and the dry-mode runs.

Results From Dry-Mode Runs

Initial simulations of the 1981 dry-mode runs did not agree well with experimental measurements. Simulations using a dry TEM surface predicted denser clouds, which propagated further from the TEM, reached peak intensity later, and dissipated more slowly, than the measured clouds. However, the dry-TEM simulations did approximately predict both cloud onset and the gross features of the space-time envelopes of the measured clouds (Fig. VII-1). On the other hand, simulations using a fully-wetted TEM surface did not resemble the observed clouds at all (Fig. VII-2). Later model runs, which simulated a partially-wetted TEM surface, greatly improved the agreement with the measurements (Fig. VII-3), except that the model clouds still did not dissipate as rapidly as the experimental clouds during heating cycles.

The partial-wetting effect was simulated by a numerical artifice which we termed the "drop-loading" method. A population of "dummy" nuclei was introduced into the grid cell which simulated the TEM surface. By appropriately matching the concentration and the critical supersaturation of the dummy nuclei, it was possible to simulate a wide range of water vapor boundary conditions, such as: fully wetted, partially wetted, or effectively dry at all times; and fully or partially wetted during cooling cycles but effectively dry during heating cycles. For very high nucleus concentrations and/or very large droplets, this method led to some numerical problems which were overcome by standard techniques.

The results of these studies have shown that a range of drop-loading parameters can be chosen for each run which optimizes the agreement between predicted and measured clouds. However, the development of the model clouds is much more sensitive to the values of these dummy parameters than to the other adjustable parameters, such as the mass accommodation coefficient (β). Since the retrieval of an experimental value for β is an important goal for the study, the uncertainty in the TEM surface condition presented a serious problem. For this reason, the 1982 flight series used fully wetted walls so that the water vapor boundary conditions on the TEM surface could be known a priori.

Results From Wet-Mode Runs

Initial comparisons of model predictions (Fig. VII-4) with experimental results for the 1982 wet-mode runs showed good qualitative agreement. Droplet clouds formed during heating cycles and partially dissipated during cooling cycles. Model and experimental clouds grew at comparable rates, and both sets of clouds developed their peak densities a few mm from the TEM surface. However, the model clouds did not dissipate as rapidly as the experimental clouds during cooling cycles.

Conclusions

The work to date has demonstrated the feasibility of the thermal wave technique for studying the growth and development of droplet clouds in low-gravity. Suitable data sets have been obtained for a number of experimental conditions, including wet-mode and dry-mode TEM surfaces, and initial heating/initial cooling cycles on the thermal wave forcing function. The thermal wave numerical model has been debugged, and is capable of qualitatively simulating most of the important cloud features observed in the test chamber for the full range of boundary conditions that have been investigated. However, the model clouds still dissipate more slowly than the observed clouds, both for dry-mode and wet-mode cases. Efforts are con-

tinuing to resolve this discrepancy by concentrating on the analysis of diffuse clouds formed during small amplitude thermal waves.

Planned Work

Upcoming improvements in the analysis techniques include fine tuning and condensing the numerical model and streamlining the data transfer from the experimental hardware to the host computer. This latter improvement will be facilitated by upgrading of the data acquisition pallet. The upgraded equipment will be flown late in FY-83.

Acknowledgments

The dedicated efforts of Robert Shurney (MSFC), Robert Williams and Lawrence Magers (JSC), and the pilots and crew of the KC-135 contributed immensely to this investigation.

References

Anderson, B. J., V. Keller, and D. Bowdle: Thermal Wave Experiment. The Marshall Space Flight Center KC-135 Zero Gravity Test Program for FY1981. R. E. Shurney (Ed.) NASA TM 82476. George C. Marshall Space Flight Center, Alabama, pp. 41-45, 1982.

TABLE VII-1. EXPERIMENTAL AND MODEL THERMAL WAVE STUDY PARAMETERS.

1A. EXPERIMENTAL PARAMETERS									
SEE TEXT FIGURE =	RUN =	DATE	TEM MODE	INITIAL CONDITIONS		THERMAL WAVE PARAMETERS			EXPANSION RATE (mb/sec)
				TEMPERATURE (°C)	PRESSURE (MB)	AMPLITUDE (°C)	PERIOD (SEC)	PHASE	
1	5	8 APRIL '81	NO WICK	17.65	680.70	5.65	10	INITIAL COOLING	-0.300
2	5	8 APRIL '81	NO WICK	17.65	680.70	5.65	10	INITIAL COOLING	-0.300
3	5	8 APRIL '81	NO WICK	17.65	680.70	5.65	10	INITIAL COOLING	-0.300
4	3	22 JULY '82	WET WICK	25.04	750.93	4.75	10	INITIAL HEATING	-0.106

2B. MODEL PARAMETERS										
SEE TEXT FIGURE =	RUN =	DATE	TEST AEROSOL		TEM DUMMY AEROSOL		CHAMBER WALL DUMMY AEROSOL		ACCOMODATION COEFFICIENT	
			CONCEN- TRATION (cm ⁻³)	ACTIVATION SUPER (%)	CONCEN- TRATION (cm ⁻³)	ACTIVATION SUPER (%)	CONCEN- TRATION (cm ⁻³)	ACTIVATION SUPER (%)	THERMAL	MASS
1	5	8 APRIL '81	1000	0.186	0	-	0	-	1.000	0.034
2	5	8 APRIL '81	1000	0.186	FULLY WETTED		FULLY WETTED		1.000	0.034
3	5	8 APRIL '81	1000	0.186	10 ⁵	5	2 x 10 ⁵	0.02	1.000	0.034
4	3	22 JULY '82	1000	0.186	FULLY WETTED		FULLY WETTED		1.000	0.034

ORIGINAL PAGE IS
OF POOR QUALITY

ORIGINAL PAGE 19
OF POOR QUALITY

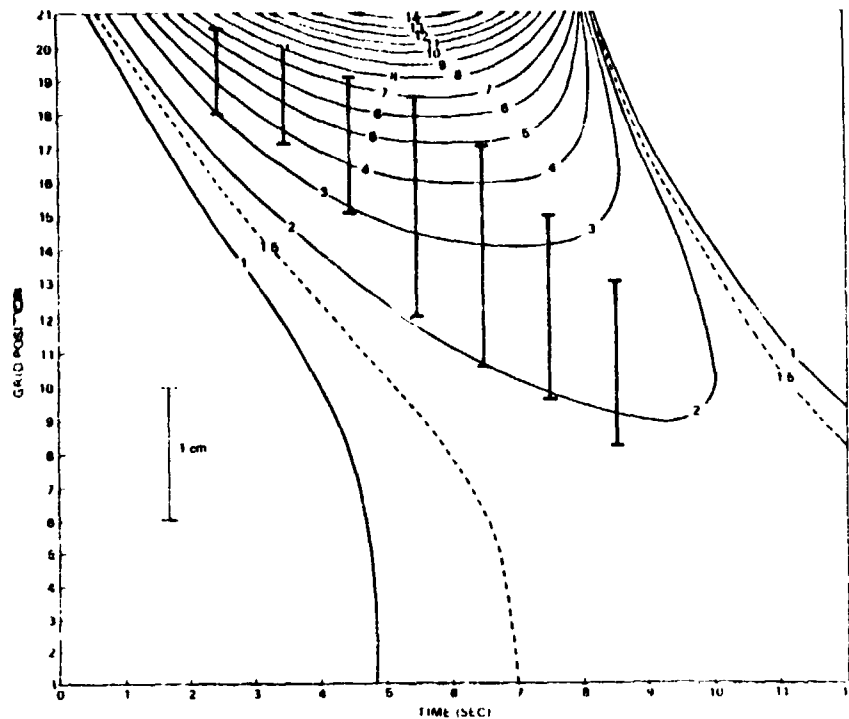


Figure VII-1. Comparison of experimental measurements and dry-mode model predictions of cloud development in space and time during a dry-mode low-gravity thermal wave experiment on the NASA KC-135 aircraft. Experimental positions of the cloud are shown by heavy solid bars, model predictions are shown by contours of drop radius. Spatial scale is shown by light solid bar. Experimental and simulation parameters are shown in Table VII-1.

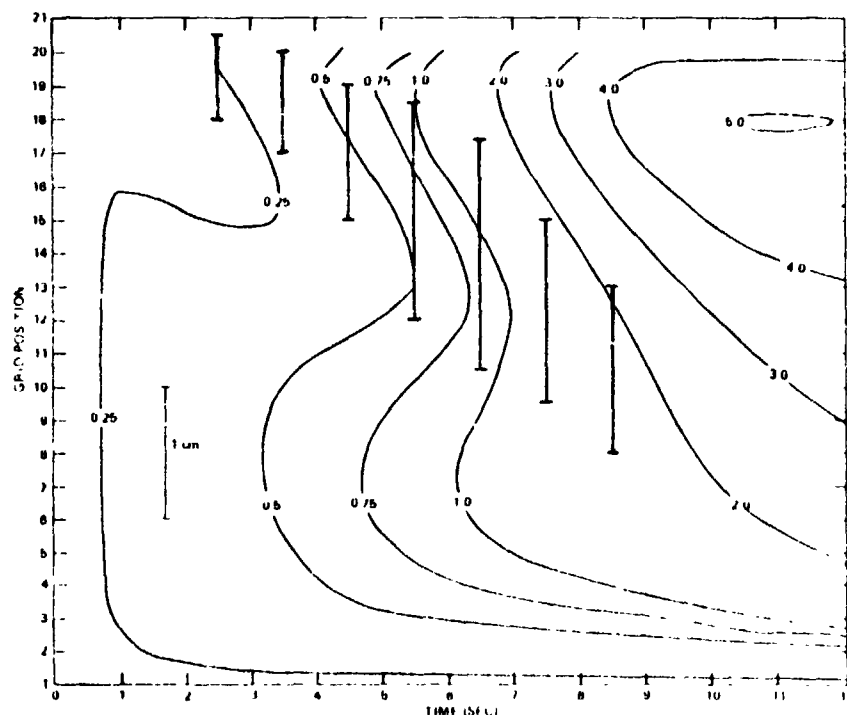
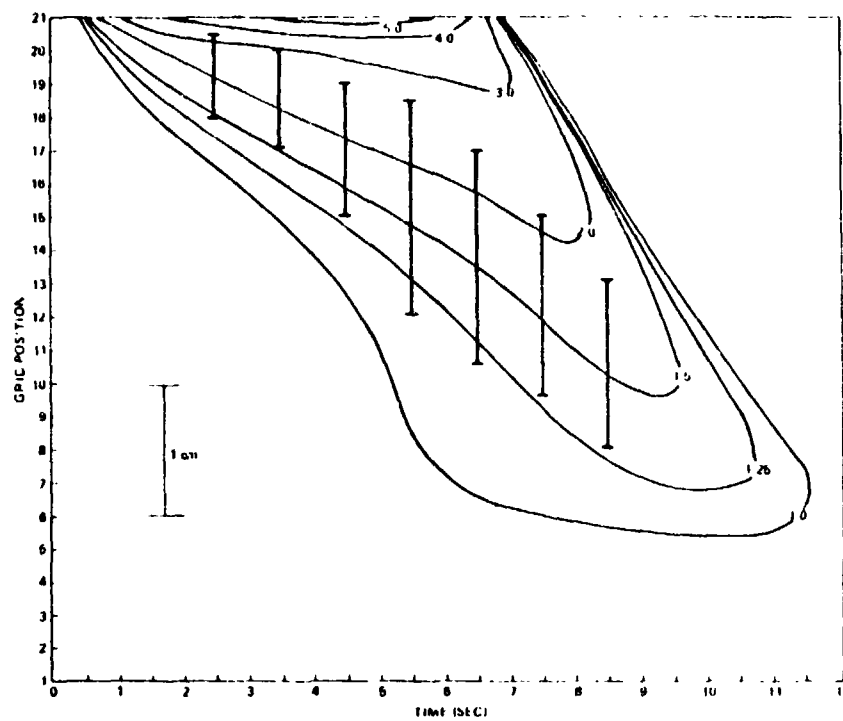


Figure VII-2. As in Fig. VII-1 except that wet-mode model predictions are shown.



ORIGINAL PAGE 78
OF POOR QUALITY

Figure VII-3. As in Fig. VII-1 except that partial-wetting model predications are shown.

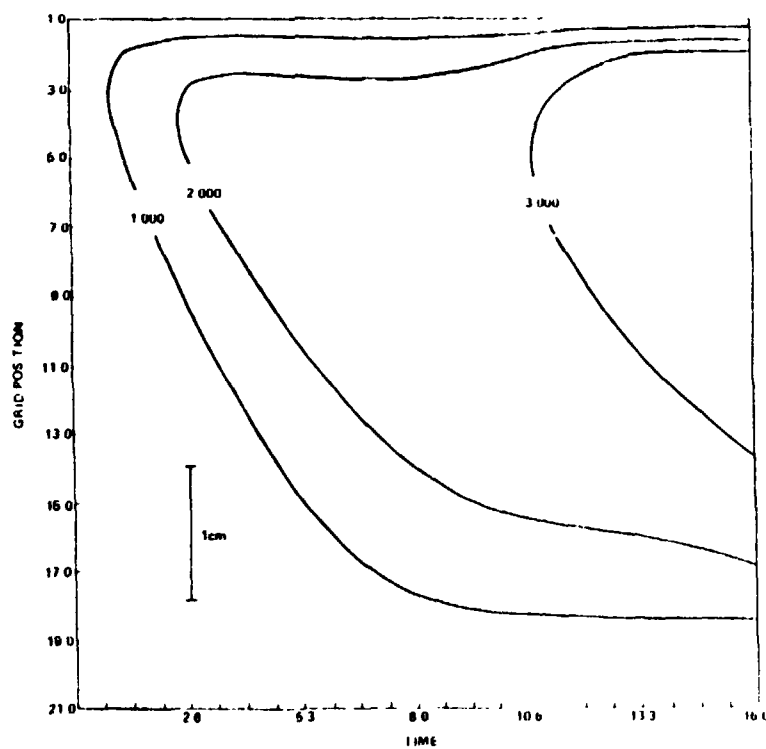


Figure VII-4. As in Fig. VII-1 except that wet-mode predictions are shown for a wet-mode experiment.

VIII. SCIENCE REPORT ON THE DIRECTIONAL SOLIDIFICATION OF HYPEREUTECTIC CAST IRON DURING KC-135 LOW-G MANEUVERS

By P. A. Curreri, D. M. Stefanescu, and J. C. Hendrix

Introduction

Alloys solidified in a low-gravity environment can, due to the elimination of sedimentation and convection, form unique and often desirable microstructures [VIII-1-VIII-4]. One method of studying the effects of low-gravity on alloy solidification has been the use of the KC-135 aircraft flying repetitive low-g maneuvers. Each maneuver gives from 20 to 30 sec of low-g which is between about 0.1 and 0.001 gravities. The frequency of KC-135 flights can provide an opportunity for a much faster learning curve than is available at the present time from either sounding rocket or orbital experiments. For experiments that require more low-g time than afforded by the droptube or droptower facilities [VIII-2-VIII-5] and which are precursorary to orbital processing experiments, the KC-135 provides a valuable research environment in which the experimenter can interact with his experiment in real time.

Previous alloy solidification experiments on the KC-135 have attempted to quench ingots of molten metal within the time span of a single low-g parabola [VIII-6-VIII-8]. Directional solidification, however, has many important advantages over the quenched ingot methods for alloy solidification experiments, especially in the KC-135. In directional solidification, the solidification interface can be slowly advanced through a rod of the sample. Controlled solidification can continue through a number of aircraft parabolas. The known solidification rate of the sample can then be correlated with accelerometer data to determine the gravity level during solidification for any location on the sample. The thermal gradient and solidification rate can be controlled independently; whereas, for the quench ingot method the complexity of the three dimensional cooling problem makes their control very difficult. Consequently, by directional solidification we can obtain fundamental scientific information not obtainable by the ingot quench techniques. Directional solidification also greatly mitigates the need to obtain one-g control samples - solidified under conditions that precisely match the flight conditions - in order to detect a gravitational effect. Directional solidification can also remove constraints on the sample cooling rates, since in directional solidification it is not necessary to completely solidify the sample in a single low-g parabola. In a collaborative effort with Dr. Mary H. Johnston, we therefore modified a G. E. built ADSS-P directional solidification furnace to make it compatible for use on the KC-135.

Cast iron has been identified [VIII-9] as a candidate material of possible value in the study of the effects of sedimentation and convection on alloy solidification. NASA is presently involved in research efforts studying low-g solidification of cast iron for its scientific value [VIII-10] and also to obtain data of possible significance to commercial casting processes [VIII-11]. Off eutectic compositions of cast iron may be especially interesting for study in low-g. For example in hypereutectic cast iron melts, a lighter graphite phase is present in a heavier melt. Sedimentation effects are likely to be significant during the solidification process [VIII-9, VIII-12].

The directional solidification furnace was first integrated in the KC-135 during the September 82 series of flights. The two objectives were: first, to flight test the furnace system, and second, to study any low-g effects on the solidification of hypereutectic cast iron and of a superalloy composition. This report deals with the results of the solidification of the hypereutectic cast iron sample.

Procedures

A G. E. prototype ADSS furnace [VIII-13] was modified for use in the KC-135 (Fig. VIII-1) primarily by adding a portable quench block water circulation system. The system consists of a 10 liter reservoir, an expansion tank, and a peristaltic pump (Fig. VIII-2). On top of the quench block in the furnace canister is an 11 cm long furnace element consisting of platinum rhodium wire double wound around an alumina core. The sample is placed in a 1/2 cm ID, approximately 40 cm long, alumina crucible. The furnace is then translated, using a motor and gearing system, and thus the sample is gradually solidified. Figure VIII-3 shows the quench block temperature versus time with the closed cooling system and a maximum furnace temperature of 1500°C. The change in quench block temperature of approximately 25°C will have an insignificant effect on the thermal gradient in the sample. A thermal profile of an empty crucible, measured with the maximum furnace temperature of approximately 1500°C, is given in Figure VIII-4. By varying the maximum or plateau temperature in the furnace cavity we can obtain various thermal gradients. Figure VIII-5 shows the thermal gradients in an empty crucible obtained for various maximum furnace temperatures. The hypereutectic iron sample solidified during the flight was prepared by adding excess carbon to a commercial cast iron composition. The compositional analysis after alloying is given in Table VIII-1.

To facilitate the analysis of any low-g effects, it is desirable to have at least 1/2 mm of solidification during the approximately 20 sec of low-g in each parabola. The commercial iron composition used could be solidified at 2 mm/min and still obtain grey iron, avoiding the metastable white phase, by employing a thermal gradient of approximately 400°C per cm. Figure VIII-6 shows the graphite microstructure at 1 and 2 mm/min translation rates.

The procedure followed during the flight experiment was as follows. The furnace temperature was brought up to 1500°C within a period of about 20 min. The furnace was then translated vertically upwards at a rate of 1.2 mm/min for 13 min during which time 10 low-g parabolas were flown. The furnace was then shut off and the translation stopped.

The directionally solidified sample was sectioned longitudinally. One half was reserved for compositional analysis while the second half was polished for photometallography. For comparison a control sample was run in the lab simulating the thermal and temporal environment experienced by the flight sample.

Results

1. Furnace Operation

The furnace operated nominally during the flight experiment except for two problems. The first was that the translation motor RPM during the flight tended to drift by a maximum of about 10 percent. This required frequent adjustment by the operator on board the airplane (Fig. VIII-7). It is not known whether the RPM fluctuation was caused by the change in gravity level or by input power fluctuations. Since the flight, however, an electronic servo motor controller, employing a photo-sensitive tachometer, has been added to the furnace system to eliminate this difficulty. Figure VIII-8 shows the motor control system prior to installation in the flight furnace. Tests of the system have shown it to be able to compensate for up to a 20 percent power fluctuation to the motor with a response time of about one second. The second difficulty was due to the limited supply of 110 V 60 cycle power on the air-

plane. Consequently, the furnace was only run at temperature for 15 min rather than the 30 min planned. This limitation could preclude running more than one sample per flight and thus could seriously limit the productivity of the system. The installation of an additional aircraft power inverter is planned which would make available unused aircraft power for 110 V 60 cycle systems.

2. Experimental Results

Figure VIII-9 shows a low magnification composite photomicrograph of the flight sample and of a ground based control sample. Also given are the position of the primary melt interface and a scale corresponding to the distance on the sample from that interface. A second scale (assuming that the solidification interface advanced at the same speed as the furnace) corresponds to the parabola number and the gravity environment for the flight sample. The position for both samples at which translation was stopped is also indicated.

One anomaly in the control sample is the porosity at about 2 mm from the primary melt interface. It was caused by the molten metal running down the side of the sample in the crucible. It precludes any comparison with the flight sample in the porous region and could also have effected the solidification of the rest of the control sample. Work is continuing to obtain a control sample that more accurately reflects the thermal conditions encountered by the flight sample.

Figure VIII-10 shows a higher magnification photomicrograph of the two samples between the primary melt interface, and the porosity in the control sample and to about the beginning of the second low-g parabola in the flight sample. Fine, apparently eutectic graphite, as well as, irregular shaped graphite is evident.

Corresponding to the width and position of the second and fourth low-g parabolas in the flight sample, there is a pronounced increase, relative to the surrounding regions, of coarser graphite flakes. A 200 Xs photomicrograph of this structure is shown in Figure VIII-11. The higher magnification reveals finer graphite flakes that exist between coarser flakes.

The microstructure between approximately 2 mm and 8 mm from the primary melt interface in the control sample remains relatively constant (Fig. VIII-12). The graphite is roughly equivalent to the fine graphite that is present in the flight sample from about 3 to 8 mm from the melt interface.

From about 8 mm to about 13 mm both samples contain a mixture of both fine and coarse graphite flakes. A typical microstructure for each sample is shown in Figure VIII-13.

In the flight sample at about 13 mm from the primary melt interface there occurs a more randomly orientated system of very large flakes in a matrix of finer flakes of graphite. This continues through the rest of the sample. In the control sample a similar microstructure is obtained but more gradually.

Discussion

A promotion of coarser graphite during solidification in low-g, relative to that in high-g, is suggested by the microstructure of that part of the flight sample that was solidified between the first and fifth parabolas. Coarsening of the graphite during low-g solidification could be explained by either of the following hypotheses:

A) Lack of convection lessens the tendency for the graphite leading the solidification front to break up.

B) Lack of flotation allows primary graphite to be incorporated into the solidification front.

The observation that microstructure in the low-g "bands" contains a matrix of fine - probably eutectic - graphite along with the coarse flakes (Fig. VIII-11) tends to favor hypothesis B.

The morphology (Fig. VIII-10) of the irregular graphite between the primary melt interface and approximately 2 mm from it is similar to the graphite in the unmelted portion of the sample prior to the melt interface. This indicates the graphite up to that point did not completely dissolve in the melt; the reason can be seen in Figure VIII-4. The thermal profile of the furnace is such that the temperature rise from the melt interface to the furnace maximum temperature occurs over approximately a centimeter of sample. Thus, it was probably not hot enough near the primary melt interface to completely dissolve all the graphite that was present. This problem could be remedied by translating the furnace approximately 1 cm before beginning directional solidification at the desired rate.

The gradual increase with distance from the primary melt interface in the amount of coarser graphite in both samples can be explained by either the rejection of sulphur [VIII-14] or of primary graphite at the solidification interface. The observation that the fine graphite remains about the same size throughout supports the latter hypothesis. The increasing concentration of primary graphite with distance from the primary melt interface could also explain why coarse bands would only be observed in the initial parabolas, since after the primary graphite concentration increases to the level where the flakes intersect flotation is no longer significant. Chemical analysis of the flight sample is planned to determine the compositional profiles of carbon and sulphur.

The microstructure in the samples from about 13 mm from the primary melt interface through the rest of the samples remains approximately the same, and it is essentially the microstructure that occurred from the slow cooling of the sample after the translation was stopped and the furnace was turned off. It should be noticed that this interface (in the flight sample) occurs at about 13.5 mm from the primary melt interface even though the furnace translation had been stopped about 2 mm later - after the tenth parabola. This indicates that 2 mm of sample melted back after the furnace was turned off.

Conclusions

1) The microstructure of the flight sample suggests that low-g promotes the incorporation of large graphite flakes into the solidification front. However, further flight and ground experiments and more detailed analysis are needed to determine with a reasonable certainty that this is a gravity induced effect and not an artifact of the experiment.

2) The conversion of additional aircraft power to 110 V 60 cycle is needed to fully support this series of experiments.

3) Directional solidification can greatly enhance the information obtained from alloy solidification experiments on board the KC-135. The method promises to be a valuable tool for the study of low-g effects on alloy solidification.

Acknowledgments

We would like to acknowledge the contributions and support to this project of the following personnel: Billy R. Aldrich, Wendy S. Alter, Mary H. Johnston, William F. Kaukler, Robert J. Naumann, Carrol Persel, Robert E. Shurney, John M. Theiss, and John R. Williams (all of MSFC); and the personnel of JSC who operate the KC-135.

References

- VIII- 1. Witt, A. F., Gatos, H. C., Lichtensteiger, M., Lavine, M. C., and Herman, C. J.: Crystal Growth and Steady-State Segregation Under Zero Gravity: In Sb. J. Electrochem. Soc.: Solid State Science and Technology, pp. 276-283, 1975.
- VIII- 2. Lacy, L. L. and Otto, G. H.: The Electrical Properties of Zero Gravity Processed Immiscibles. AIAA Paper 74-208, Washington, D.C., January 30 - February 1, 1974.
- VIII- 3. Larson, D. J.: The Zero-G Processing of Magnets, ASTP Experiment MA-070 Preliminary Science Report. Johnson Space Center, NASA Report No. TXM-58173, February 1976.
- VIII- 4. Wouch, G. Frost, R. T., Pinto, N. P., Kieth, G. H., and Lord, Jr., A. E.: Uniform Dispersion of BeO Particles in Be Casting Produced in Rocket Free Fall. Nature, Vol. 274, pp. 235-237, 1978.
- VIII- 5. Lacy, L. L., Robinson, M. B., and Rathz, T. J.: Containerless Undercooling and Solidification in Drop Tubes. J. Cry. Growth, Vol. 51, pp. 47-60, 1981.
- VIII- 6. Alter, W. S., unpublished results.
- VIII- 7. Johnston, M. H. and Parr, R. A.: Low Gravity Solidification structures in the Tin - 15 Wt % Lead and Tin - 3 Wt % Bismuth Alloys. Materials Processing in the Reduced Gravity Environment of Space, Ed. G. E. Rindone, Elsevier Science Publishing Company, Inc., New York, pp. 303-346, 1982.
- VIII- 8. Fosbinder, L. L. and Klann, R. W.: NASA Solidification of Cast Iron in Zero Gravity. Deere and Co. Technical Report No. 173, August 1982.
- VIII- 9. Frankhouser, W. L.: Materials Processing Threshold Report, II. Use of Low Gravity for Cast Iron Process Development. Final Report NAS8-33518, February 1980.
- VIII-10. Stefanescu, D. M.: Graphite Formation in Cast Iron. NAS8-34724, March 1981.
- VIII-11. Technical Exchange Agreement Between National Aeronautics and Space Administration and Deere and Company in the Area of Materials Processing in Low-Gravity, signed June 29, 1981.
- VIII-12. Schobel, J. D.: Precipitation of Graphite During the Solidification of Nodular Iron. Recent Research in Cast Iron, Ed. M. D. Merchant, Gordon and Breach Science Publishers, New York, pp. 303-346, 1968.

- VIII-13. General Electric, Space Science Laboratory, Phila., PA., NASA Contract Number NAS8-31536, November 1975.
- VIII-14. Fredriksson, H. and Remaeus, B.: The Influence of Sulphur on The Transitions White to Grey and Grey to White in Cast Iron. Recent Research in Cast Iron, Ed. M. D. Merchant, Gordon and Breach Science Publishers, New York, pp. 303-346, 1968.

TABLE VIII - 1. CHEMICAL ANALYSIS OF HYPEREUTECTIC CAST IRON

Element	C	Si	S	P	Mn	Cr	Ni
Wt %	4.52	2.047	0.0102	0.013	0.039	0.026	0.030
Element	Mo	Cu	Mg	Sn	Al	Ce	
Wt %	<0.001	<0.010	<0.002	0.005	0.002	<0.001	
Element	Ti	Te	V				
Wt %	0.028	<0.001	0.025				

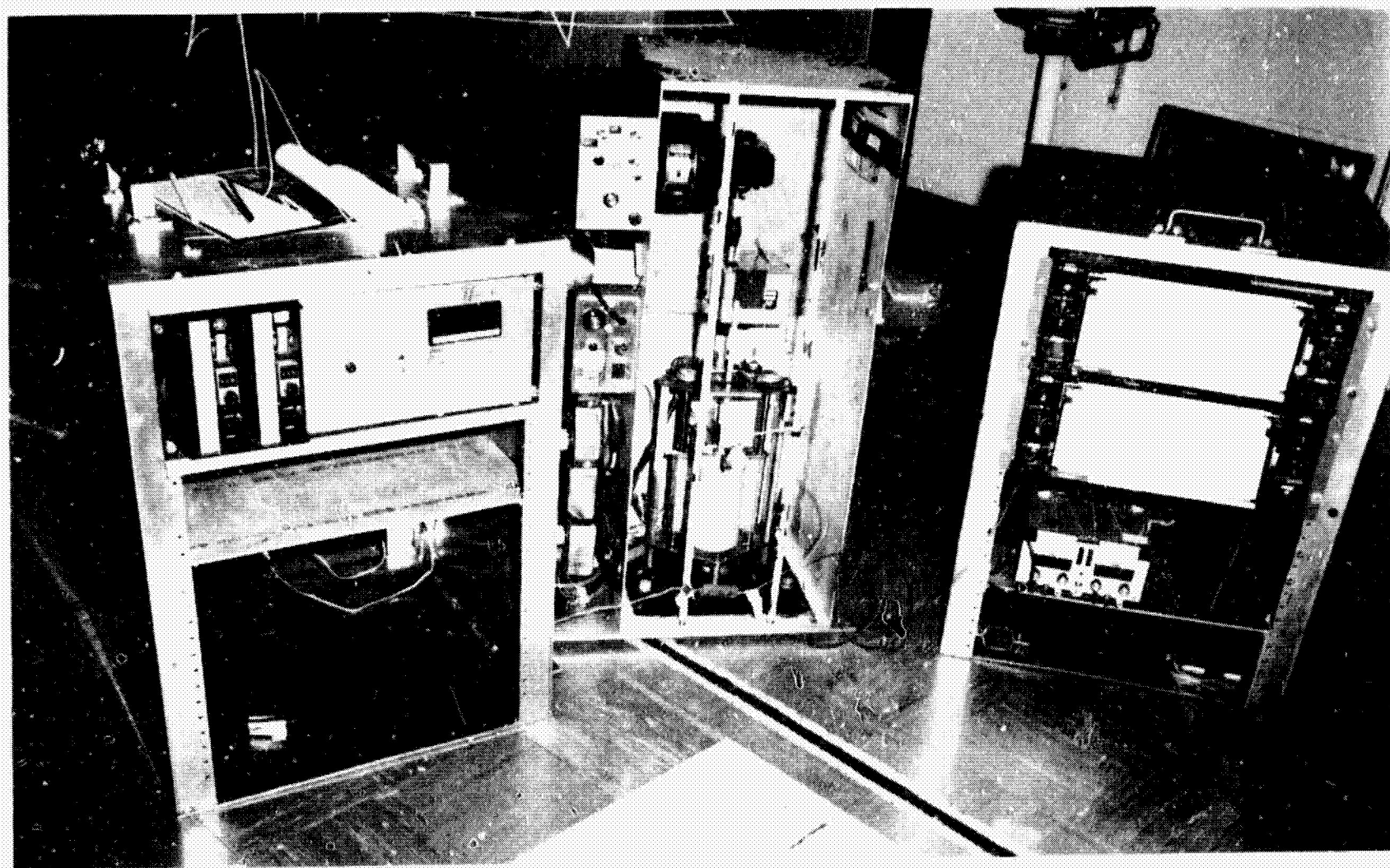


Figure VIII-1. Hardware for the ADSS-P KC-135 experiment: temperature controller and phaser package (left), automatic directional solidification furnace (center), accelerometer and recorder package (right).

ORIGINAL PHOTO IS
OF POOR QUALITY.

ORIGINAL PAGE IS
OF POOR QUALITY

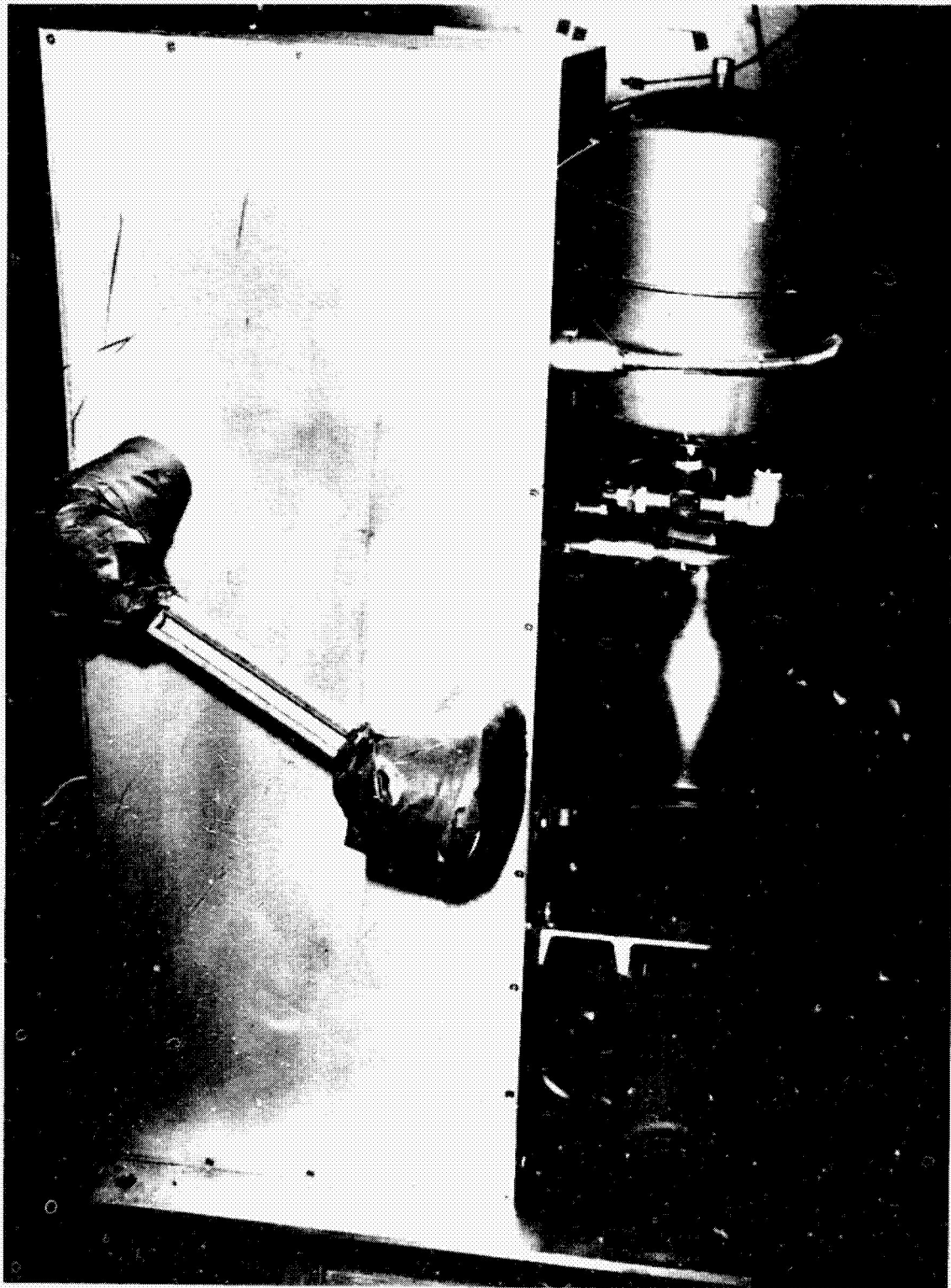


Figure VIII-2. Directional solidification furnace showing the portable quench block water circulation system - expansion tank (top), 10 liter reservoir (center), and peristaltic pump (bottom).

ORIGINAL PAGE IS
OF POOR QUALITY

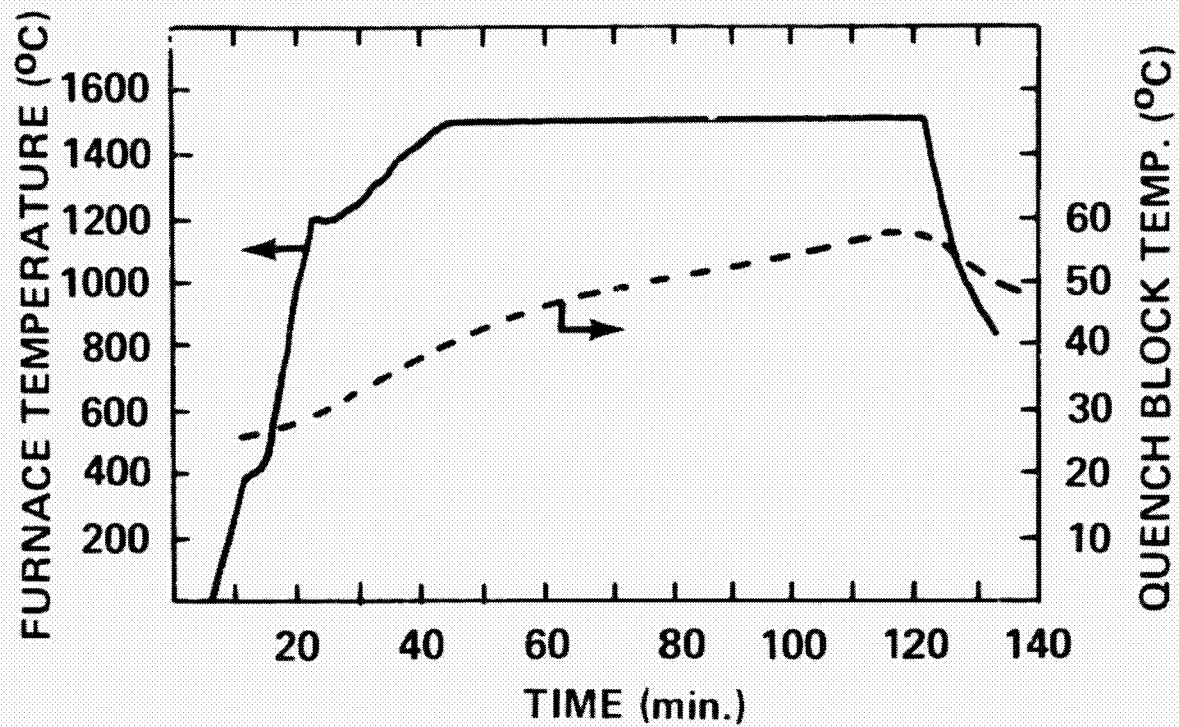


Figure VIII-3. The change in quench block temperature with time for a furnace temperature of 1500°C.

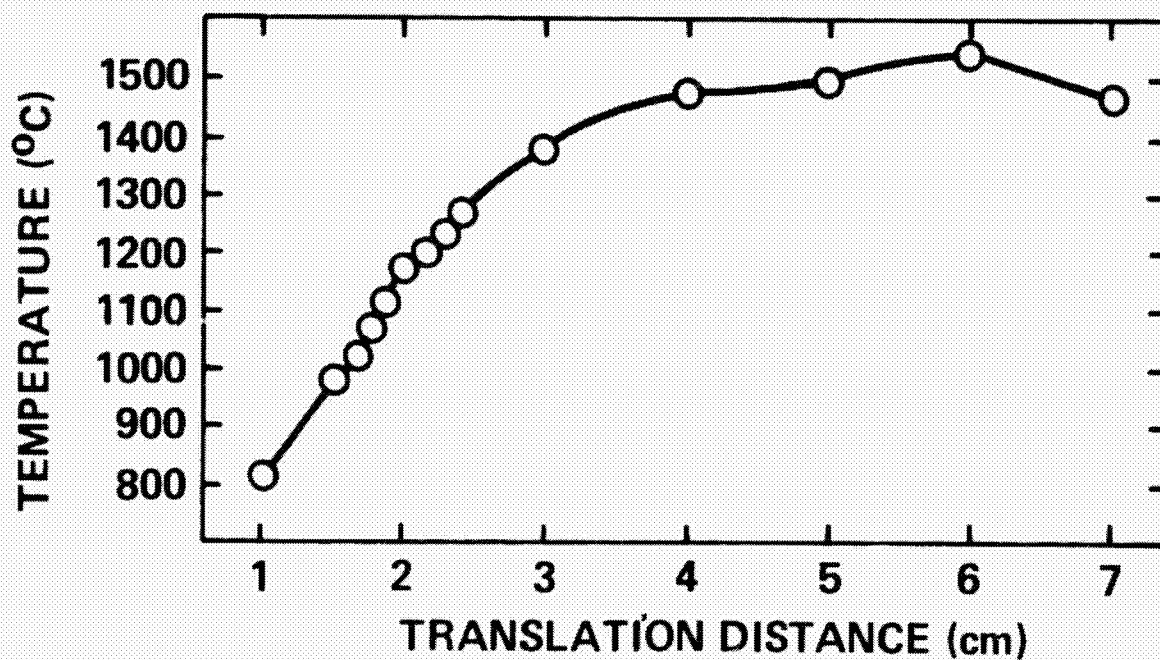
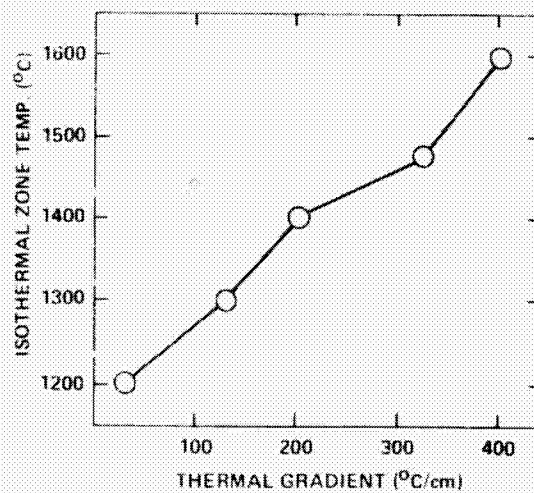


Figure VIII-4. The thermal profile of an empty crucible for a furnace temperature of 1500°C.



ORIGINAL PAGE IS
OF POOR QUALITY

Figure 5. Thermal gradient (in an empty crucible) versus furnace temperature.

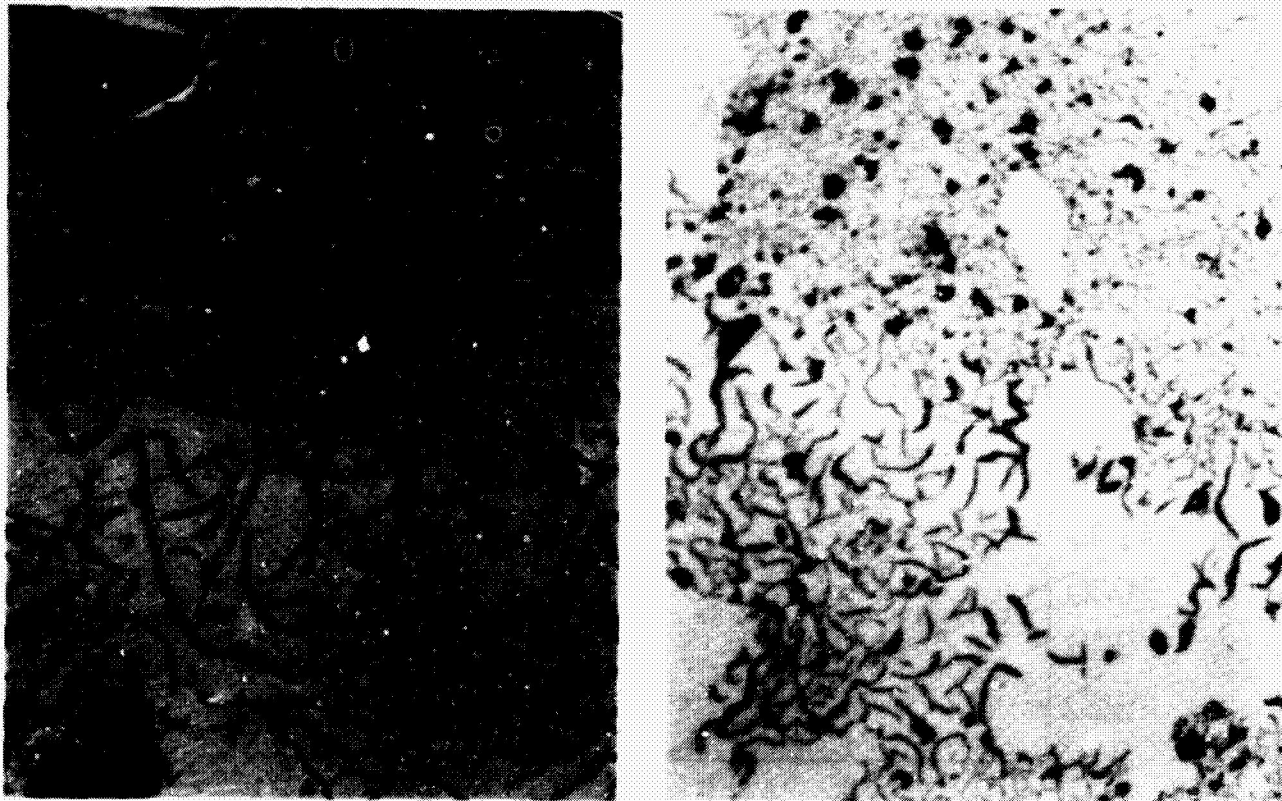


Figure VIII-6. Microstructure of commercial grey iron solidified in a thermal gradient of 403°C/cm and at translation rates of 1 mm/min and 2 mm/min.

ORIGINAL PAGE IS
OF POOR QUALITY

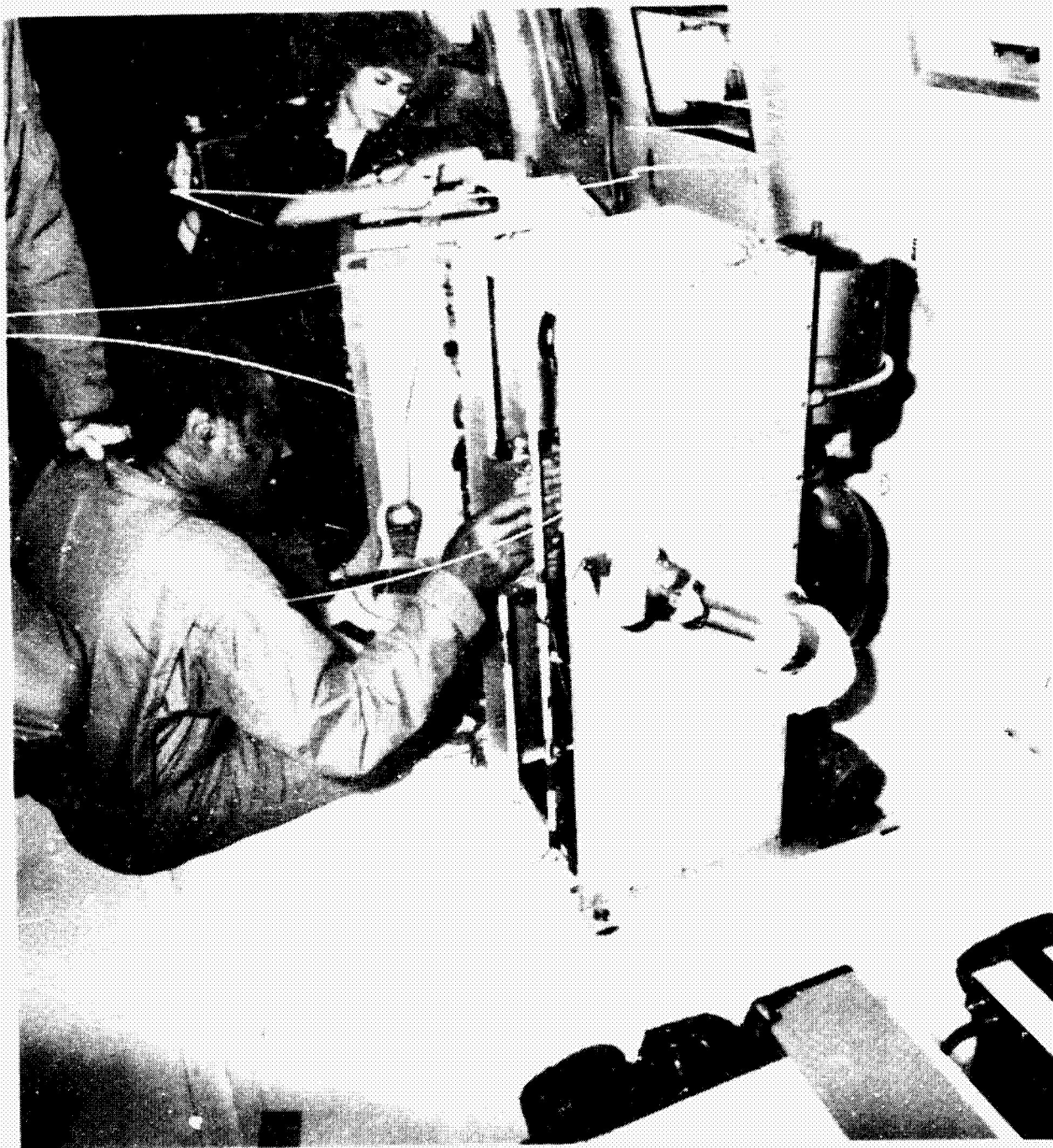
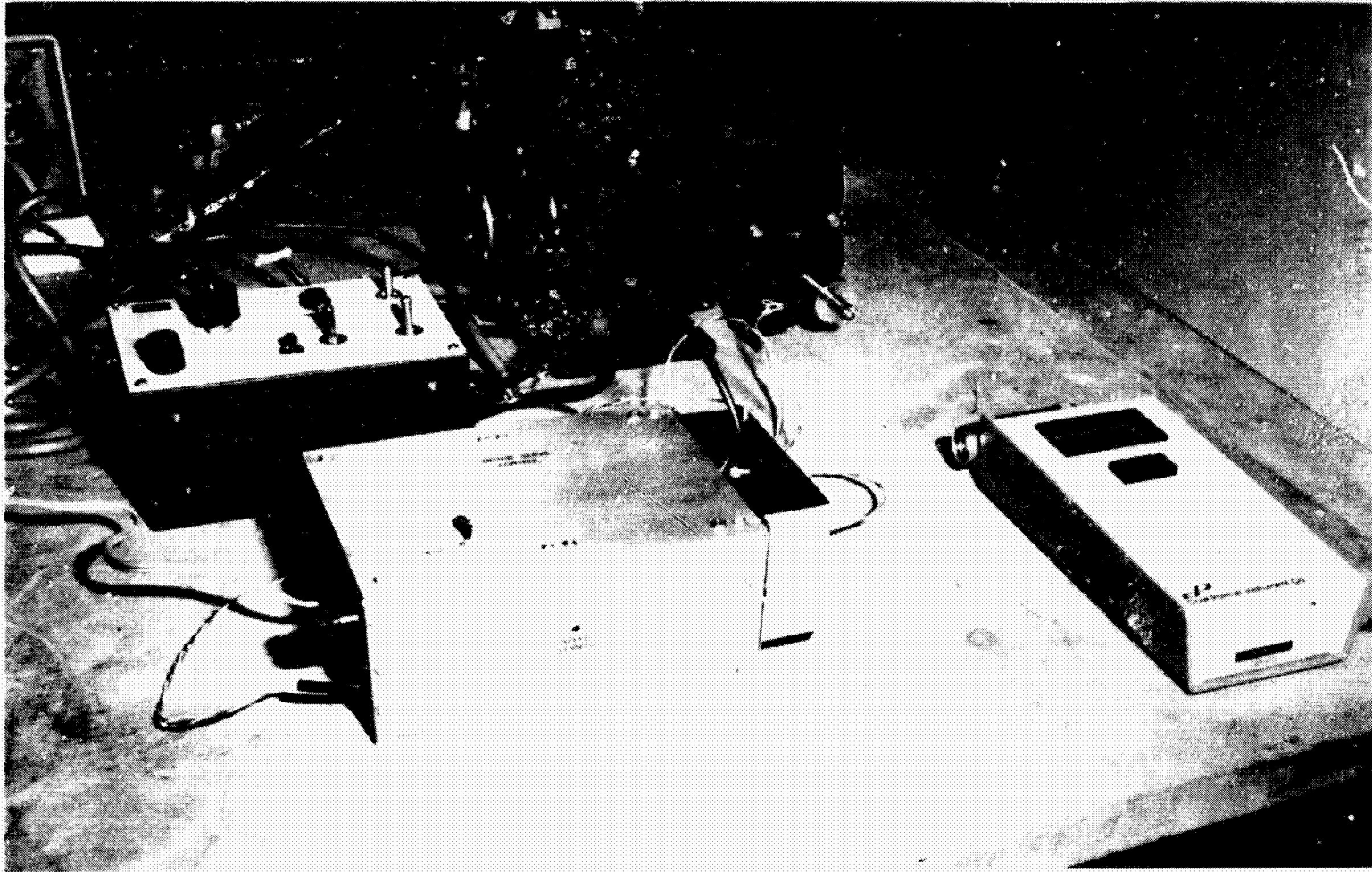
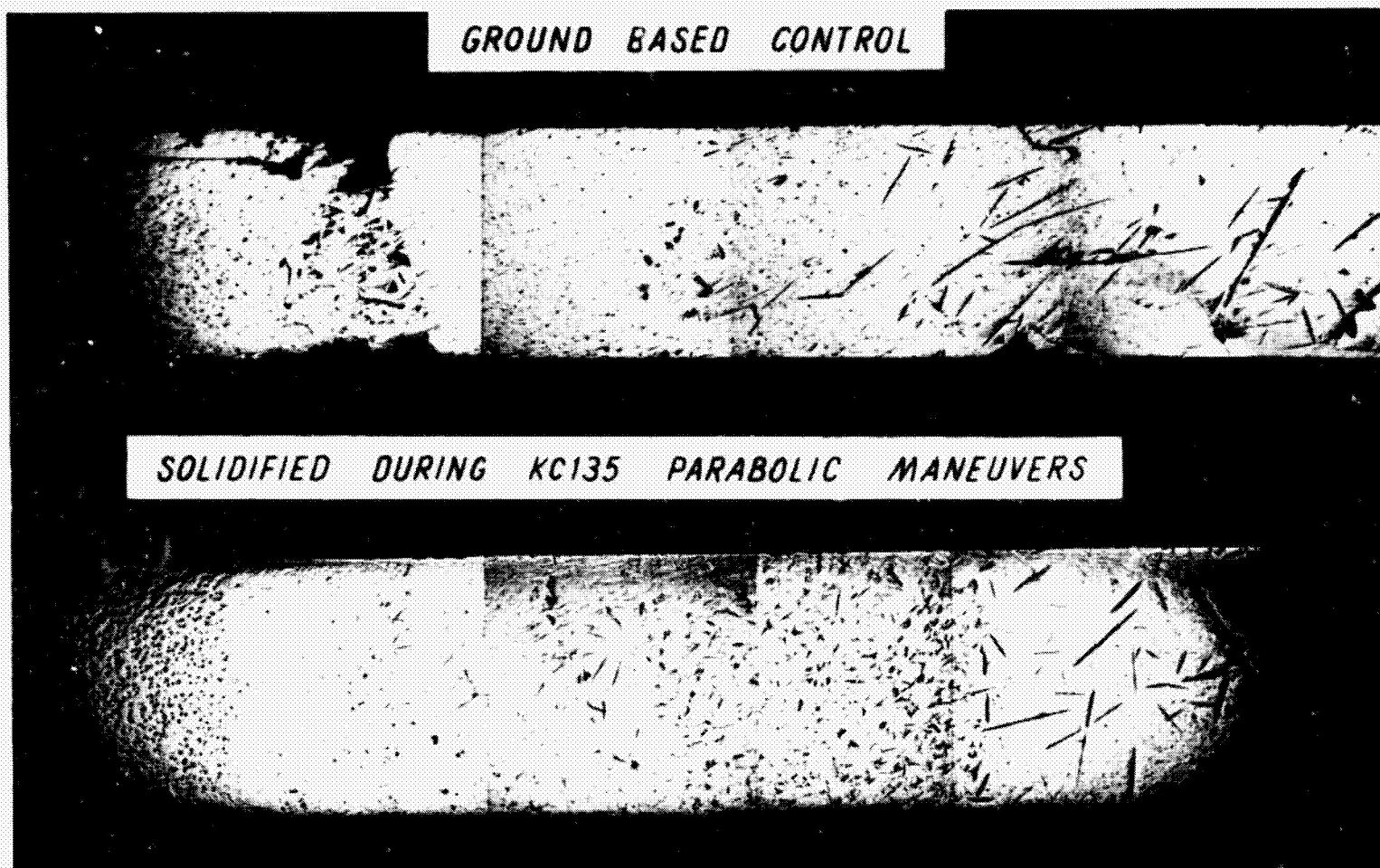


Figure VIII-7. Directional solidification system being operated during the 9-22-82 KC-135 flight. MSEC personnel Robert Shurney is measuring furnace RPM, and Wendy Alter is taking data.



ORIGINAL PAGE IS
OF POOR QUALITY

Figure VIII-8. Servo motor control system before installation into the flight furnace.



ORIGINAL PAGE IS
OF POOR QUALITY

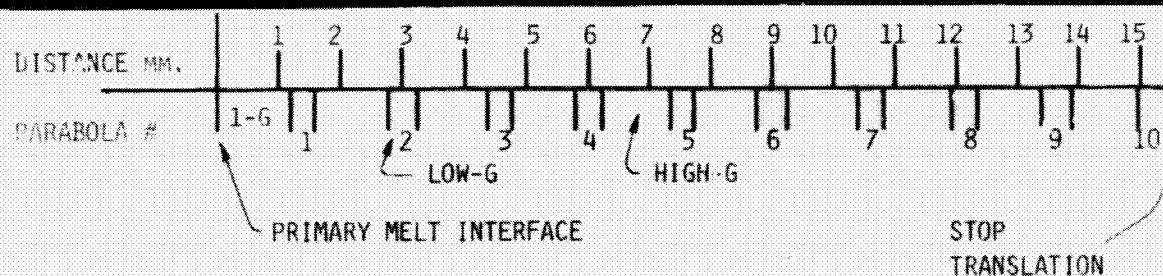


Figure VIII-9. Low magnification composite micrograph of the KC-135 directionally solidified hypereutectic cast iron flight sample and a control sample.

ORIGINAL PAGE IS
OF POOR QUALITY

200 X



FLIGHT SAMPLE



CONTROL

Figure VIII-10. Microstructure for the flight sample and control at 2 mm after the primary melt interface.

ORIGINAL PAGE IS
OF POOR QUALITY

200 X



FLIGHT SAMPLE

Figure VIII-11. Microstructure for the flight sample 2.5 mm from the primary melt interface.

ORIGINAL PAGE IS
OF POOR QUALITY

200 X



FLIGHT SAMPLE



CONTROL

Figure VIII-12. Microstructure for the flight sample and control at 4 mm from the primary melt interface.

ORIGINAL MICROGRAPH
OF POOR QUALITY

200 X



FLIGHT SAMPLE



CONTROL

Figure VIII-13. Microstructure for the flight sample and control at 10 mm from the primary melt interface.

IX. INFLUENCE OF LOW CONVECTIVE VELOCITIES ON CRYSTAL GROWTH

By John Hallett, Gary Keyser, Rick Purcell, Nam Cho,
Anna Lord, Clive Saunders, and V. Keller

Introduction

The purpose of the experiments undertaken in this study is to investigate the influence of convective velocities induced by the density difference between the fluid close to a growing crystal or freezing drop and its more distant environment. It is anticipated that convective velocities enhance the heat and mass transfer and hence the growth rate, and possibly change growth habit of the crystals and the freezing rate of the drops. This latter effect may change the symmetry of freezing of a drop, and its ability to shatter and produce secondary ice particles. Results are to be obtained on crystals grown from solution, from the melt, or from the vapor. The former are carried out in a small liquid cell and viewed by an optical system, which reveals differences of refractive index related to temperature and density around the growing crystal; vapor growth is not susceptible to such analysis. These studies are carried out in the laboratory in 1-g and in low gravity and are planned to demonstrate directly the influence of convection through comparison of the two situations.

The Experiments - Zero g

An experimental system, comprising a thermal diffusion chamber operating between +5°C and -20°C, has been designed and constructed for studies of ice crystal growth from the vapor and the freezing of small supercooled water droplets under the conditions of a low gravity environment. The experiment has been flown in parabola of NASA KC-135 flights, which permit sequential periods of $\sim 10^{-3}$ g of 20 sec interspersed with periods 2.0 g at the lower part of the aircraft trajectory. Ice crystals are produced which grow from the vapor after CO₂-cooled wire nucleation, or from a vertical fiber. The growth of these crystals is recorded photographically. Droplets are produced by a vibrating capillary and injected into the chamber to be nucleated either by AgI particles in suspension or by contact with ice crystals previously nucleated by the cold wire. This system has been flown in two KC flights. Preliminary results show particle motions dying out as the parabola is entered; data is currently being analyzed in detail.

The Experiments - 1g

In the laboratory, a thermal diffusion chamber similar to the aircraft system has been used for studying the growth transition near -6°C of ice crystals from the vapor as influenced by supersaturation. Results show that in a narrow range of temperature, the growth is unlimited by surface kinetic effects; at temperatures both colder and warmer, growth is limited by kinetic effects and requires a critical supersaturation for initiation on the basal plane. This result is to be compared with low-g studies where lack of residual motion may inhibit growth found under 1g conditions. The slow growth rate of crystals from the vapor may be insufficient to detect this particular effect, a question to be answered in planned future studies.

Growth of H₂O and D₂O from their melts, ice from NaCl solution and

$\text{Na}_2\text{SO}_4 \cdot 10\text{H}_2\text{O}$ crystals from supersaturated solution have been undertaken in a Schlieren system. Crystals grow as dendrites from a centrally located capillary tube, either stationary or in motion through the solution, and show convective plumes rising from the growing tips. Limits exist for the visualization of refractive index, which requires a concentration (for NaCl) >0.2 M; neither H_2O nor D_2O ice growing in pure water gives convection with a sufficient refractive index change to be viewed by this technique.

Preliminary results show that self-induced convective velocities are insufficient to break growing dendrites under any condition but have an influence on the growth velocity. Parallel studies, where growing crystals are moved at a known velocity through a supersaturated/supercooled solution, visualize the interaction of the growing crystal with a concentration boundary layer modified by the fluid flow. The crystal growth velocity is, in general, increased by the transport velocity.

Results

Diffusion Chamber Growth from the Vapor

Shown in Figure IX-1 schematically is the cross-sectional view of the static thermal diffusion chamber constructed. The chamber was formed by two 2.5 cm thick stainless steel plates 28 cm in diameter. A water-absorbing, stainless steel wicking material was diffusionally bonded to both plates and spaced 3 cm apart.

Machined into the side wall of a thick plexiglass ring were two access ports and two window openings. Windows were double pane to minimize the heat transfer from the ambient and provided with provisions for circulating dry air between the windows to prevent any vapor condensation that might impede viewing.

Of the two windows, one was used for viewing and the other, which was placed at 180° orientation, provided lighting from a water-filtered tungsten lamp. A hole was provided at the top center of the chamber in order to insert a fine glass fiber into the chamber vertically. The fiber was able to be rotated, and raised or lowered to control either supersaturation exposure or view position while the chamber was kept air tight.

Calibrated copper-constantan thermocouples were installed on both of the wicking surfaces to monitor temperatures at the vapor source and sink.

A third thermocouple, inserted horizontally through the chamber wall to the middle by the use of a glass tube (2 mm O.D), was used to obtain the growth temperature of crystals. The thermal plates were controlled independently by the use of chilled methanol fed from two circulators. The 0.5 cm thick copper discs were brazed to the outer surface of both thermal plates as a thermal buffer in order to achieve a uniform temperature distribution in the plates.

After flushing the chamber with bottled air, both plates were cooled close to 0°C while the upper one was supplied with distilled water in order to saturate the wicking material. As enough water was collected, the upper plate was cooled below 0°C to freeze. Saturation was controlled by varying the plate temperature appropriately such that the growth temperature remained near constant throughout supersaturation ranges.

When the center temperature was stabilized and the deposition of ice onto the lower plate was observed, a glass fiber cooled in liquid nitrogen was inserted. The position of growing ice crystals was marked microscopically by bringing the center thermocouple into view. This thermocouple was kept away from the fiber in the actual experiments in order to avoid introducing an additional vapor sink around the crystals.

All the growth measurements were done on the projected images of 16 mm movie film recorded via a stereo microscope. The rate of filming was 4 to 30 frames per hour depending on the growth rate and supersaturation. The experimental set-up for the diffusion chamber study of ice crystal growth is shown in Figure 1a.

The temperature profile inside the chamber was linear as shown in Figure 2, assuming the linear gradient of vapor pressure, supersaturation at the chamber center was calculated using the relation,

$$S = \frac{[e_o(T_l) + e_o(T_u)]/2}{e_o(T_m)}$$

where $e_o(T_l)$ and $e_o(T_u)$ is the saturation vapor pressure over ice at the lower and upper plate temperature, with their average being T_m .

Experimental Results

A high density of small crystals were nucleated and grew as thin plates at the early stages of growth throughout the temperature range -5 to -9°C . At relatively high supersaturation, some of these plates grew quickly clear of neighboring crystals and transformed into hollow columns. Further increase in supersaturation caused the preferential growth of corners to result in a multiple needle-like structure as shown in Figure IX-3.

At low supersaturations, the growth rate of thin plates could be measured as they grew to a fairly large size; however, these plates usually began to thicken as they outgrew the neighboring crystals. Occasionally layers which originated at the crystal periphery were seen to spread across the basal plane of these thickening crystals as shown in Figure IX-4.

It was obvious that densely populated crystals were mutually competing for the available water vapor. Such local depletion of water vapor made it impractical to determine the dependence of growth form on supersaturation. For a better assessment on this, hollow prisms on the order of $400\text{ }\mu\text{m}$ in size were grown at high supersaturation. The growth rate of one of these prisms, which was free of neighbors, was measured at a stepwise decrease in supersaturation at near constant temperature.

Both the c- and a-axial growth slowed down in response to a decrease in supersaturation; however, at 0.9 percent supersaturation, a thin plate originated at the corners of prism and spread toward the hollow portions of crystal covering them at its tip. Formation of this thin plate was more pronounced as the c-axial growth became immeasurably small ($<0.001\text{ }\mu\text{m/sec}$) at less than 0.6 percent supersaturation. typical form of this thin cap and its development in time are illustrated in Figure 17

and Figure IV-6, respectively. Represented in Figure IX-7 is the measured rate of growth normal to the basal and prism planes. A curve fitting based on the least square criterion was applied to the c-axial rate only. The important conclusion from this work is that under quite specific conditions, the growth rate is very sensitive to the environmental supersaturation. Since environmental supersaturation has been shown to be equivalent to ventilation (Keller and Hallett, 1982) the growth kinetics under low-g may be expected to be influenced by lack of convection in quite specific situations. In particular, the growth form of the crystals near -7°C would be expected to show such differences.

Isothermal Chamber: Growth from the Melt or Solution

Crystals are grown from supercooled melt or supersaturated solution in $\sim 1/2\text{l}$ of liquid uniformly ($\pm 0.01^{\circ}\text{C}$) cooled below its equilibrium melting point. Crystal growth rates and convective velocity is measured from projected movie film.

In the case of a moving crystal, the growth is measured from a fixed point on the support (Fig. IX-8). Convective velocities are measured from rising irregularities in the plume viewed by the Schlieren technique; under steady state conditions the angle of the plume gives the ratio of the (transport + growth) to the rise velocity. The shape of the plume away from the tip gives the variation of low density fluid generated back from the tip; this increases with distance under some conditions (Fig. IX-9).

The limits of resolution are set by the integrated path $\int (n_{\infty} - n_0) dx$ along the path (x) of the Schlieren system as it traverses the boundary layer of the growing crystal. Refractive index concentration/temperature data is not readily available. 0.2 M NaCl has refractive index of 1.3340 at 25°C ; temperature coefficient for sea water (0.4 M) is $.00001^{\circ}\text{C}^{-1}$ (estimate). With supercooling of -1°C and path width $\sim \text{mm}$, this gives optical path differences of 10^{-6} cm ; this shows that appreciable higher resolution should be obtainable with an interferometric technique.

Figure 10a, b, c, gives results for convective and growth velocity for 1 M, 0.5 M and 0.2 M NaCl transported at between 0.15 and 0.2 cm s^{-1} , showing absolute crystal growth rate and convection rate becoming equal at -1.4°C supercooling. Figures 11a, b show results of growth with pure $\text{D}_2\text{O}/\text{H}_2\text{O}$ showing enhanced transport velocity giving enhanced growth rate, and that $\text{D}_2\text{O} < \text{H}_2\text{O}$ for identical velocity / supercooling.¹

It is concluded that horizontal transport velocities as low as 0.1 cm s^{-1} influence the growth rate of the crystals to give a 50 percent increase; since in these studies the growth form is dendritic, this implies a transport effect rather than a kinetic effect demonstrated for vapor growth. Since convective velocities are measured as 0.05 cm s^{-1} to 0.1 cm s^{-1} in the growth regime, it is to be expected that they would give an enhancement of growth velocities by a comparable amount compared with the low-g case without convection. This has to be demonstrated.

¹Movies of these events are available.

Low Gravity Studies

The chamber utilized for the laboratory studies described earlier was mounted for flight tests on KC-135. Two series of flights were carried out under the present contract.

OPERATIONAL SUMMARY

Report of KC-135 Flights, 1982

May 1982 - Flight Scientists:

Vern Keller (NASA, MSFC)

John Hallett (DRI, ASC)

The technical purpose of these flights was to test the temperature control and stability of the diffusion chamber, the drop producing system, the seeding system, the accelerometer system and the photographic and chart recording system. The scientific purpose was to assess the growth rate of crystals following seeding and the freezing of drops during the low-g trajectory.

Flight 1: (25 Parabolas) 25 May 1982

Time: 10.04 - 11.34 hrs

1. Cooling set at -2°C , -11°C , worked satisfactorily.
2. There was a problem of reloading 35 mm camera without removal of the 16 mm camera.
3. Pressure trace fortuitously overlaid accelerometer trace.
4. Seeding procedure (cooled wire in solid CO_2) worked well.

Flight 2: (25 Parabolas) 26 May 1982

Flight Time: 10.07 - 12.00 hrs

1. Cooling failed 10 min after takeoff.
2. Primary effort concentrated on drop injection and positioning - shows need for better in-flight viewing.
3. Condensation of water between windows is a problem - also water slopping around on bottom plate, but this would go away in a cooled condition, as it would be frozen.

Flight 3: (25 Parabolas) 27 May 1982

Flight Time: 9.15 - 11.07 hrs

1. Efforts to repair cooling failed.
2. Continued tests on drop injection and positioning.
3. Condensation of water between windows is a problem - also water slopping around on bottom plate, but this would go away in a cooled condition, as it would be frozen.

Conclusions and Recommendations from Flights of 28 May 1982 - Post Analysis

The nucleation system appeared to work well in the first flight. The cooling appeared satisfactory, but the trace on the printout required an offset to avoid confusion. The tests of drop injection system during flights 2/3 showed that the control and operation needed improvement; in particular, the filling procedure was not satisfactory. Due to the cooling failure, the ice crystal growth tests were not carried out. Satisfactory 35 mm and 16 mm movies were obtained, and showed that improvement in the illumination system was required.

1. Cooling failure was caused by chip failure in the control system. This could have been caused by a noise spike in the power supply, or possibly static from the operator.
Action: (a) change of circuitry to reduce noise susceptibility.
(b) use an antistatic floor mat for the operator.
(c) add filter to input power supply.
2. Condensation occurred between the windows.
Action: improve dry air circulation between windows.
3. The water supply to the drop producer had inadequate control and leaked slightly.
Action: Provide pressure relief valve for water supply and improve the mechanical construction of the bladder system. An override should also be added to give continuous drop input on demand.
5. Quick release for 35 mm camera required.
6. An offset for vertical accelerometer is required; also a lateral accelerometer should be installed for monitoring possible lateral drop motion.

SEPTEMBER, 1982

The action items of the May flight were carried out prior to this flight. Flight Scientists: J. Hallett, V. Keller Assistant: L. Kennedee

These series of flights were planned to check out the electronics of the cooling system and to assess its stability. In addition, it was intended to carry out the following experiments:

1. Ice growth from the vapor by seeding. Chamber set 0, +5°C
temperatures: -10 -15°C
2. As (1), with presence of water drop and cloud.
3. Assess injected drop residual motion in low-g and investigate nucleation of such drops.
4. Ice growth rate on fiber during whole parabola sequence from takeoff.

General:

The cooling system performed well during flights, without failure. It turned out that operating on the ground, with airplane temperatures above +30°C, that the display overflow gave an apparent temperature of -59°C - which led to some confusion in interpretation until cooling had begun.

As of the date of this report, only the 35 mm films are available for analysis.

Tuesday, September 21, 1982: 1.17 - 2.57 hrs (40 Parabolas)

Flight 1: Temperature +5°C, -9°C

1. Tests on drop injection
2. Tests on CO₂ seeding
3. A defect developed in a leg of the chamber suspension, which was removed after the flight and repaired for Flight 2.

Wednesday, September 22, 1982: 9.45 - 10.28 hrs

Flight 2:

A difficulty arose in entering the computer program, so the chamber was operated isothermally -5° during this flight; it maintained temperature and stability.

Thursday, September 23, 1982: 11.00 hrs (40 Parabolas)

Flight 3: Temperature set at +4) and worked well.

-7)

Power available only in parabola sequences 2/3, parabolas 11→40. A problem developed in the 35 mm film transport for this flight - a faulty cassette appeared to be the problem.

Conclusions from September Flights:

1. Necessary to improve the entry procedure for temperature program. A series of pre-selected entries will be coded, to be easily inserted.

Action: Requisite program to give temperature set points:

+10°C	+5°C	0	-10°C	-5°C
-20°C	-15°C	-10°C,	-20°C	-25°C

The last sequence may be beyond the capability of the cooling system and will be investigated in the laboratory.

2. It will be necessary to heat the top plate during flight to maintain a given temperature above 0°C. This can be achieved by reversing the thermo-electric power.

Action: Rewrite program.

3. Further improvement of illumination is required to facilitate inflight adjustment.

Action: Awaiting 16 mm movie results; installation and testing of closed circuit TV system for possible aircraft use.

4. The 35 mm camera quick release still needs improvement to give rapid access during flight.

Action: Redesign

5. The piezo-electric system was damaged in transit by moisture and required replacement.

Action: The system should be redesigned to improve this operation and prevent entry of water during transport.

Preliminary analysis of the 35 mm film has shown satisfactory exposure and illumination.

The success of a program of this kind depends critically on the cooperation of the science personnel and the NASA personnel responsible for the operation. I would like to give special thanks for the assistance provided by the staff at Marshall - particularly Bob Shurney, and the staff at Johnson, for help in the field.

1. Preliminary Conclusions from Zero-g Studies

The system is now performing as intended, and with planned modifications, should give satisfactory performance for the next series of flights planned for April/September 1983.

1) Water cloud and ice crystal clouds can be formed in the chamber in low-g and can be observed.

2) Larger drops can be satisfactorily formed and injected.

2. Remaining Operating Questions:

1) Can injected drops be positioned well enough to remain in the field of view

long enough to study their freezing behavior?

2) Can crystals be grown on a fiber prior to low-g parabola so that their differential behavior can be examined?

3) Can growth rate of small nucleated crystals be determined in the chamber from Brownian oscillation (twinkling frequency) to give growth rate?

Negative answers to these questions will preclude the KC-135 study and lead to the longer shuttle times as a possibility.

Conclusions

Fundamental Questions

The scientific thrust of these studies has been the role of small scale convection in phase change events. This is important in rate processes for crystal growth limited by both kinetics and mass/heat transport; it could be important in both growth and evaporation or melting. In addition, the degree of perfection of the growing crystal and its impurity content (partition coefficient) are all likely to be influenced by the convective velocity.

The role of this convection on individual particles is of importance in understanding the growth mechanism; however, the role of convection in bulk material should not be underestimated. For example, snow metamorphosis in a snow pack depends on vertical thermal/moisture gradients which are dramatically influenced by convection in the air cells between the snow grains; a critical value (Rayleigh $\# \propto d^3$) and could have a considerable effect. This metamorphosis takes place over a period of days, so cannot be done in KC-135 -- shuttle/space station is more appropriate.

A second possibility for application of these studies is in heat/mass transport in a plant system. This has a close analogy to crystal growth, since CO_2/O_2 /heat is limited by similar transport processes, and the kinetic effect is comparable to the opening and closing of the stomata which occurs under quite specific conditions. Here again, the time scale is long, so that KC is too short, and the shuttle/space station can give the required times.

In all of these studies, progress is to be made by direct comparison of 1.0g and 0g studies; these necessarily go hand in hand to provide the comparisons necessary to test our hypotheses.

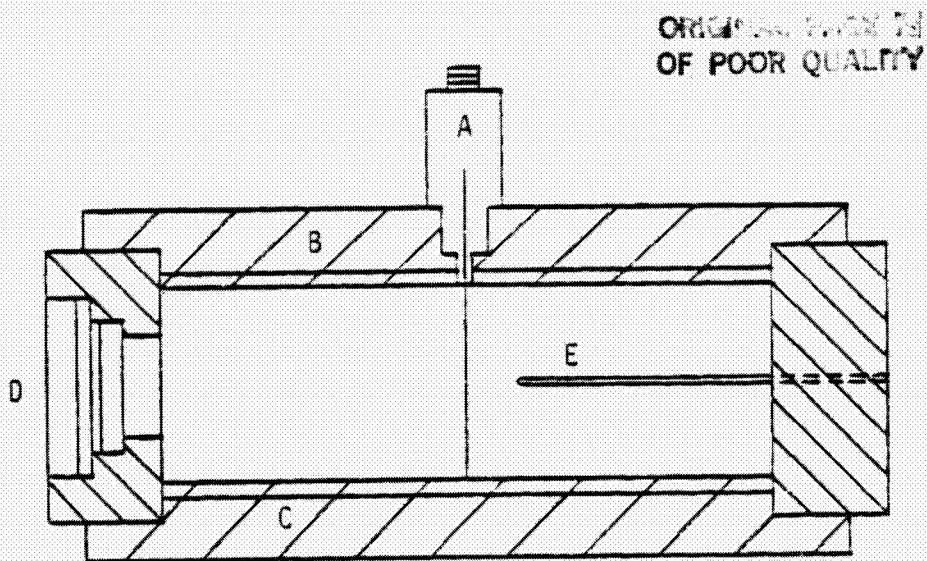


Figure IX-1a. Cross-sectional schematic of the static thermal diffusion chamber.
 A: glass-fiber manipulator B: upper thermal plate
 C: lower thermal plate D: window
 E: center thermocouple.

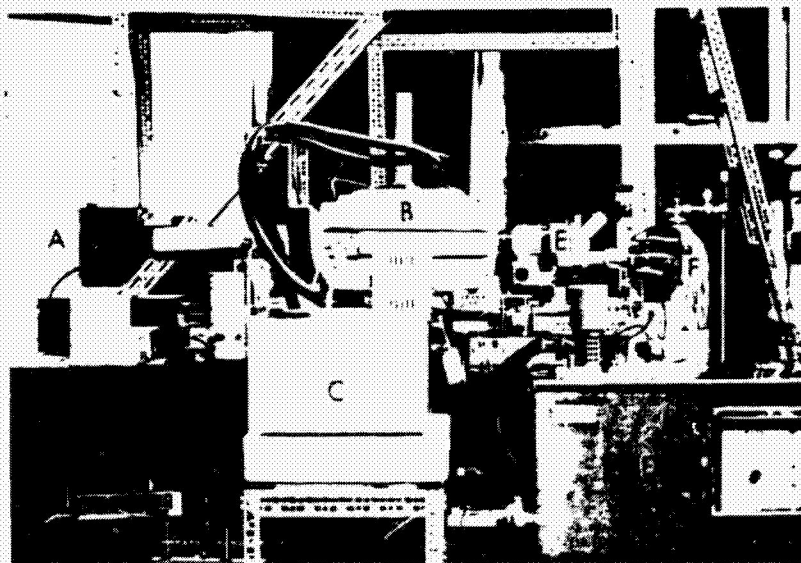


Figure IX - 1b. Experimental set-up for the diffusion chamber study.
 A: illuminator B: diffusion chamber C: upper plate cooling bath
 D: lower plate cooling bath E: microscope
 F: time lapse camera

ORIGINAL PAGE IS
OF POOR QUALITY

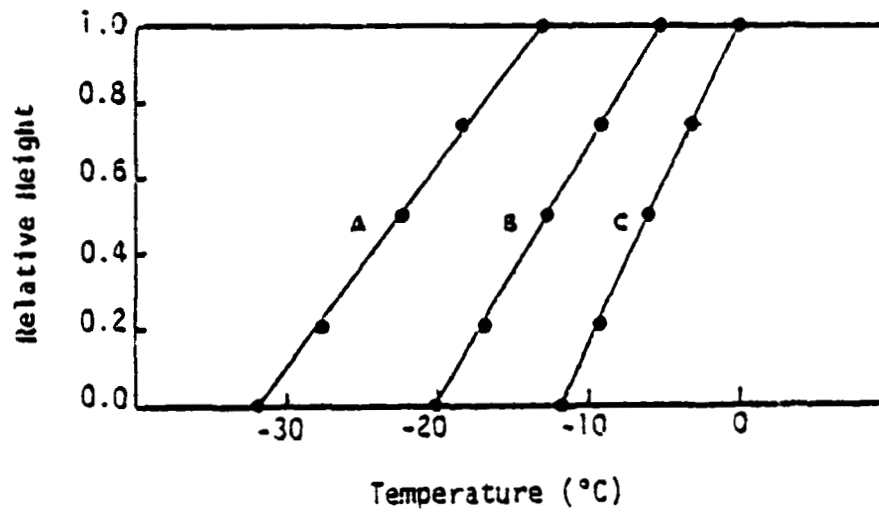


Figure 2. Temperature profile inside the thermal diffusion chamber at various temperature gradients. A: $0.59^{\circ}\text{C}/\text{mm}$
B: $0.47^{\circ}\text{C}/\text{mm}$ C: $0.37^{\circ}\text{C}/\text{mm}$

X. OPTICAL OBSERVATIONS OF UNIDIRECTIONAL SOLIDIFICATION IN MICROGRAVITY

By M. H. Johnston, R. B. Owen and R. E. Shurney

Introduction

Since gravity-induced effects are thought to impede structural and compositional control during solidification of materials, the application of the low gravity space flight environment to the advancement of materials science and technology constitutes one of the more active NASA research programs [X-1]. Although several solidification experiments have already been conducted in a low-gravity environment [X-2, X-4], none of these has utilized optical systems such as interferometers to study the fluid thermal and concentration profiles.

The present experiments used advanced optical measurement techniques to observe unidirectional solidification of a saturated solution of $\text{NH}_4\text{Cl-H}_2\text{O}$. This material has been used extensively as a transparent metal-model system in solidification experiments [X-5] and in low-gravity suborbital rocket studies [X-6]. In particular, it is a good analog for the casting of complex materials such as superalloys. Experimentation has included studies of growth morphology, dendrite remelting and coarsening, and fluid instabilities. In this material system the fluid ahead of the interface is lighter than the initial fluid, causing the eruption of jet-like plumes. This phenomena is associated with freckling in superalloys [X-7]. The present study was undertaken to quantify the changes occurring as a result of gravity forces on the liquid phase during solidification.

Preliminary studies included development of low-gravity optical systems by theoretical and experimental approaches [X-8, X-9] and laser shadowgraph/schlieren observations of low-gravity fluid flow [X-10, X-11]. This earlier work measured reduction of natural convection fluid flows resulting from thermally and compositionally induced density gradients. Such flows are important during compositional segregation in crystal growth and solidification processes [X-12].

Instrumentation

Experimental Environment

All low-gravity experiments were conducted in the NASA KC-135 aircraft. This experimental environment has been described in detail elsewhere [X-10]. In brief, the KC-135 low-gravity simulation aircraft flies a series of parabolic (Keplerian) trajectories, each of which yields approximately 25 sec of low ($1 \times 10^{-2}g$) gravity environment. A typical parabola is shown in Figure X-1.

Mach-Zehnder Interferometer

The Mach-Zehnder interferometer is probably the most versatile interferometric configuration for the observation of refractive index fields. It allows one to arbitrarily orient, space, and localize the interference fringes, and it separates the reference and test beams, allowing the reference beam to pass through a uniform field. Also, with this arrangement the test beam passes through the disturbed region only once,

resulting in a sharp image and a well-defined test path. Operational details of this instrument have been well described [X-13, X-14], and a system diagram is shown in Figure X-2.

We will consider two-dimensional liquid test fields in which the only refractive index variations along the test beam are the sharp discontinuities at the entrance and exit of the test cell. In such cases when the beams are recombined parallel to each other, each interferometric fringe represents the locus of points (in a two-dimensional field) where the fluid density is constant. These fringes can then yield qualitative temperature or concentration data, provided the fluid refractive indices are known in these terms and temperature and concentration profiles are not mixed. Normal operation requires a reference point in the test beam cross section where the properties are known, and then all properties at other locations in the test cell are measured relative to the properties there.

For such a field the refractive index at any point in the test cell is given by

$$n = \frac{\lambda_0 \epsilon}{L} + n_{\text{ref}} \quad . \quad (X-1)$$

ORIGINAL PAGE IS
OF POOR QUALITY

where

λ_0 = vacuum wavelength

ϵ = optical path length difference in terms of λ_0

L = length of test cell

n_{ref} = refractive index at reference point .

In practice a Mach-Zehnder interferometer is commonly used with the beams slightly diverging at an angle θ . Recombination of the test and reference beams then gives rise to wedge fringes separated by a space d , where

$$d = \frac{\lambda/2}{\sin \theta/2} \quad . \quad (X-2)$$

This configuration allows measurement of fraction values of ϵ .

Since light has an extremely short wavelength, equations (X-1) and (X-2) infer that the system is extremely sensitive to vibration and requires careful alignment. For example, if the fringes are separated by 6 mm, this means that θ is approximately 10^{-4} rad; thus the two beams must be aligned to this divergence. Further, since changes in path length are measured in terms of λ , slight movements in mirrors or beam splitters cause violent fringe shifts. An extremely rugged system was, therefore, required in order to operate successfully in the aircraft experimental environment outlined earlier.

To satisfy these design requirements, all system components were mounted onto a custom Newport Research optical breadboard. This slab was a 90- x 120- x 10-cm aluminum honeycomb with stainless steel top, bottom, and sides. The slab was vibration isolated from the aircraft using Varray W. Series ring and bushing elastic mounts. Mirrors and beam splitters were positioned using reinforced Newport Research mounts. The laser, a 4 mW He-Ne Spectra-Physics Model 144, had its beam expanded to 2.54 cm and collimated by a Spectra-Physics Model 332 spatial filter and an S-P Model 333 collimator. The 3-micron spatial filter pinhole was aligned using a modified NR Model 600 A-2 mount which stayed in place even while the 180-kg system was loaded onto the KC-135 by forklift. Interferograms were recorded by a Nikon 35 mm motor-driven camera with a 250-exposure film cassette. Pan-X film was used, and exposure times were set at 1/1000 sec, which solved any remaining vibration problems. The laser, camera, and test cell were controlled from a central power strip on the slab.

3. Laser Shadowgraph System

The operation of a shadowgraph system depends upon the deflection of a light beam, unlike interferometry in which such refractive effects are undesirable. In a shadowgraph system the linear displacement of the perturbed light beam is measured, and the end result is an image whose contrast is given by [X-14]

$$\frac{\Delta I}{I_T} = - \frac{z_{sc}}{n_a} \int \frac{\partial^2 n}{\partial y^2} dz ,$$

ORIGINAL PAGE IS
OF POOR QUALITY

(X-3)

where

I_T = initial beam intensity

$\Delta I = I_O - I_T$ where I_O = beam intensity in image plane

z_{sc} = distance from test cell to image plane

n_a = refractive index of air

n = refractive index of perturbing medium (assumed to vary in y only)

z = direction of initial light beam .

Unlike interferometry, shadowgraph is rarely used for quantitative measurements, since the contrast would have to be accurately measured and equation (X-3) integrated twice to obtain the distribution of interest. However, if large density gradients are present, shadowgraph pictures can be very useful.

In the present study, a laser shadowgraph system was used to track concentration boundary layer transitions in a rotating sample. A system diagram is shown in Figure X-3. Components were mounted similarly to those utilized in the Mach-Zehnder interferometer described, and several identical items were used in both systems.

4. Laser Streak Photograph System

ORIGINAL PAGE IS
OF POOR QUALITY

In laser streak photography, the fluid of interest is seeded with tracer particles which are then illuminated by a sheet of laser light [X-15]. A system diagram is shown in Figure X-4. By setting the camera shutter for one long exposure, streak photographs are obtained which indicate fluid velocity vectors in the plane of illumination. In the present study, streak photography was used to measure fluid motion independent from temperature and concentration profiles.

Results

A saturated $\text{NH}_4\text{Cl-H}_2\text{O}$ solution was prepared at 22°C and then encapsulated in a quartz cuvette sealed with a teflon cork. The cuvette was contained in an assembly (Fig. X-5) previously developed for sounding rocket flights, allowing the sample to be heated and cooled as required. The solution was then studied during solidification both on the ground and in the KC-135 low-gravity simulation aircraft.

1. Interferometric Results

The interferograms in Figures X-6 through X-9 show temperature and concentration profiles. Figure X-6 shows fluid temperature profiles as the solution is undercooled prior to solidification. Figure X-7 compares ground-based and low-gravity temperature profiles. Figure X-8 shows concentration profiles in growth plumes resulting from gravity-induced convection, and Figure X-9 shows stabilized concentration profiles in the absence of gravity-induced convection.

In order to analyze these interferograms, refractive index data were taken for $\text{NH}_4\text{Cl-H}_2\text{O}$. These indices were obtained using a Bellingham and Stanley Model 60/ED refractometer with test cell temperature determined by a Neslab Model RTE-4 circulating bath controlled at $\pm 0.02^\circ\text{C}$. These data are shown in Figures X-10 and X-11. From Figure X-10 a 1 percent change in concentration $\rightarrow \Delta n = 0.00187$ is calculated, and from Figure X-11 a 1°C change in temperature $\rightarrow \Delta n = 0.00012$ is calculated. Using equation (X-1)

$$\Delta n = \frac{\lambda_0 \epsilon}{L} \quad (\text{X-4})$$

Thus, for $\lambda_0 = 632.8 \text{ nm}$ and $\epsilon = 1$,

$$\Delta n = 6.33 \times 10^{-5} \text{ for } L = 1 \text{ cm}$$

$$\Delta n = 6.33 \times 10^{-4} \text{ for } L = 1 \text{ mm}$$

Therefore,

$$\epsilon = 1.95 \text{ for } T = 1^\circ\text{C} \text{ (1 cm test cell)}$$

$$\epsilon = 2.95 \text{ for } C = 1 \text{ percent (1 mm growth plume)} \quad .$$

The results were used to calculate the temperature and concentration profiles shown in Figures X-12 and X-13.

Thermocouple measurements were made to provide data in the instances where the magnitude of flow precluded analyses of the optical test results. Chromel-alumel thermocouples were first coated with a thin layer of epoxy to protect them from the corrosive liquid and then placed at 1 cm intervals inside the cuvette. Since there was concern that the thermocouples might affect the flow, they were used two at a time over different heights. In the rotating assembly, the millivolt signal was transmitted through a slip ring. In all instances, the data were recorded on a Honeywell recorder using a hot-pen stylus to eliminate gravitational effects on the ink flow.

Particularly in the assembly which was rotated for 5 sec during the low-gravity period, the data had to be obtained with thermocouples. As shown in Figure X-14, at the onset of spinning, each TC saw a pulse of cool fluid, then the overall temperature increased. The upper TC showed a greater cooling pulse, but less overall temperature change; whereas, the lower TC had the opposite effect. Figure X-15 shows split screen photographs of the fluid motion decay on the ground and in low gravity. When the apparatus was stationary, it was possible to use optical techniques to study the plumes occurring ahead of the interface as a result of gravity created instabilities. The concentration shift from the bulk to the center of the plumes is given in Figure X-13 for the two gravity levels.

Discussion

The change in temperature with time in the cuvette was determined from the thermal profiles and is shown in Figure X-16. The low-g and 1-g cases parallel each other for the first 15 sec of cooling. Then the 1-g fluid cooling rate begins to decrease while the low-g fluid continues to cool at the initial constant rate. Although nothing was visible in the interferometric photographs to explain this divergence, the streak photographs showed convection cells at the base of the cuvette within 20 sec after cooling began. Cool liquid flowed down the walls of the cuvette, initiating the cells. Particles in the fluid were moving on the order of 0.05 mm/sec. This convection would decrease the rate of cooling by mixing warmer fluid with the liquid. The effect can be seen in the temperature gradient. After only 20 sec, the temperature gradient in 1-g is 40°C/cm, 15 percent less than the 46°C/cm gradient in low-gravity.

Once a growth front has begun, a layer of less dense liquid forms ahead of the interface. In 1-g, this reached a width of 0.17 cm whereupon plumes broke loose and rose upwards [X-11]. In low-gravity interface, layers varied between 0.18 and 0.27 and no plumes occurred. The sample was able to establish and maintain a layer of concentration change ahead of the interface, with no perturbations.

In the instances where solidification and subsequent fluid plumes were allowed to begin prior to the low-gravity time period, the plumes reacted oppositely under the two gravity forces. During the low-gravity parabola, the plume movement halted within 8 sec and the concentration gradient between the plume and the surrounding liquid decreased. It is probable that with sufficient time, diffusion would totally eliminate the plume. But in 1-g, the concentration gradient increased, causing the plume to continue growing. In this case the plume is being replenished by light, cool liquid while it is rising into the denser, warmer surrounding fluid.

These effects would tend to decrease the overall stability of directional solidification in l-g. The rate of heat removal changes as convection cells begin, and the temperature gradient ahead of the interface is less, decreasing the effective temperature gradient to growth rate (G/R) ratio. In materials such as $\text{NH}_4\text{ClH}_2\text{O}$ and some of the superalloys in which the eutectic liquid is lighter, flow instabilities like plumes can develop creating freckles and small grains in l-g castings.

Summary

Gravity has both subtle and dynamic effects on the temperature profiles in solidifying materials. Shortly after the onset of cooling, low levels of fluid flow begin in l-g, decreasing the temperature gradient. This does have a concurrent effect on the G/R ratio and tends to decrease the stability of the interface. In low-gravity the interface appears to be more stable since the temperature gradient is steeper.

The gravity-driven pulses of liquid, causing freckling in superalloys, do not occur in low-gravity. Any existing plums of this rich eutectic liquid dampen quickly and diffuse into the surrounding fluid. This is opposite to what happens in l-g, where the density difference between the freckle plume and the surrounding liquid continues to increase as the plume rises, leading to greater instability.

References

- X- 1. Naumann, R. J. and Herring, H. W.: Materials Processing in Space: Early Experiments. NASA SP-433, 1980.
- X- 2. Wiedemeier, H., Klaessig, F. C., Irene, E. A., and Wey, S. J.: J. Crystal Growth, vol. 31, 1975, pp. 36-43.
- X- 3. Witt, A. F., Gatos, H. C., Lichtensteiger, M., Lavine, M. C., and Herman, C. J.: J. Electrochem. Soc., vol. 122, 1975, pp. 276-283.
- X- 4. Lid, M. D.: AIAA J., vol. 16, 1978, pp. 458-462.
- X- 5. Jackson, K. A. and Hunt, J. D.: Acta Met., vol. 13, 1965, pp. 1212-1215.
- X- 6. Johnston, M. H., Griner, C. S., Parr, R. A., and Robertson, S. J.: J. Crystal Growth, vol. 50, 1980, pp. 831-838.
- X- 7. Giamei, A. F. and Kear, B. H.: Met. Trans, vol. 1, 1970, p. 2185.
- X- 8. Owen, R. B.: Opt. Letters, vol. 6, 1981, pp. 331-333.
- X- 9. Owen, R. B.: Appl. Opt., vol. 21, April 15, 1982.
- X-10. Owen, R. B.: Opt. Eng., vol. 20, 1981, pp. 634-638.
- X-11. Owen, R. B. and Johnston, M. H.: Opt. Lasers Eng., vol. 2, 1981, pp. 129-146.
- X-12. Carruthers, J. R.: J. Cryst. Growth, vol. 42, 1977, pp. 379-385.

- X-13. Miller, R. H.: **Advances in Electrochemistry and Electrochemical Engineering**. Edited by P. Delahay and C. W. Tobias, vol. 9, John Wiley and Sons, N.Y., 1973, pp. 281-368.
- X-14. Goldstein, R. J.: **Measurements in Heat Transfer**. Edited by E. R. G. Eckert and R. J. Goldstein, McGraw-Hill, New York, 1976, pp. 241-293.
- X-15. Owen, R. B. and Campbell, C. W.: **Rev. Sci. Instrum.**, vol. 51, 1980, pp. 1504-1508.

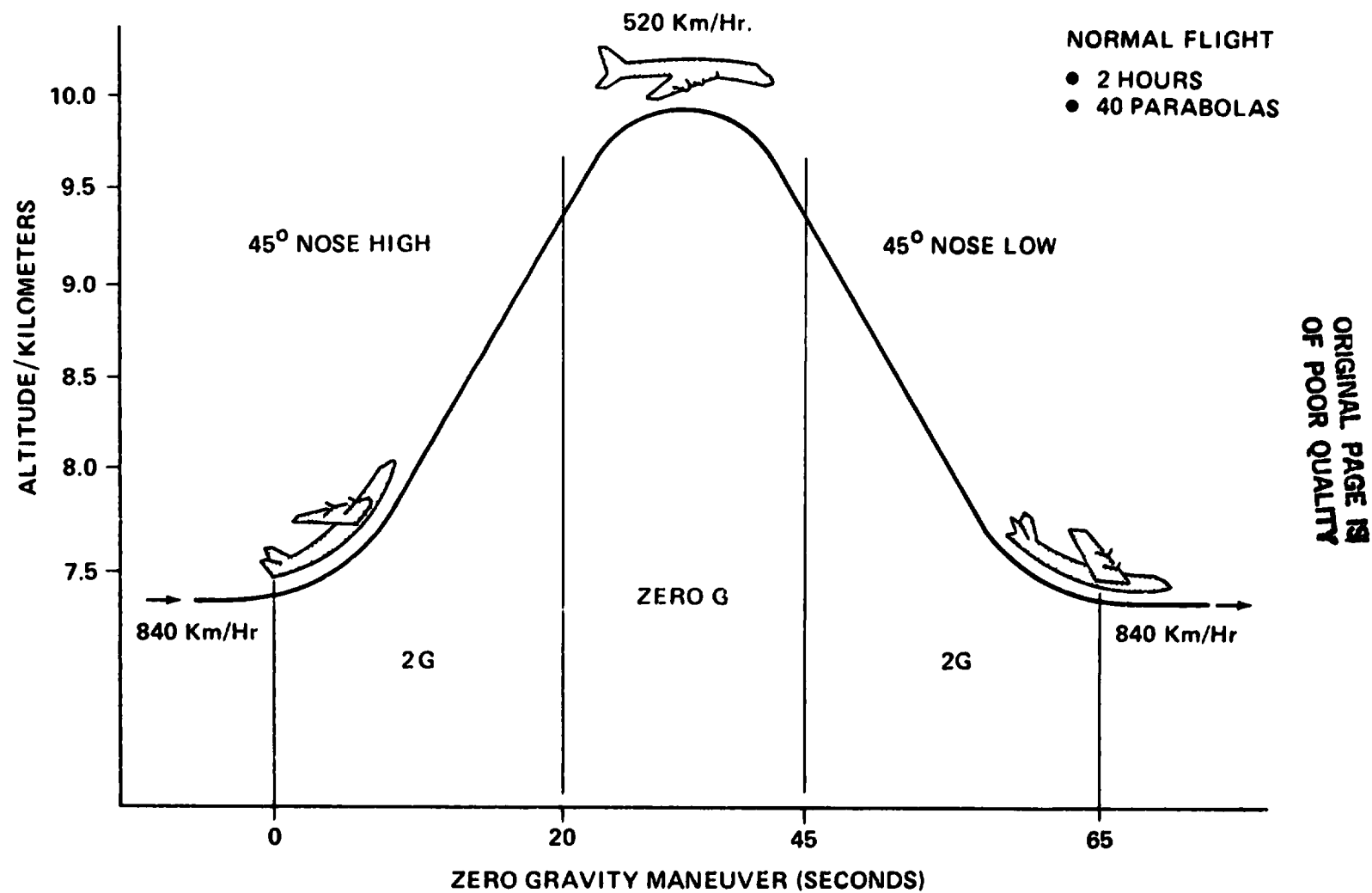
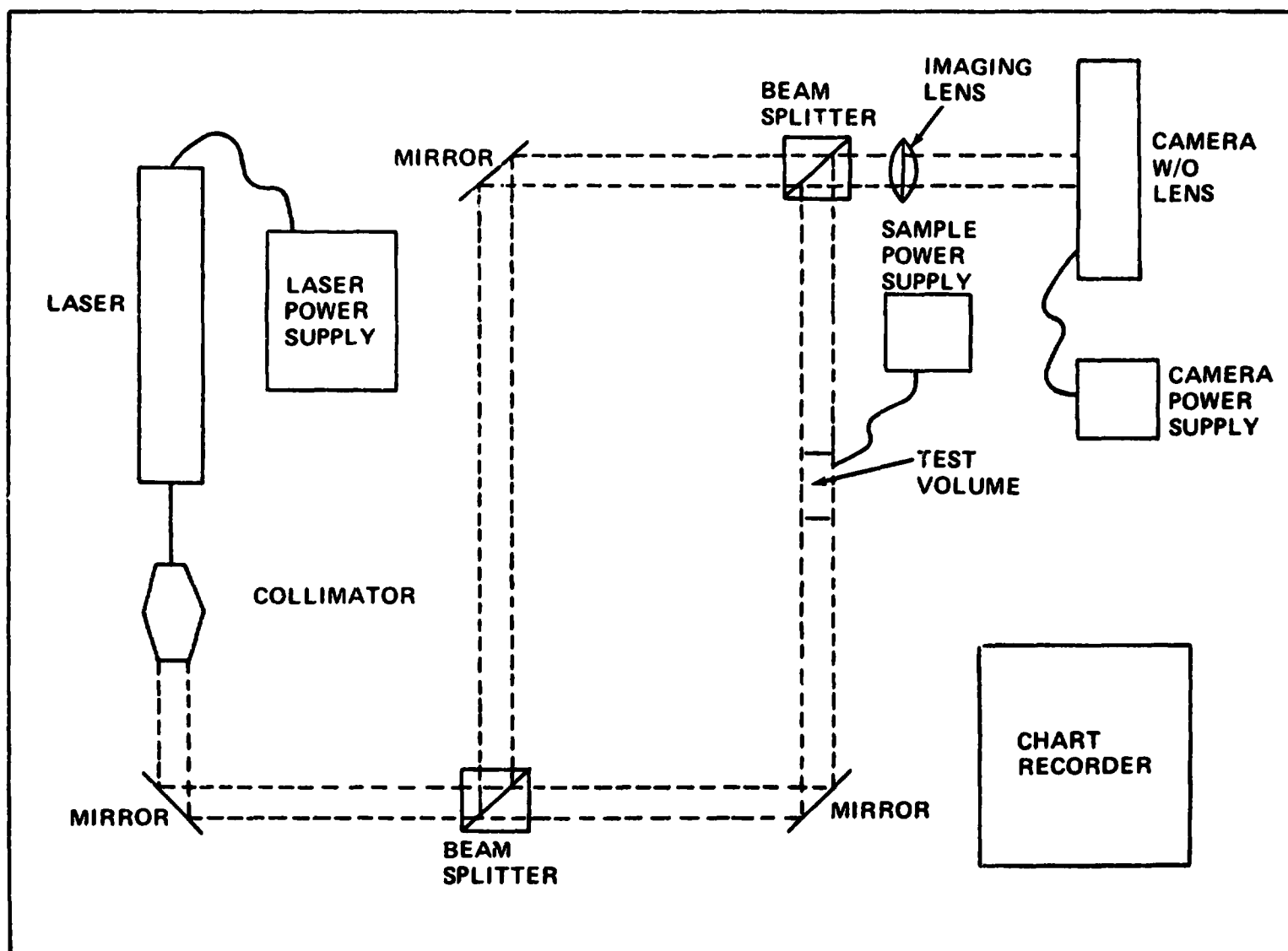
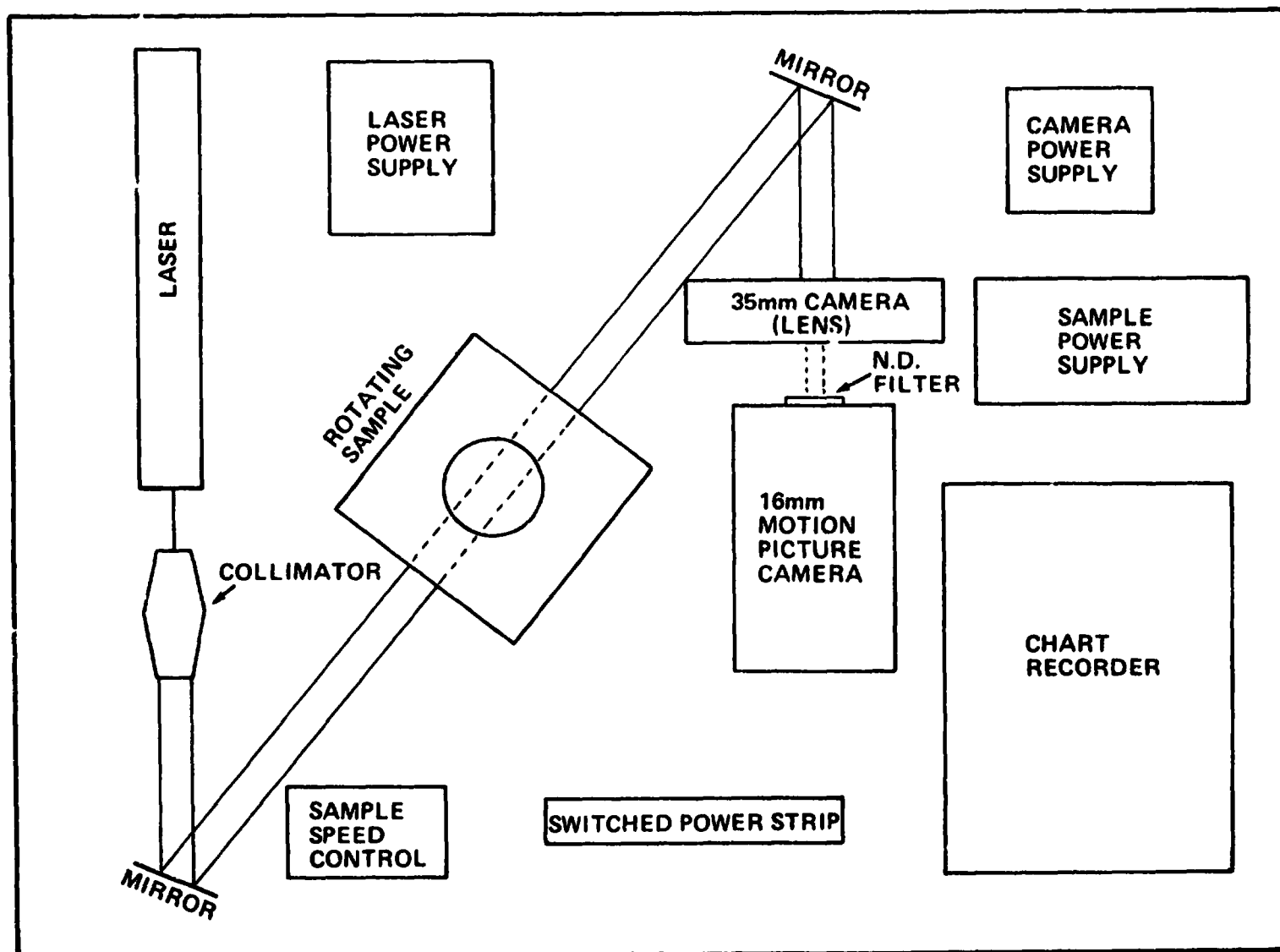


Figure X-1. Flight parabola of KC-135 low-gravity simulation aircraft.



ORIGINAL PAGE IS
OF POOR QUALITY

Figure X-2. Diagram of Mach-Zehnder interferometer.



ORIGINAL PAGE IS
OF POOR QUALITY

Figure X-3. Laser shadowgraph SPAR fluid motion simulator.

ORIGINAL PAGE IS
OF POOR QUALITY

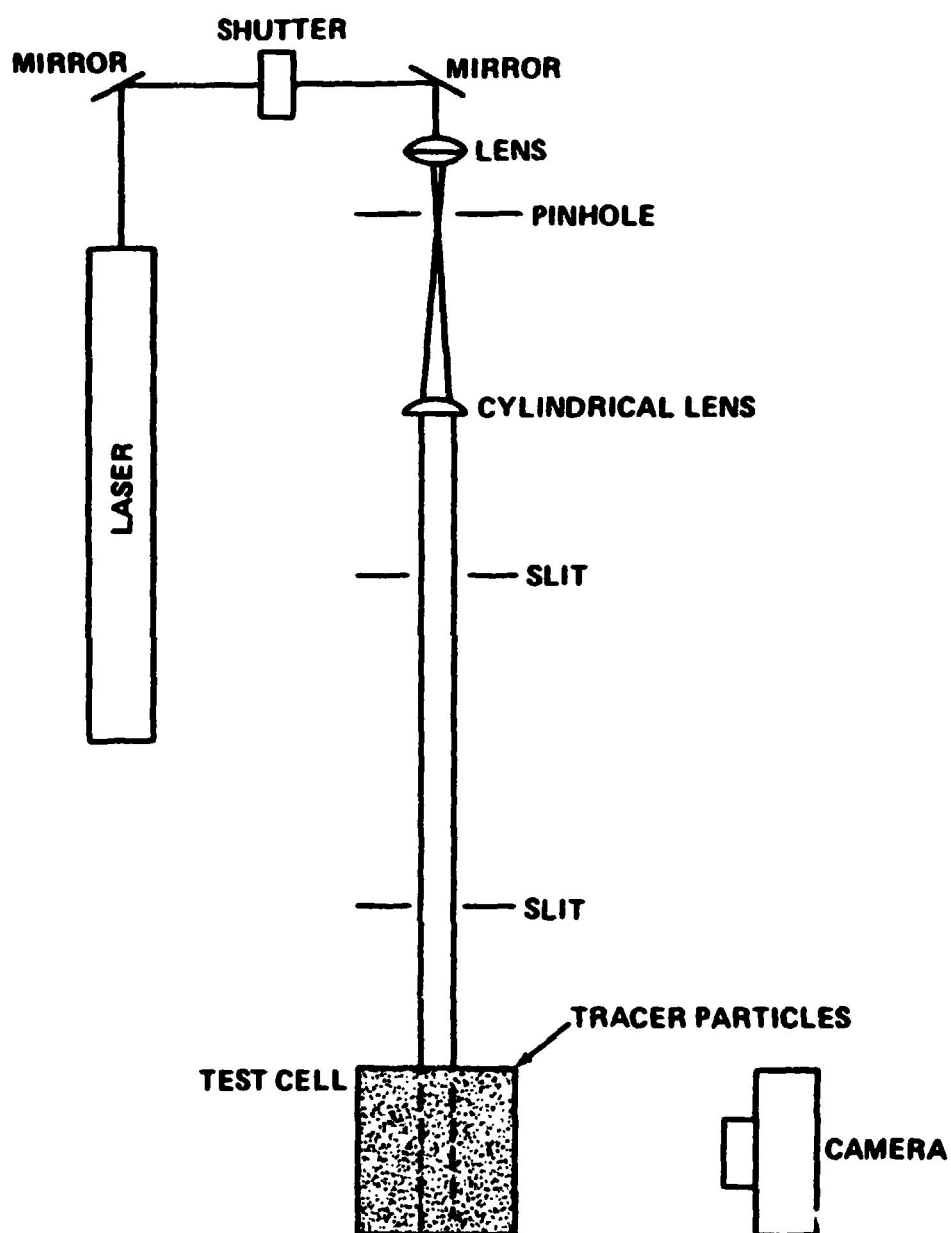


Figure X-4. Diagram of laser streak photography system.

ORIGINAL PAGE 13
OF POOR QUALITY

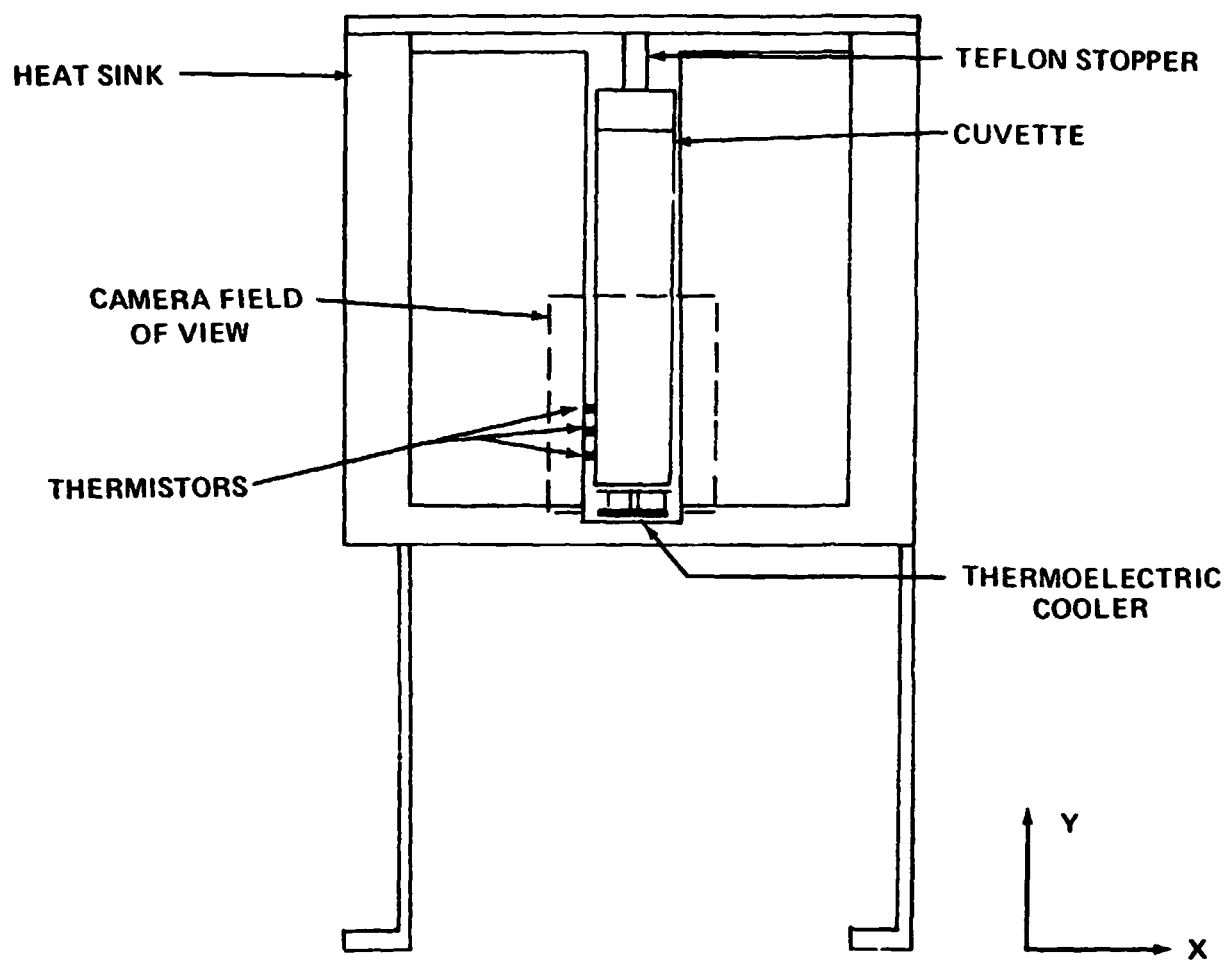
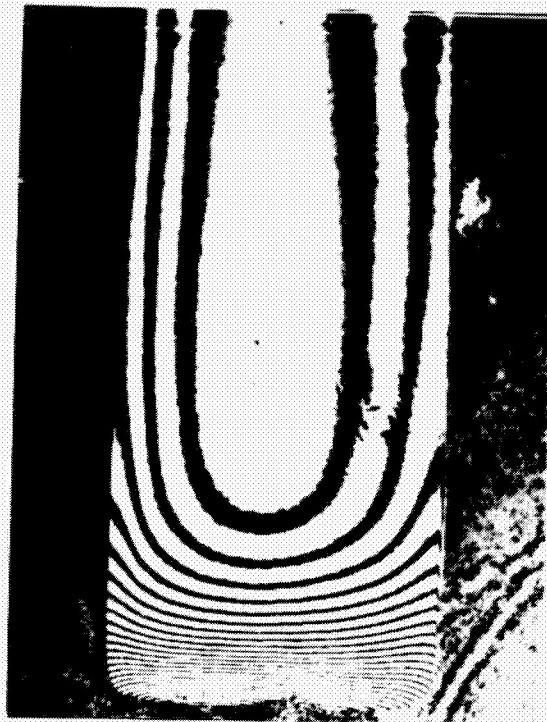


Figure X-5. Cuvette assembly viewed along Z-axis.

ORIGINAL PAGE IS
OF POOR QUALITY



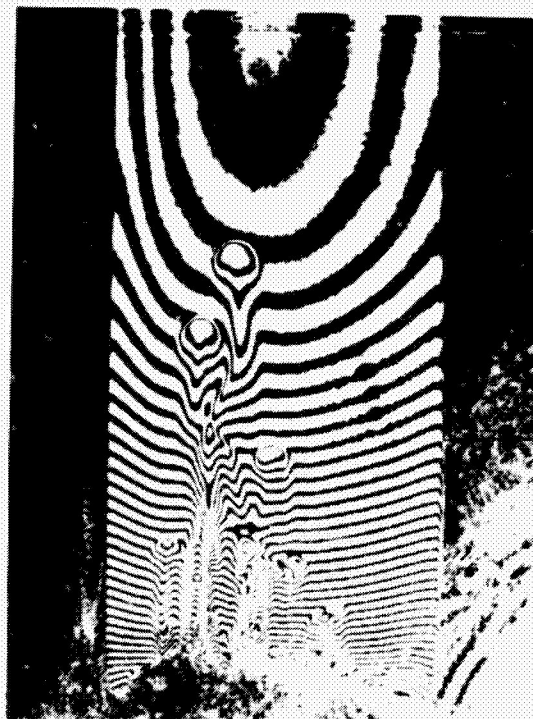
t=0



t=30 seconds

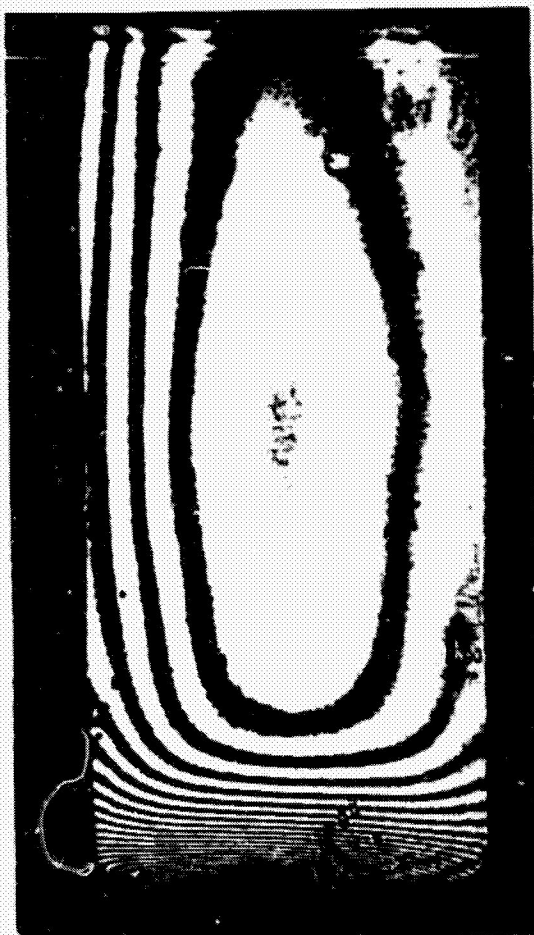


t=90 seconds

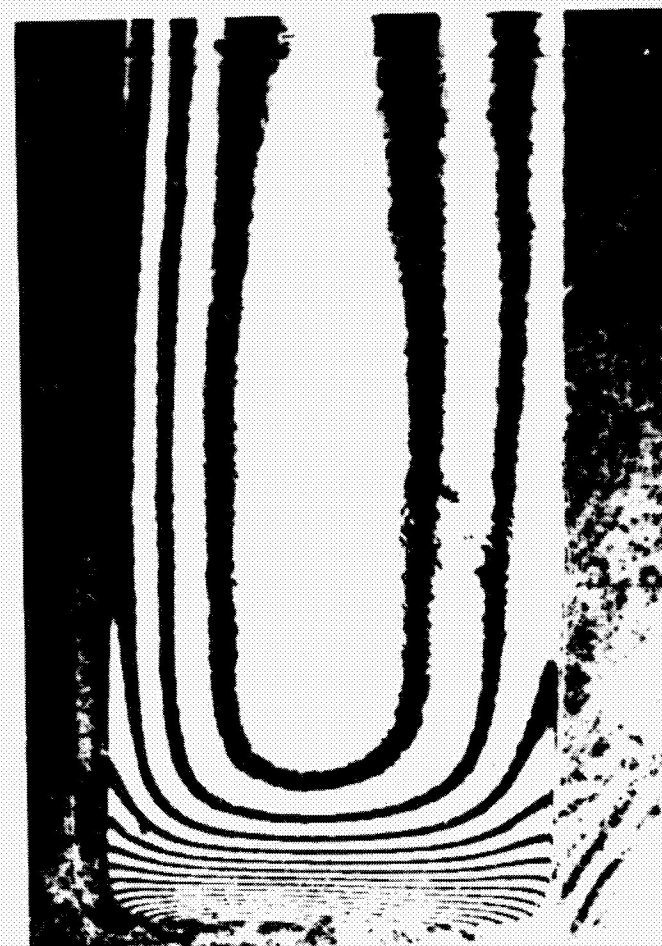


t=120 seconds

Figure X-6. Ground-based interferograms of NH_4Cl metal-model solution during initial solidification.



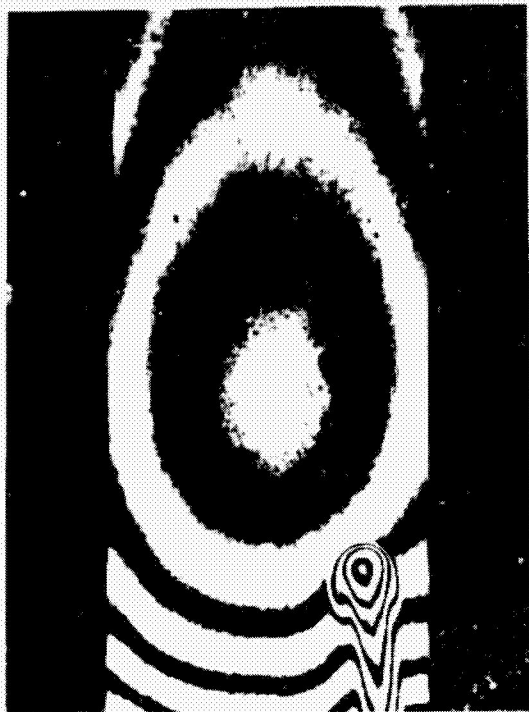
**LOW-g
TEMPERATURE PROFILE**



**ONE-g
TEMPERATURE PROFILE**

ORIGINAL PAGE IS
OF POOR QUALITY

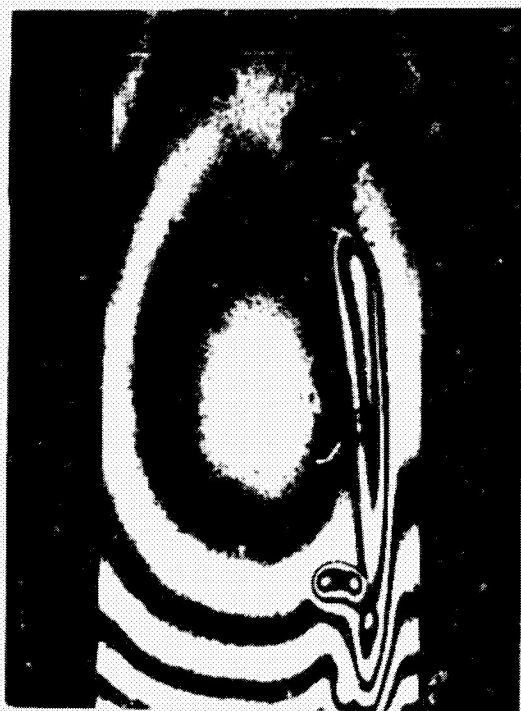
Figure X-7. Interferograms of NH_4Cl metal-model solution after 15 sec of cooling.



t=0



t= 5 seconds



t= 10 seconds



t= 20 seconds

Figure X-8. Ground-based interferograms of NH_4Cl metal-model solution during solidification.

ORIGINAL PAGE IS
OF POOR QUALITY.



TIME = 0 SECONDS



TIME = 5 SECONDS



TIME = 10 SECONDS



TIME = 15 SECONDS

Figure X-9. Low-gravity interferograms of NH_4Cl metal-model solution during solidification.

ORIGINAL PAGE IS
OF POOR QUALITY

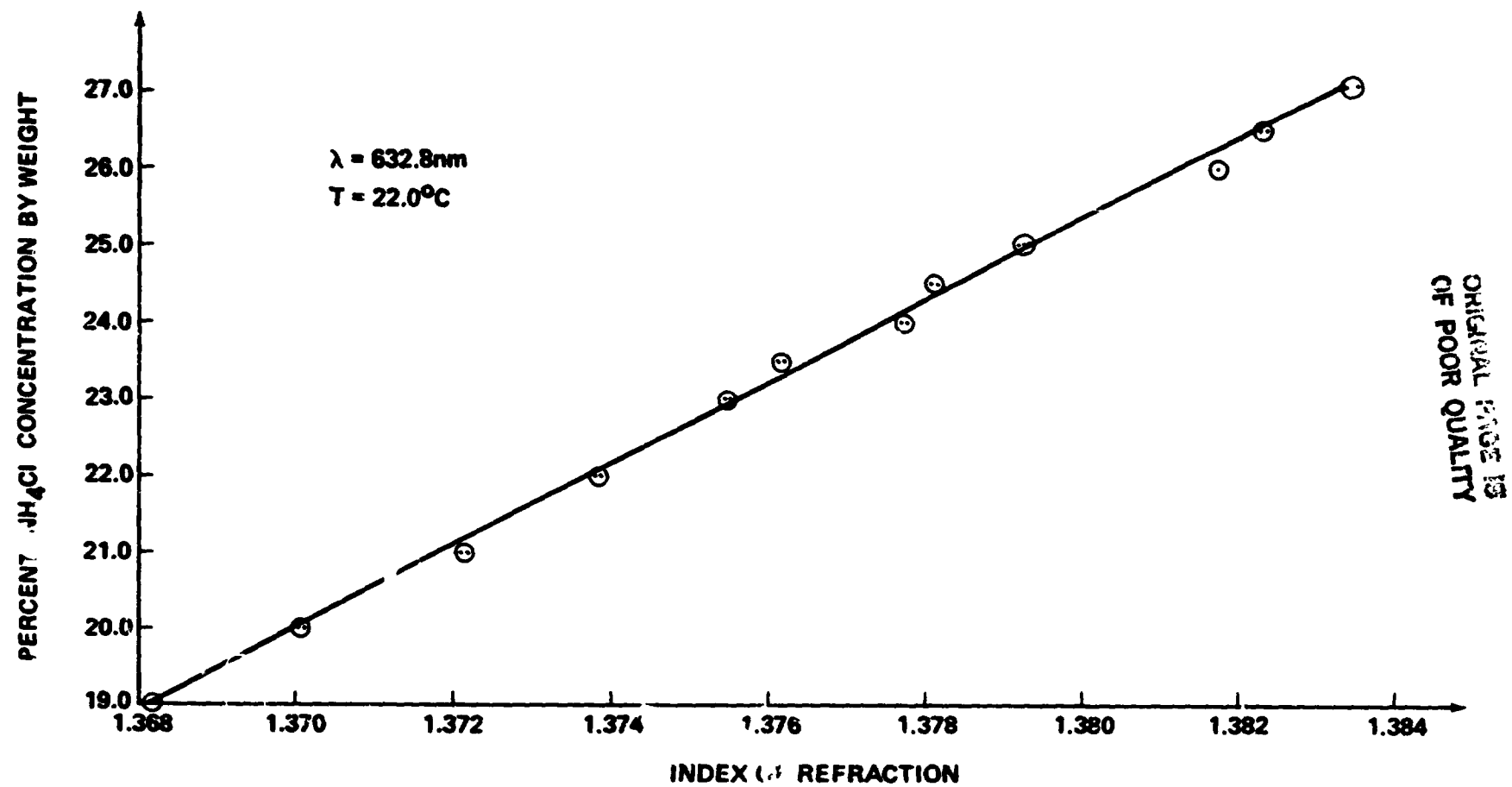


Figure X-10. NH_4Cl solution refractive indices versus concentration.

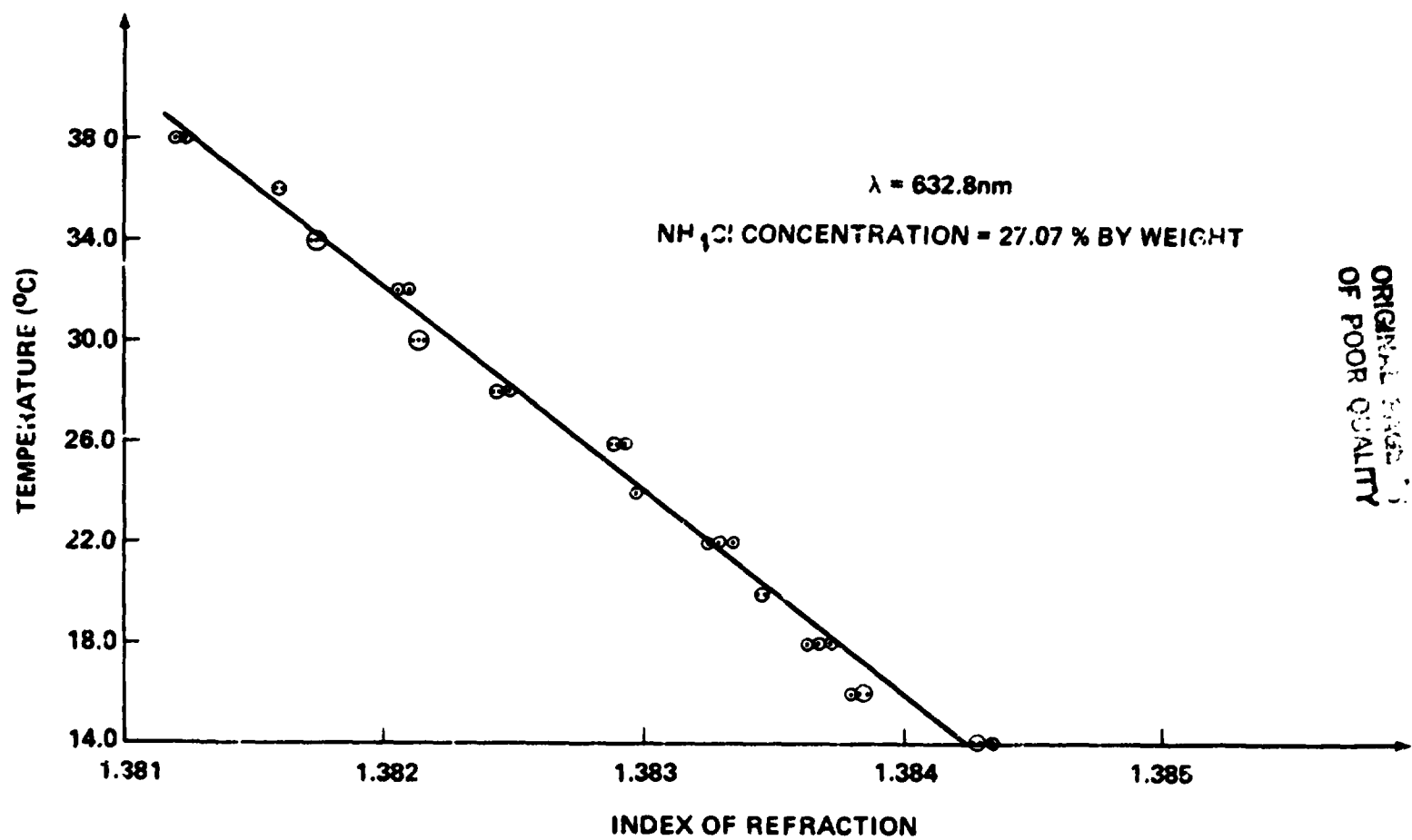


Figure X-11. NH_4Cl solution refractive indices versus temperature.

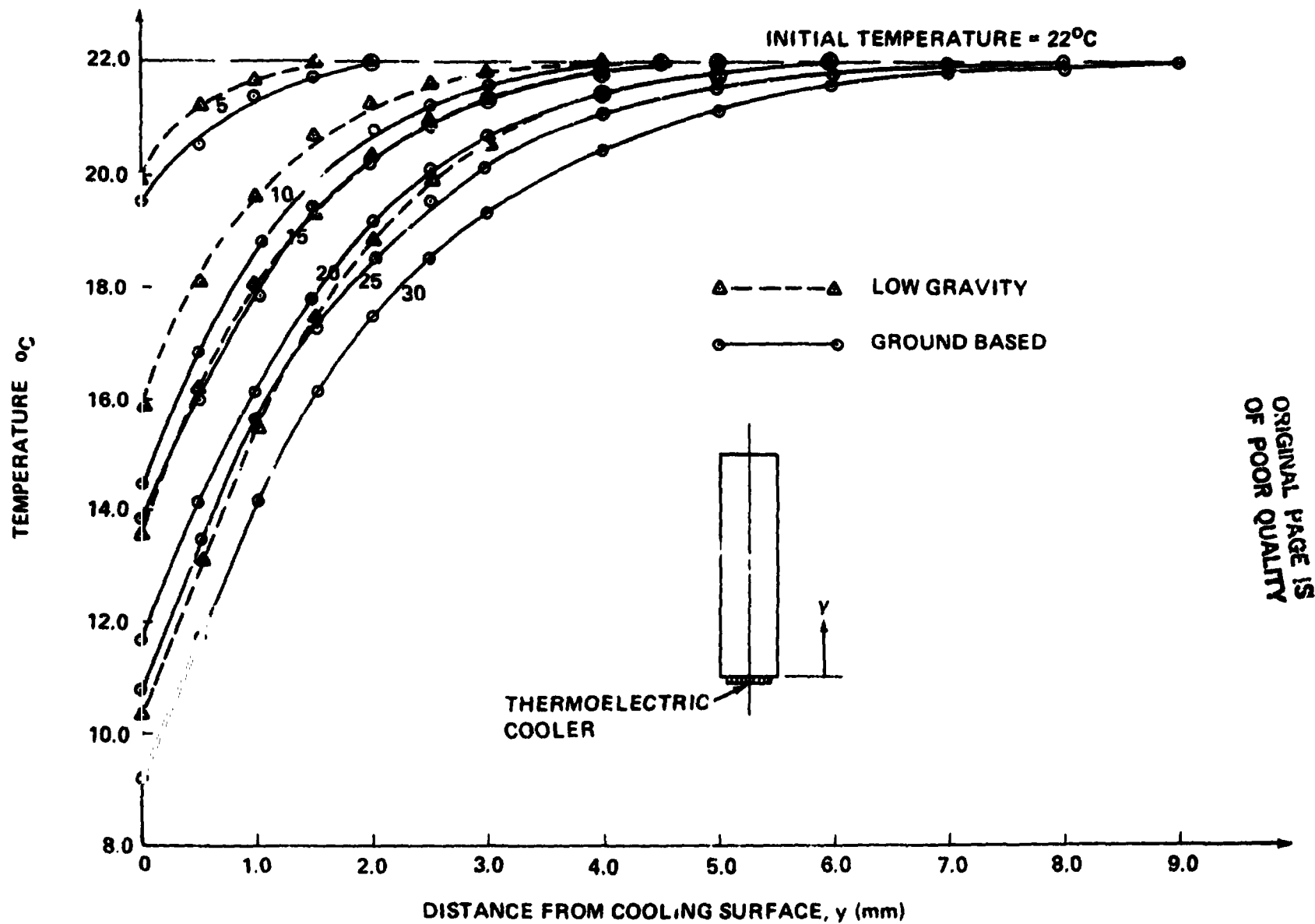


Figure X-17. Low-g and ground based experimental NH_4Cl centerline temperature distributions for various times (sec).

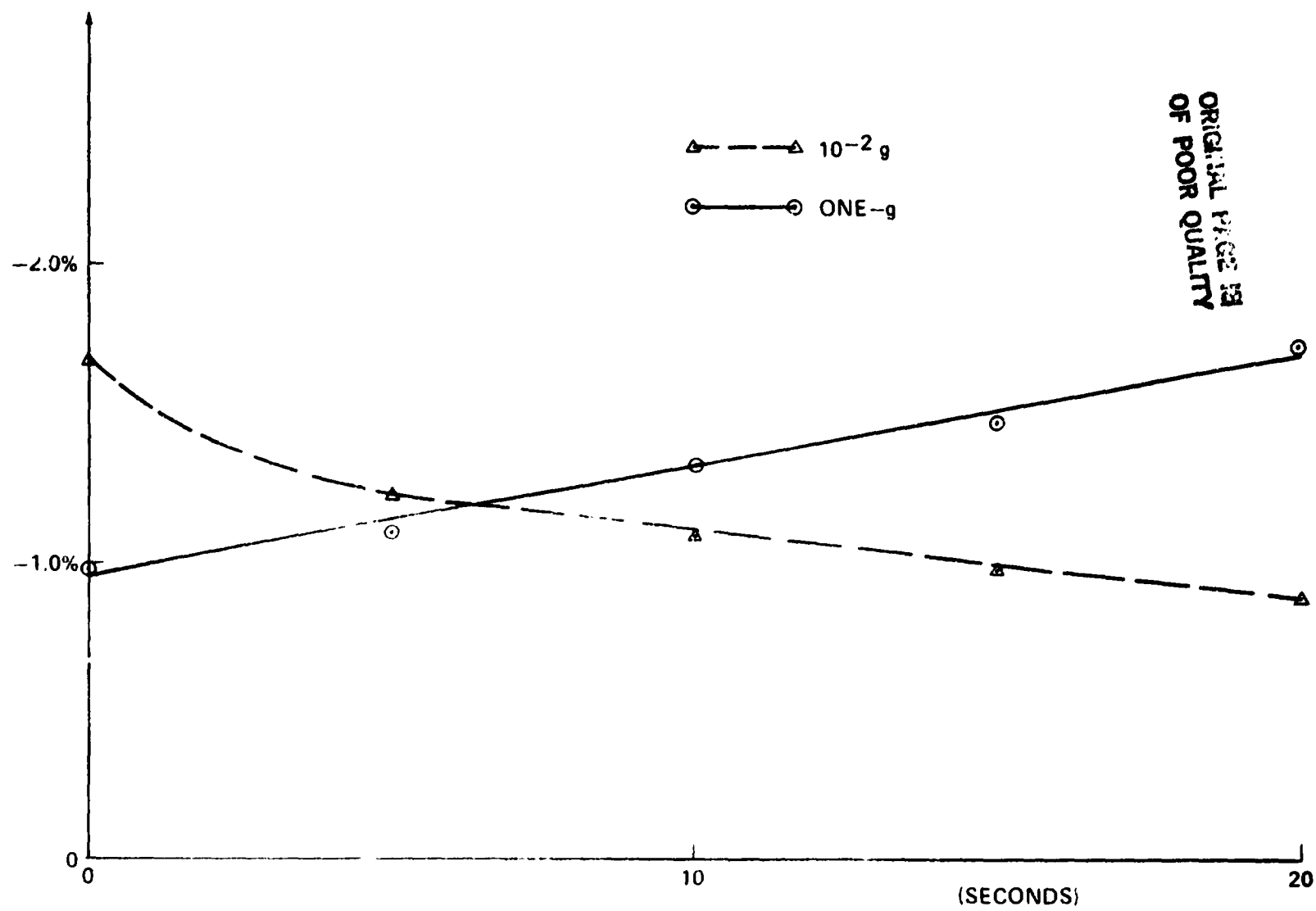
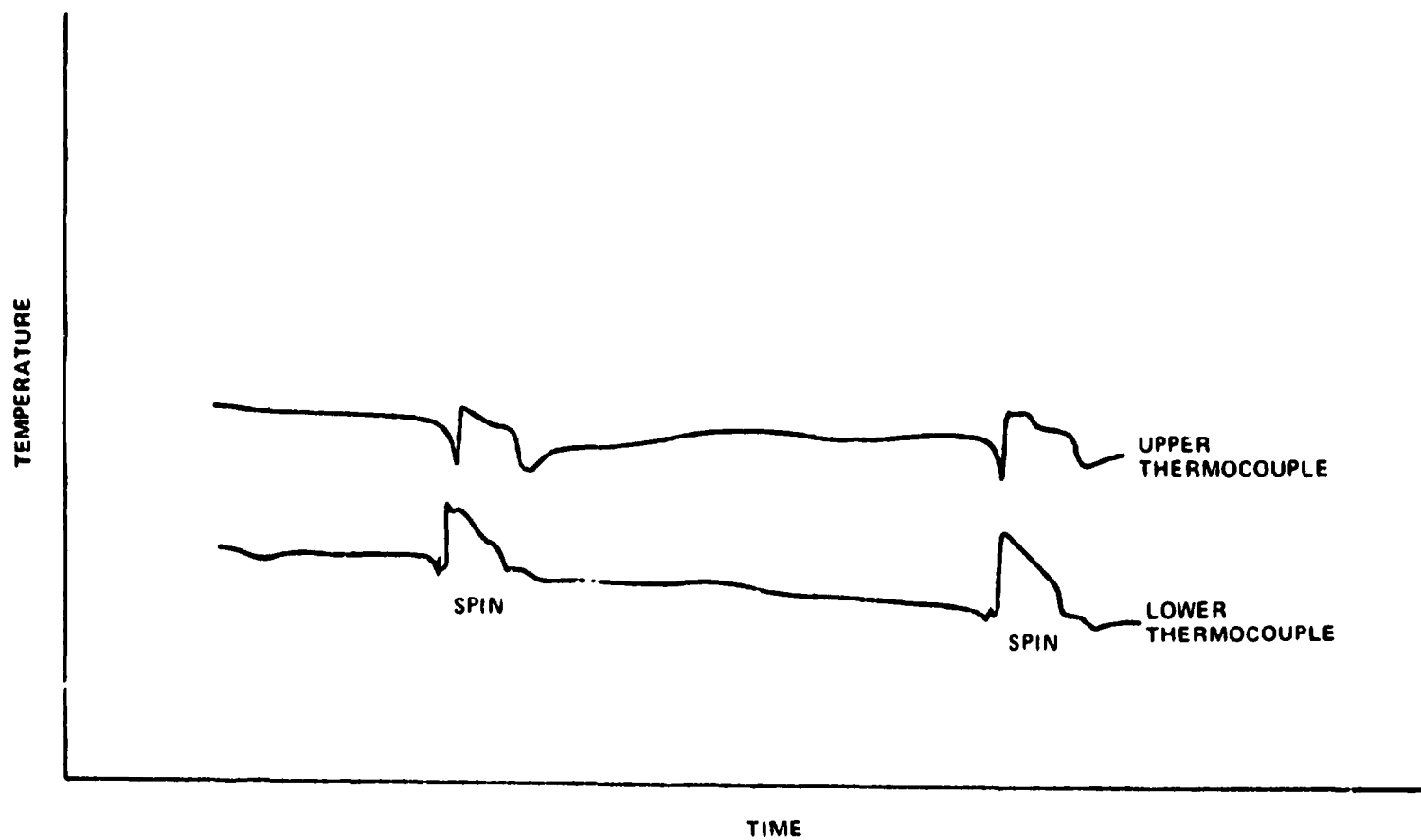
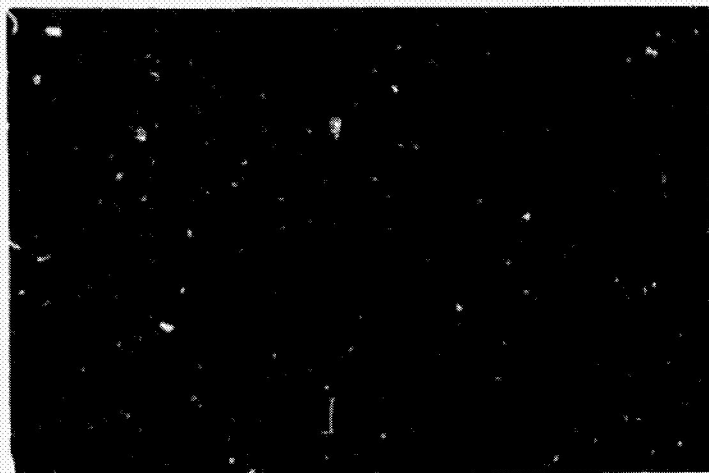


Figure X-13. Concentration shift from bulk to center of plume.

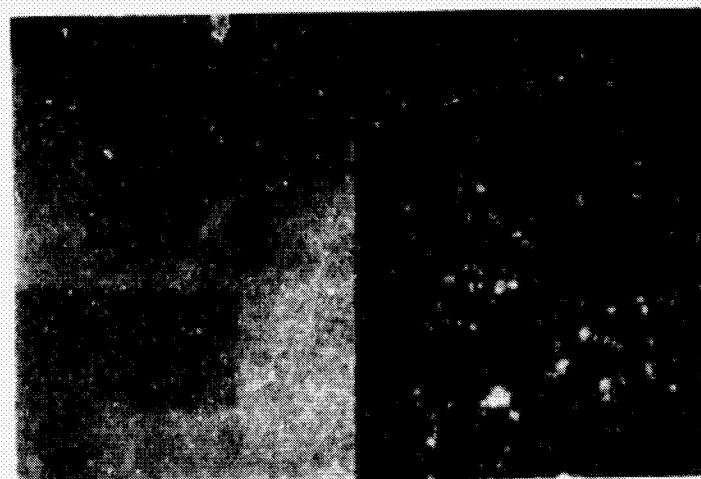


ORIGINAL PAGE IS
OF POOR QUALITY

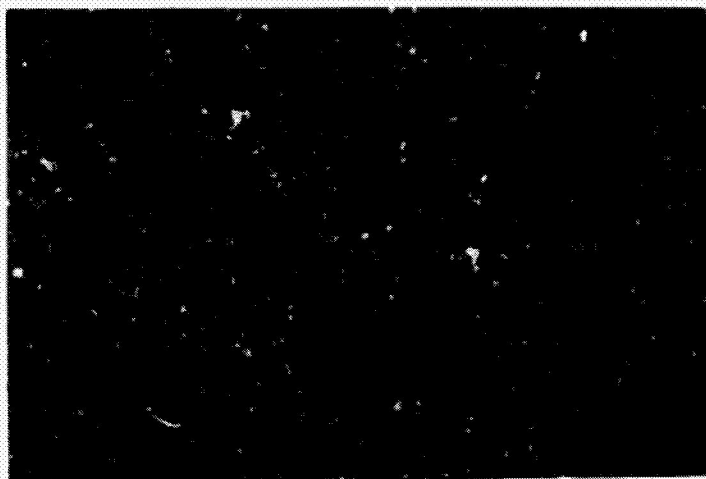
Figure X-14. Low-gravity temperature profiles during and after crucible rotation.



TIME: 0 SECONDS



TIME: 5 SECONDS



TIME: 10 SECONDS



TIME: 15 SECONDS

ORIGINAL PAGE IS
OF POOR QUALITY

Figure X-15. Split screen photographs of fluid motion decay on the ground (left half of photos) and in low-gravity (right half of photos.)

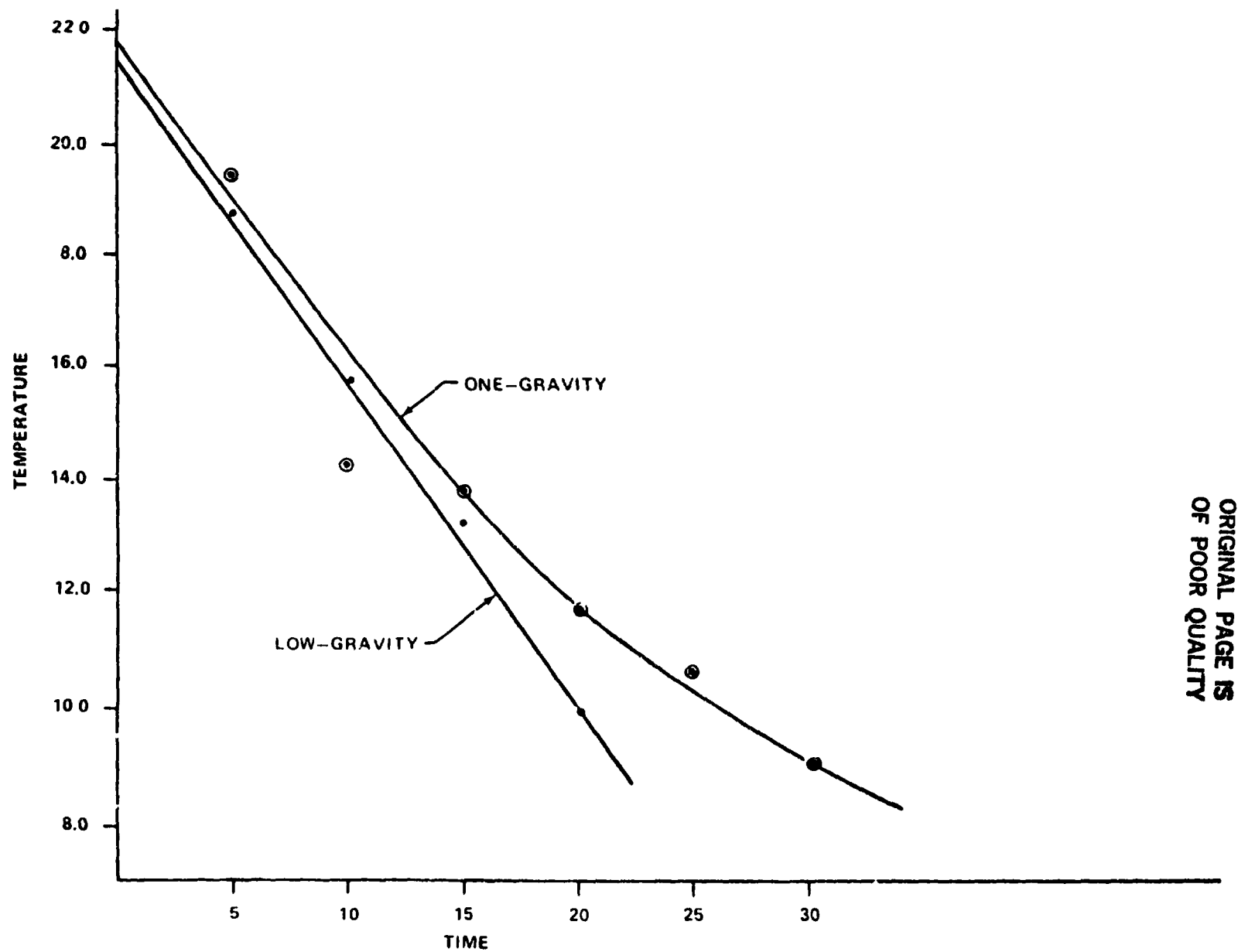


Figure X-16. Temperature versus time at bottom of cuvette after start of cooling.


ORIGINAL PAGE IS
OF POOR QUALITY

APPROVAL

OPTICAL OBSERVATIONS OF UNIDIRECTIONAL
SOLIDIFICATION IN MICROGRAVITY

By Mary H. Johnston, Robert B. Owen, and Robert E. Shurney

The information in this report has been reviewed for technical content. Review of any information concerning Department of Defense or nuclear energy activities or programs has been made by the MSFC Security Classification Officer. This report, in its entirety, has been determined to be unclassified.



G. D. HOPSON
Director, Systems Analysis
and Integration Laboratory